Herbivorous insects independently evolved salivary effectors to regulate plant immunity by destabilizing the malectin-LRR RLP NtRLP4

Xin Wang[1,2], Jia-Bao Lu[1], Yi-Zhe Wang[1], Xu-Hong Zhou[3], Jian-Ping Chen[1,2], Chuan-Xi Zhang[1], Jun-Min Li[1,#], Hai-Jian Huang[1,#]

[1] State Key Laboratory for Quality and Safety of Agro-Products, Key Laboratory of Biotechnology in Plant Protection of MARA, Zhejiang Key Laboratory of Green Plant Protection, Institute of Plant Virology, Ningbo University, Ningbo 315211, China

[2] Institute of Applied Ecology, Fujian Agriculture and Forestry University, Fuzhou 350002, China

[3] Office of Science and Technology, Yunnan University of Chinese Medicine, Kunming 650205, China

Abstract

Plants depend on receptor-like proteins and receptor-like kinases (RLPs/RLKs) to detect a variety of invading pathogens and insects. Although the mechanisms of microbial pathogens in suppressing plant immunity have been well investigated, it remains unclear how herbivorous insects overcome receptor-mediated defenses. Here, we show that salivary effectors evolve independently in whiteflies and planthoppers to target defensive RLP4, therefore minimizing the plant immunity. RLP4, as a leucine-rich repeat RLP (LRR-RLP), confers plant resistance against herbivorous insects by forming the RLP4/SOBIR1 complexes. In the whitefly *Bemisia tabaci*, BtRDP, the Aleyrodidae-specific salivary sheath protein, interacts with RLP4 from multiple plant species and promotes its ubiquitin-dependent degradation. Overexpression of NtRLP4 in transgenic plants exerts a detrimental impact on *B. tabaci* by exploiting the crosstalk between the salicylic acid (SA) and jasmonic acid (JA) pathways. Conversely, overexpression of BtRDP or silencing of NtRLP4 effectively alleviates such negative effects. In planthopper *Nilaparvata lugens*, the Delphacidae-

* Corresponding authors: Jun-Min Li, lijunmin@nbu.edu.cn; Hai-Jian Huang, huanghaijian@nbu.edu.cn

restricted salivary protein NlSP104 also targets and promotes the degradation of OsRLP4 from rice plants. Our results reveal the convergent evolution of salivary proteins in insects, and highlight the complex interactions between plants and herbivorous insects.

Keywords

salivary effector, insect-plant interaction, receptor-like protein, convergent evolution

Introduction

Plants have evolved sophisticated defense systems to survive the constant attacks of pathogens and herbivorous insects. These defenses function at multiple levels, encompassing physical barriers such as the cuticle and cell wall, chemical defenses that include toxic secondary metabolites and anti-nutritive compounds, and indirect defenses that involve the emission of herbivore-induced volatiles to attract natural enemies of the herbivores [1, 2]. Beyond these general strategies, plants also rely on the highly specialized molecular immune responses to detect and rapidly respond to invaders. The activation of innate immunity by membrane-localized receptors is a highly conserved mechanism among eukaryotes [3]. In sessile plants, the first line of defense against potential pathogenic microbes or insects relies on cell surface pattern-recognition receptors (PRRs) [4]. The plant genome encodes hundreds of PRRs, including receptor-like kinases (RLKs) and receptor-like proteins (RLPs) [4]. RLKs are consisted of different types of N-terminal ectodomains, a single transmembrane domain, and a cytoplasmic protein kinase domain, while RLPs have a similar structure but lack the kinase domain [5, 6]. As RLPs lack the intracellular signaling domains, they usually bind to SOBIR1 or SOBIR1-like adaptors to form the bimolecular receptor kinases [6]. Despite the large number of PRRs encoded by plant genomes, only a few of them have been well characterized regarding their functions in recognizing microbial-associated molecular patterns (MAMPs), damage-associated molecular patterns (DAMPs), and herbivore-associated molecular patterns (HAMPs) [5, 7]. For instance, FLS2 is known to recognize bacterial flagellin [8], EFR can recognize the bacterial elongation factor Tu [9], and EIX2 is responsible for the recognition of the fungal ethylene-inducing xylanase [10].

Piercing-sucking insects, such as whiteflies, aphids, and planthoppers, damage plants by feeding or transmitting viruses. They inject a mixture of saliva into plant tissues, which enhances

58 their feeding efficiency by binding to leaked calcium, degrading extracellular DNA, and regulating
59 plant hormonal signals [11-14]. In response, plants have evolved the ability to detect herbivores by
60 sensing HAMPs present in insect saliva [7, 15]. This triggers pattern-triggered immunity (PTI),
61 including mitogen-activated protein kinase (MAPK) cascades, reactive oxygen species (ROS), and
62 hormone signaling [16-18]. A few salivary proteins have been reported to activate plant PTI, but the
63 specific PRRs that recognize these proteins and trigger plant immunity are largely unclear [19-21].
64 One exception is the inceptin receptor (INR), which is a legume-specific LRR-RLP that can
65 recognize the Vu-In in insect oral secretions [7]. Moreover, plant PRRs have been extensively
66 reported to be targeted by pathogen effectors [22-24]. However, it remains unknown how insects
67 cope with the immune recognition system.

68 The whitefly *Bemisia tabaci* (Hemiptera: Aleyrodidae) and brown planthopper *Nilaparvata*
69 *lugens* (Hemiptera: Delphacidae) are notorious pests globally. During their feeding process, both
70 insects secrete abundant species-specific salivary proteins into host plants [25, 26]. It is reported
71 that plants initiate defense responses when they recognize insect feeding [19, 27]. However, the
72 specific PRRs responsible for this process are still unknown. Both insects can successfully ingest
73 phloem saps with limited plant defenses. At present, it remains unknown how insects attenuate plant
74 defenses. Given that numerous defense mechanisms are conserved across plants [3, 28], it is
75 interesting to investigate whether insect evolves a similar strategy to aid feeding during convergent
76 evolution. In this study, the functions of RLPs in the plant immunity responsive to piercing-sucking
77 insects were investigated, and *B. tabaci* and *N. lugens* were demonstrated to independently evolve
78 salivary proteins to regulate the post-translational modification of RLPs.

79

80 ## Results

81 **BtRDP is most abundantly expressed in salivary glands and secreted into host plants**

82 Based on the transcriptomic results, BtRDP (*B. tabaci* RLP-degrading protein; GenBank
83 accession: MN738093) was the most abundant gene in salivary glands [26]. It was a secretory
84 protein that contained a signal peptide at the N-terminal, and totally 6 unique peptides from BtRDP
85 were detected in the *B. tabaci* watery saliva (Fig. S1). As there was no gene homolog identified in
86 the NCBI nr database, BtRDP was subjected to BLAST analysis against the transcriptomic or
87 genomic data of 30 insect species. RDP was distributed in all the analyzed Aleyrodidae species,

88 while no RDP homolog was detected in other species (Table S1). Phylogenetic analysis indicated
89 that RDPs from five *B. tabaci* cryptic species were clustered in the same clade, exhibiting a close
90 correlation with RDP from *Aleurocanthus spiniferus* (Fig. S2).

91 A group of *B. tabaci* were allowed to feed on *Nicotiana tabacum* plants for 24 h, and the
92 presence of BtRDP in the infested and non-infested samples were assayed. One band between 26-
93 33 kDa was detected in the *N. tabacum* plants infested by *B. tabaci*, but not in the non-infested
94 plants (Fig. 1a). This band matched the molecular weight of BtRDP identified in the salivary glands.
95 The detection of BtRDP in the infested plants (Fig. 1a) and in watery saliva (Fig. S1) collectively
96 indicated that BtRDP was a salivary protein. According to Western-blotting, qPCR and
97 transcriptomic analysis, BtRDP was nearly exclusively expressed in the salivary glands (Fig. 1b, c;
98 Fig. S3a), which was significantly different from the actin or ribosomal 18S rRNA (Fig. S4a). In
99 addition, BtRDP was highly expressed in the adult stages, but lowly expressed in the egg, nymph,
100 and pseudopupa stages (Fig. 1d; Fig. S3b), similar to another salivary protein BtFTSP [29] but
101 different from actin and ribosomal 18S rRNA (Fig. S4b). According to immunohistochemical (IHC)
102 staining, BtRDP was specifically distributed in the principle salivary gland, but not in the accessory
103 salivary gland or other tissues (Fig. 1e). For most piercing-sucking insects, two types of saliva (gel
104 and watery saliva) are secreted into plant tissues. The salivary sheath, formed from gel saliva, serves
105 as an insoluble lining along the stylet path, potentially providing a scaffold for effector delivery [30].
106 The salivary sheath secreted by *B. tabaci* was also stained with the anti-BtRDP serum. The BtRDP
107 signal was mainly detected in the protuberant structure of sheath (Fig. 1f), suggesting that BtRDP
108 attaches to salivary sheath after secretion.

109

110 **BtRDP is important for *B. tabaci* feeding on tobacco plants**

111 RNA interference was conducted to investigate the role of BtRDP in whitefly feeding.
112 Treatment with ds*BtRDP* efficiently and specifically suppressed the target gene at both the transcript
113 and protein levels (Fig. 2a; Fig. S5). There was no significant difference in the morphology of the
114 salivary sheath between ds*BtRDP*-treated and ds*GFP*-treated *B. tabaci* (Fig. S6a). However, the
115 salivary sheath length of ds*BtRDP*-treated *B. tabaci* was significantly shorter than that of the
116 ds*GFP*-treated control (Fig. S6b). Furthermore, treatment with ds*BtRDP* did not affect the
117 survivorship of whiteflies (Fig. S6c). Upon conducting a reproduction analysis, it was found that

118 the ds*BtRDP*-treated whiteflies oviposited fewer eggs than the control (Fig. 2b). The feeding
119 behavior of whiteflies was monitored using the electrical penetration graph (EPG) technique, which
120 distinguishes nonpenetration (np), pathway (C), phloem salivation (E1), and phloem ingestion (E2)
121 phases [31] (Fig. S7). Compared to the ds*GFP* control, ds*BtRDP*-treated *B. tabaci* exhibited a
122 significant reduction in phloem ingestion and an extended pathway duration, indicating that BtRDP
123 is necessary for efficient feeding (Fig. 2c).

124 Salivary proteins are reported to function in intercellular space and/or extracellular space after
125 being secreted into host plants [30, 32]. To investigate the role of BtRDP in different subcellular
126 locations of host plants, we constructed two transgenic *N. tabacum* lines overexpressing BtRDP:
127 one carrying the full-length coding sequence that included the signal peptide (oeBtRDP), which is
128 expected to be secreted into the apoplast (extracellular space), and the other lacking the signal
129 peptide (oeBtRDP^{-sp}), which is likely to be retained in the cytoplasm. The flag tag was fused to the
130 C-terminal ends of the recombinant proteins, respectively. Transgenic plants containing the empty
131 vector (EV), which exerted no significant influence on insect performance compared with the WT
132 (Fig. S8), were used as negative controls. Fecundity and two-choice assays demonstrated that
133 BtRDP, whether localized in the apoplast (oeBtRDP) or cytoplasm (oeBtRDP^{-sp}), enhanced whitefly
134 settling and oviposition relative to the EV controls (Fig. 2d-i; Fig. S9), indicating that BtRDP
135 promotes whitefly feeding behavior irrespective of its subcellular location.

136

137 **BtRDP interacts with the NtRLP4/NtSORBIR1 complex**

138 To investigate the underlying mechanism of BtRDP in improving whitefly feeding, yeast two-
139 hybrid (Y2H) screening against a *N. benthamiana* cDNA library was conducted using BtRDP^{-sp} as
140 a bait. Totally seven proteins were found to potentially interact with BtRDP^{-sp} (Table S2), including
141 an NbRLP4 (accession Niben261Chr07g1310001.1 in Niben261 genome). NbRLP4 possesses a
142 predicted N-terminal signal peptide, a malectin-like domain, a LRR domain, and a transmembrane
143 domain. NbRLP4, as well as its closest homology in *N. tabacum* (NtRLP4; GenBank accession:
144 XM_016601109), did not contain the kinase domain (Fig. 3a).

145 The relative expression of *NtRLP4* in response to *B. tabaci* infestation was investigated. Based
146 on qRT-RCR results, the transcript level of *NtRLP4* was not significantly influenced by *B. tabaci*
147 (Fig. S10). However, a decrease in the protein level of NtRLP4 was detected by Western-blotting

148 assay (Fig. 3b). Point-to-point Y2H assays revealed that NtRLP4$_{(23-541)}$ (a truncated version lacking
149 the signal peptide and transmembrane domains) interacted with BtRDP^{-sp} (Fig. 3c). To investigate
150 the specificity of the NtRLP4-BtRDP interaction, another RLP protein NtCf9 with the highest
151 sequence similarity to tomato resistance protein Cf9 (Fig. S11) [33], as well as three randomly
152 selected salivary proteins from *B. tabaci* (BtFTSP, QHB15613; BtSP16.3, MN738005; BtSP37.4,
153 MN738158), were used as controls. As a result, BtRDP^{-sp} did not interact with the truncated NtCf9
154 construct, in which the signal peptide and transmembrane domains were removed (Fig. 3c). Also,
155 NtRLP4$_{(23-541)}$ could not interact with the other three salivary proteins without signal peptides (Fig.
156 S12a, b). These findings raised the question of which domain of NtRLP4 is responsible for binding
157 to BtRDP, as identifying the interacting domain can help to infer where the salivary protein contacts
158 the receptor in plants. We therefore dissected the NtRLP4 domains accordingly. The results showed
159 that it was the LRR domain, rather than the malectin-like domain or the short intercellular region,
160 that was required for the NtRLP4-BtRDP interaction (Fig. 3c). To investigate the shortest LRR
161 sequence responsible for BtRDP interaction, the LRR domain was divided into three segments.
162 However, none of these segments interacted with BtRDP^{-sp} (Fig. S12a). Co-immunoprecipitation
163 (Co-IP) assays further confirmed the specific interaction between BtRDP and NtRLP4 (Fig. 3d). It
164 was the C-terminal myc tag-fused NtRLP4 (NtRLP4-myc), but not the NtCf9 (NtCf9-myc), that
165 could be immunoprecipitated by the C-terminal flag tag fused BtRDP (BtRDP-flag). In the
166 bimolecular fluorescence complementation (BiFC) assay, YFP fluorescence was observed upon co-
167 expression of the N-terminal nYFP tag fused NtRLP4 and N-terminal cYFP tag fused BtRDP^{-sp} (Fig.
168 S12c). Furthermore, in oeBtRDP transgenic plants, endogenous NtRLP4 was specifically
169 immunoprecipitated with BtRDP-flag, which was significantly different from the control (Fig.
170 S12d). These results suggest that BtRDP interacts with NtRLP4.

171 The absence of kinase motifs in the C-terminal region of NtRLP4 suggests that it may function
172 in cooperation with other proteins to initiate signaling. The receptor-like kinase SOBIR1, which
173 contained a kinase domain (Fig. S13a), has been widely reported to be required for the function of
174 RLPs in the innate immunity [6]. Through Co-IP assays, our study demonstrated that NtSOBIR1
175 was capable of interacting with NtRLP4 but not BtRDP (Fig. S13b, c).

176

177 **NtRLP4 and NtSOBIR1 are resistant to *B. tabaci* infestation**

178 The transgenic *N. tabacum* overexpressing NtRLP4 (oeRLP#1 and oeRLP#2, without any tags)
179 was constructed (Fig. 3e). Compared with the EV control, both oeRLP lines were less attractive to
180 *B. tabaci*, alongside less settling and ovipositing insects (Fig. 3f; Fig. S14a). Also, *B. tabaci* had a
181 significantly decreased fecundity in oeRLP plants (Fig. 3g; Fig. S14b). Similar results were
182 observed after transient overexpression of NtRLP4-GFP in *N. tabacum* (Fig. S14c, d), indicating
183 that NtRLP4 is resistant to *B. tabaci* infestation.

184 Thereafter, the EV and oeRLP#1 plants underwent transcriptomic sequencing (Fig. S15a). A total
185 of 729 differentially expressed genes (DEGs) were identified, comprising 423 up-regulated and 306
186 down-regulated genes (Table S3). Enrichment analysis demonstrated that the majority of up-
187 regulated DEGs were associated with plant-pathogen interaction, environmental adaptation, MAPK
188 signaling pathway, and signal transduction (Fig. S15b). In contrast, the glutathione metabolism,
189 carbohydrate metabolism, and amino acid metabolism pathways were significantly enriched in
190 down-regulated DEGs (Fig. S15c). Noteworthily, numerous DEGs were annotated as RLK/RLP or
191 WRKY transcription factor, with the majority of them being significantly upregulated (Fig. S15d,
192 e). These results suggested an enhanced defense response in oeRLP plants. The crosstalk between
193 salicylic acid (SA) and jasmonic acid (JA) pathways was critical for plant defenses [14]. The
194 increased defense of oeRLP transgenic plants was partially caused by the altered hormonal signaling.
195 The JA-associated gene *FAD7* was significantly induced, while the SA-associated genes *PAL* and
196 *NPR1* were repressed in oeRLP plants (Fig. 3h). Transient overexpression of NtRLP4-GFP in *N.*
197 *tabacum* plants via *Agrobacterium* infiltration exerted similar effects (Fig. S14e). Furthermore,
198 NtRLP4-GFP significantly enhanced H_2O_2 accumulation (Fig. S14f).

199 The function of NtSOBIR1 was also investigated by transient overexpression and hairpin RNAi
200 (Fig. S16). Overexpression of NtSOBIR1-GFP induced the cell death phenotype five days post agro-
201 injection (Fig. S16). Insects preferred to settle and oviposit on GFP-expressed *N. tabacum* than on
202 NtSOBIR1-GFP-expressed control, even though no obvious death phenotype was observed two
203 days post agro-injection (Fig. S16c, d). For NtSOBIR1 silencing, no cell death phenotype was
204 observed, while the NtSOBIR1-silenced leaves exhibited reduced growth (Fig. S16f). Compared
205 with the EV-silenced control, NtSOBIR1-silenced *N. tabacum* was slightly attractive to *B. tabaci*
206 (Fig. S16g, h). Collectively, these results demonstrate that NtSOBIR1 is resistant to *B. tabaci*
207 infestation.

208

209 **BtRDP attenuates plant defenses by promoting the degradation of host RLP4**

210 To investigate the interplay between NtRLP4 and BtRDP, transgenic *N. tabacum* silencing
211 NtRLP4 (*RNAi-RLP*#1 and *RNAi-RLP*#2) plants were constructed. Both *RNAi-RLP* lines showed
212 reduced NtRLP4 levels compared with EV plants, with *RNAi-RLP*#2 exhibiting a stronger silencing
213 effect (Fig. S17a). Compared with EV plants, *B. tabaci* showed a tendency to settle on NtRLP4-
214 silenced plants and lay more eggs (Fig. S17b, c). Thereafter, ds*GFP*- and ds*BtRDP*-treated *B. tabaci*
215 were reared on EV, *RNAi-RLP*#1, and *RNAi-RLP*#2, respectively. The ds*BtRDP*-treated *B. tabaci*
216 produced less offspring than the control (decreased by 28.3%; P=0.0007) on EV plants (Fig. 4a),
217 consistent with the results obtained from WT plants (Fig. 2b). On the *RNAi-RLP*#1 plant, the
218 impaired insect reproduction was still observed after ds*BtRDP* treatment, but the extent was slightly
219 reduced (decreased by 23.7%; P=0.002) (Fig. 4a). On the *RNAi-RLP*#2 plant, there was no
220 significant difference between the ds*GFP* and ds*BtRDP* treatments (Fig. 4a). The differential rescue
221 effect between the two RNAi lines likely resulted from their different NtRLP4 silencing efficiencies,
222 with the lower NtRLP4 level in *RNAi-RLP*#2 leading to a more complete rescue phenotype (Fig.
223 S17a; Fig. 4a). Collectively, these results suggest that *RNAi-RLP* plants are beneficial for insects
224 and can partially, but not completely, rescue the impaired feeding performance of ds*BtRDP*-treated
225 insects.

226 To investigate the influence of BtRDP on NtRLP4, GFP-tagged NtRLP4 (NtRLP4-GFP) was
227 transiently co-expressed with mCherry-tagged BtRDP (BtRDP-mCherry), red fluorescent protein
228 (RFP)-mCherry, and BtFTSP1-mCherry through agroinfiltration, respectively. All tags were fused
229 with the C-terminal region. As discovered, BtRDP-mCherry did not influence the location patterns
230 of NtRLP4-GFP (Fig. S18). However, a significant reduction in the fluorescent signal of NtRLP4-
231 GFP was detected after co-expression with BtRDP-mCherry, but not with the controls (Fig. S18).
232 Besides, co-expression with BtRDP-mCherry/NtRLP4-GFP significantly reduced H_2O_2
233 accumulation (Fig. 4b), suppressed the expression of JA-associated genes *FAD7* and *PDF.12*, and
234 induced that of the SA-associated genes *PAL* and *NPR1* (Fig. 4c). It was discovered by insect
235 bioassays that, transient overexpression of BtRDP-mCherry rescued the negative effects on whitefly
236 performance caused by NtRLP4-GFP overexpression (Fig. 4d, e). In the host choice experiments,
237 *B. tabaci* displayed a preference for settling on *N. tabacum* leaves co-expressing BtRDP-

238 mCherry/NtRLP4-GFP over those co-expressing RFP-mCherry/NtRLP4-GFP (Fig. 4d). However,
239 almost no preference was observed in *B. tabaci* feeding on *N. tabacum* plants co-expressing BtRDP-
240 mCherry/NtRLP4-GFP and plants expressing GFP alone (Fig. S19).

241 The attenuated NtRLP4-GFP fluorescent signal (Fig. S18), along with the observed decrease
242 in the protein level of NtRLP4 during *B. tabaci* infestation (Fig. 3b), led us to speculate on whether
243 BtRDP influenced the accumulation of NtRLP4. To this end, the BtRDP^{-sp}-his and GFP-his proteins
244 were prokaryotically expressed in *Escherichia coli*. Different concentrations of purified BtRDP^{-sp}-
245 his and GFP-his proteins were infiltrated into *N. tabacum* plants overexpressing NtRLP4-myc.
246 Interestingly, the protein level of NtRLP4-myc slightly decreased with the increasing amount of
247 BtRDP^{-sp}-his, while no such effect was observed with GFP-his (Fig. S20). Moreover, the BtRDP^{-sp}-
248 his protein did not have any significant effect on the accumulation of another RLP NtCf9-like (Fig.
249 S20). We further assessed the impact of BtRDP on NtSOBIR1 following NtRLP4 destabilization.
250 As the amount of BtRDP-flag increased, NtRLP4-myc accumulation was markedly reduced, while
251 NtSOBIR1-flag levels remained unchanged (Fig. S21).

252 Then, the NtRLP4 levels in oeBtRDP and oeBtRDP^{-sp} plants were detected. Compared with
253 the EV control, a reduced NtRLP4 abundance was observed in both oeBtRDP#1 and oeBtRDP#2
254 transgenic lines, but not the oeBtRDP^{-sp} plants (Fig. 4f), suggesting the importance of BtRDP
255 secretion in extracellular space. BtRDP attached to salivary sheath that was localized in plant
256 apoplast (Fig. 1f). The presence of signal peptide promoted the secretion of BtRDP into the
257 extracellular space. Therefore, the complete coding region of *BtRDP* was used in subsequent
258 experiments. The NtRLP4-myc and BtRDP-flag were transiently co-expressed in *N. benthamiana*
259 plants through *Agrobacterium* infiltration. As a result, BtRDP-flag significantly decreased the
260 protein level of NtRLP4-myc, but not NtCf9-myc (Fig. 4g). qRT-PCR analyses demonstrated that
261 the transcript level of *NtRLP4* remained unchanged (Fig. S22). These findings indicate that the
262 reduction in the protein level of NtRLP4 is not caused by transcriptional changes but rather by
263 degradation.

264 The ubiquitin system and autophagy are two major pathways regulating protein degradation
265 [34]. At first, MG132, a 26S proteasome inhibitor known to inhibit the degradation of ubiquitin-
266 conjugated proteins, was employed [35]. The results showed that MG132 efficiently prevented the
267 degradation of NtRLP4-myc by BtRDP-flag (Fig. 4h). Then, the autophagy inhibitor 3-

268 Methyladenine (3-MA) and bafilomycin A1 (BAF) that can block autophagy in plants were used
269 [36]. However, the decreased protein level of NtRLP4-myc was still observed in the presence of 3-
270 MA or BAF (Fig. S23). Additionally, NtRLP4-myc and HA-tagged ubiquitin (HA-UBQ) were co-
271 expressed in *N. benthamiana*. Total proteins were extracted from *N. benthamiana* leaves and then
272 subjected to immunoprecipitation with anti-myc beads. The ubiquitin attached to NtRLP4 was
273 determined by immunoblot using the anti-HA antibody. Leaves expressing NtRLP4-myc or UBQ-
274 HA along were used as negative controls. The results showed that a strong UBQ signal was detected
275 in the immunoprecipitated product only when NtRLP4-myc and UBQ-HA were co-expressed (Fig.
276 4i). The molecular weight of UBQ-attached NtRLP4-myc was remarkably larger than NtRLP4-myc
277 itself (Fig. 4i). These results suggest that BtRDP promotes NtRLP4 degradation through the
278 ubiquitin system, but not the autophagy pathway.
279
280 **Degrading plant RLP4s by salivary effectors is a common strategy for insects**
281 To investigate the ability of BtRDP to degrade RLPs from other host plants of *B. tabaci*,
282 *Solanum lycopersicum* RLP4 (SlRLP4; GenBank accession: XP_004232910) was selected for
283 further analysis. Sequence analysis revealed a similar gene structure between SlRLP4 and NtRLP4
284 (Fig. S24; Fig. S25a). Moreover, the interaction between BtRDP and SlRLP4 was confirmed
285 through Y2H and Co-IP assays (Fig. S25b, c). Additionally, SlRLP4-myc and SlCf9-like-myc were
286 transiently co-expressed with varying concentrations of BtRDP-flag or GUS-flag, with the myc and
287 flag tags fused with the C-terminus. The results showed that BtRDP-flag exerted no influence on
288 the accumulation of SlCf9-like-myc protein. In contrast, the protein level of SlRLP4-myc was
289 significantly reduced in the presence of BtRDP-flag (Fig. S25d), indicating the conserved function
290 of BtRDP in *B. tabaci* adaptation to different host plants.
291 BtRDP was a gene specific to the Aleyrodidae family, lacking homologues in other species.
292 To explore whether the degradation of RLPs by salivary effectors was a conserved mechanism
293 among different herbivorous insects, a RLP4 homology from *Oryza sativa* (OsRLP4; GenBank
294 accession: XP_015645303; Fig. 5a) and twenty salivary proteins from planthopper species lacking
295 signal peptides were paired to identify the potential interactions using Y2H assays. As a result, only
296 the salivary protein NlSP104^{-sp} (*N. lugens* salivary protein consisting of 104 amino acids, GenBank
297 accession: MF278694) interacted with OsRLP4$_{(29-551)}$ (OsRLP4 lacking signal peptides and

298 transmembrane domains), while the other salivary proteins tested did not show any interaction (Fig.
299 5b, c; Fig. S26). NlSP104 did not exhibit any sequence or structural similarity to BtRDP (Fig. S27).
300 Truncation analysis revealed that NlSP104^{-sp} interacted with both the LRR domain and the malectin-
301 like domain of OsRLP4 (Fig. 5c), which was slightly different from the BtRDP-NtRLP4 interaction
302 (Fig. 3c). Given that both BtRDP and NlSP104 interacted with the LRR domain of RLP4, further
303 investigation focused on the specific region of the LRR domain responsible for NlSP104 binding.
304 The LRR domain of OsRLP4 was divided into three segments, mirroring the division of the LRR
305 domain in NtRLP4 (Fig. S12a). NlSP104^{-sp} interacted with the truncated LRR domain (OsRLP4$_{(480-}$
306 $_{526)}$) (Fig. 5c). In contrast, none of the truncated LRR domain of NtRLP4 interacted with BtRDP^{-sp}
307 (Fig. S12a). These findings suggest that the binding sites for salivary proteins to RLP4 may differ
308 between *N. lugens* and *B. tabaci*.

309 NlSP104 was a planthopper-specific salivary protein nearly exclusively expressed in salivary
310 glands (Table S1; Fig. 5d; Fig. S28). The function of NlSP104 or its gene homologs in other
311 planthopper species has not been well investigated previously. Silencing NlSP104 did not affect
312 insect survivorship (Fig. 5e). However, significant reductions in honeydew excretion and impaired
313 fecundity were observed in ds*NlSP104*-treated *N. lugens* (Fig. 5f, g), indicating the importance of
314 NlSP104 in insect feeding.

315 Subsequently, OsRLP4-myc was transiently co-expressed with a complete coding region of
316 *NlSP104* (C-terminal flag tagged, NlSP104-flag). Another salivary protein NlSP7-flag and NtCf9-
317 myc were used as negative controls. It was found that NlSP104-flag specifically and significantly
318 decreased the protein level of OsRLP4-myc, which differed significantly from that of the NlSP7-
319 flag (Fig. 5h). Additionally, NlSP104-flag failed to decrease the protein level of NtCf9-myc (Fig.
320 5h). These findings suggest that *N. lugens* potentially evolves salivary effectors to target rice RLPs.
321

322 **Discussion**

323 Plants have evolved a complex innate immune system to protect themselves against
324 pathogen/insect invasion, and the cell surface-localized PRRs function on the frontline [4]. To
325 counteract this response, the pathogens have developed various strategies to avoid plant PRR-
326 mediated PTI for their own advantage [37]. However, it remains unknown whether insects take the
327 similar strategy to sabotage plant immunity. In this study, we demonstrate that the RLP4/SOBIR1

complexes confer plant resistance against herbivorous insects. In response, both planthoppers and whiteflies secrete salivary effectors that facilitate the degradation of defensive RLP4, leading to the attenuated plant immunity. Our results suggest that manipulation of PRRs may be a conserved strategy for herbivorous insects.

PRRs detect modified-self or non-self patterns and initiate a cascade of immune signaling events, which subsequently regulate downstream defense responses, conferring plant resistance against invaders [4, 5]. Although various insect salivary components have been identified as triggers for plant immune responses, the specific PRRs involved in this process remain unclear. Our study indicates that RLP4 significantly influences insect performance by modulating plant hormones and ROS (Fig. 3f-h; Fig. S14), highlighting the critical role of RLP4 in plant immunity. However, the precise ligand for RLP4 has yet to be identified. The malectin-LRR receptor RLP4 may respond to the DAMPs or HAMPs released during insect feeding [38], a hypothesis that warrants further investigation. RLP4 lacks an intracellular kinase domain, and instead forms bimolecular receptor kinases by interacting with SOBIR1 (Fig. S13). Overexpression of NtRLP4 or NtSOBIR1 in *N. tabacum* attracts *B. tabaci* and promotes insect reproduction, whereas silencing of either gene exerts the opposite effect (Fig. S14-S17). The association between RLPs and SOBIR1 protein kinases is structurally and functionally analogous to that of genuine receptor kinases [6]. Therefore, destabilizing the RLP4/SOBIR1 complex can potentially disrupt the immune recognition processes. It is noteworthily that although NtRLP4 interacts with SOBIR1, this alone does not confirm that it operates strictly through this canonical module. Evidence from other RLPs shows that co-receptor usage can be flexible, and some RLPs function partly or conditionally independent of SOBIR1 [39]. Therefore, a more definitive assessment of NtRLP4 signaling will therefore require genetic dissection of its co-receptor dependencies, including but not limited to SOBIR1.

As pivotal regulators in immune signaling, PRRs are frequently targeted by multiple pathogens through diverse mechanisms. For example, *Pseudomonas syringae* hampers the functionality of receptor complexes by disrupting the ligand-dependent association between receptor-like kinase BAK1 and the flagellin receptor FLS2 [24], while *Phytophthora infestans* promotes alternative splicing of the host RLPKs to enhance infection [23]. PRRs are usually subjected to degradation via post-translational modifications [40]. In plants, the activity and stability of PRRs are under stringent regulation since excessive activation of PRRs could be detrimental [22, 41]. One prevalent

358 regulatory mechanism involves ubiquitination followed by subsequent degradation mediated by the
359 26S proteasome [40]. Mounting evidence has demonstrated that bacteria, fungi, viruses, and
360 oomycetes exploit such mechanisms to facilitate PRR degradation [42-45]. Nevertheless, the
361 occurrence of effector-mediated PRR degradation in insects is unreported. Our study reveals that
362 the salivary effectors BtRDP from *B. tabaci* and NlSP104 from *N. lugens* interact with plant RLP4s,
363 resulting in their degradation in a ubiquitin-dependent manner (Fig. 4f-i).

364 Notably, BtRDP and NlSP104 exhibit neither sequence nor structural similarity and do not
365 resemble the known eukaryotic ubiquitin-ligase domains. Their interaction with RLP4s occurs in
366 the extracellular space (Fig. 3d; Fig. 5c), whereas the ubiquitin-proteasome system primarily
367 functions within the cytosol and nucleus [46]. Furthermore, NtRLP4 reduction is observed solely in
368 oeBtRDP transgenic plants, not in oeBtRDP^{-sp} plants (Fig. 4f), indicating that BtRDP exerts its
369 influence on NtRLP4 in the extracellular space. These observations collectively refute the
370 possibility that BtRDP or NlSP104 possesses the intrinsic E3 ligase activity capable of directly
371 ubiquitinating RLP4s within plant cells. Importantly, the reduced NtRLP4 levels may not stem from
372 a direct physical interaction between BtRDP and NtRLP4. Instead, BtRDP may indirectly affect
373 RLP4 post-translational modification, thereby accelerating its degradation, which warrants further
374 investigation. Additionally, the independent evolution of RLP4-targeting effectors in various insect
375 lineages may expedite plant-insect co-evolution. Plants with robust RLP4-mediated defenses can
376 select for herbivores carrying effective effectors, driving an evolutionary "arms race". Conversely,
377 insects targeting similar host proteins may exert parallel selective pressures on unrelated plant
378 species, potentially shaping defense diversification across plant communities. Understanding these
379 dynamics provides insight into how molecular interactions scale up to influence herbivore
380 adaptation, host range, and the ecological outcomes of plant-insect interactions.

381 Herbivorous insects employ a mix of salivary components to ensure successful feeding [30].
382 Previous research has indicated that *B. tabaci* suppresses plant defenses by utilizing SA-JA crosstalk,
383 with the salivary protein Bt56 playing a crucial role in this process [14]. Bt56 activates the SA-
384 signaling pathway by directly interacting with a KNOTTED 1-like homeobox transcription factor
385 [14]. This study investigates the effects of another salivary effector, BtRDP, on plant hormones, and
386 finds that it elicits similar effects to Bt56, albeit primarily impacting the signal recognition process
387 (Fig. 3h; Fig. S14e). This leads us to speculate that different salivary effectors from the same insect

388 species may simultaneously target the same signaling pathway to ensure effective immune
389 suppression. Our analysis reveals that BtRDP interacts with other host genes apart from NtRLP4
390 (Table S2), and silencing NtRLP4 cannot completely rescue the impaired feeding performance of
391 ds*BtRDP*-treated insects (Fig. 4a). Salivary proteins exert a crucial effect on mediating the
392 interactions between herbivores and plants. The dynamic interplay between plants and insects may
393 be highly complex, one salivary protein can target multiple plant pathways, and one plant pathway
394 is influenced by multiple salivary proteins.

395 In conclusion, this study shows that suppressing PRR-mediated plant immunity may be the
396 common strategy for the successful feeding of herbivorous insects. Whiteflies and planthoppers
397 independently evolve salivary effectors that facilitate the degradation of defensive RLP4 in host
398 plants in an ubiquitin-dependent manner, therefore disrupting the RLP4/SOBIR1 complexes for
399 signal recognition (Fig. 6).

400

401 ## Material and methods

402 **Insects and plants**

403 A colony of *B. tabaci* (cryptic species MED) was originally collected from a soybean field in
404 Suzhou, Anhui Province, China. The insects were subsequently maintained on *N. tabacum* cv. K326
405 plants under controlled laboratory conditions (25 ± 1 °C, 50–70% relative humidity, 16:8 h
406 light:dark photoperiod). For experimental use, *N. benthamiana* and *N. tabacum* plants were grown
407 in a climate-controlled growth chamber (23 ± 1 °C, 16:8 h light: dark cycle).

408

409 **Phylogenetic analysis of RDP**

410 To identify potential RDP homologs across insect species, we performed a BLASTp search using
411 the BtRDP protein sequence as a query against the predicted proteomes of 30 insect species. Hits
412 were filtered using an E-value cutoff of 10^{-5}. The retrieved RDP homologs were aligned using
413 MAFFT (v7.310) with default parameters [47]. To improve alignment quality, we removed
414 ambiguously aligned regions using Gblocks with default settings. The optimal amino acid
415 substitution model (JTT+G) was determined using ModelTest-NG (v0.1.6). Phylogenetic
416 relationships were inferred using maximum likelihood analysis in RAxML (v0.9.0) with 1000
417 bootstrap replicates to assess branch support [48]. The final tree was visualized and annotated using

418 iTOL (https://itol.embl.de/).

419

420 **Preparation of anti-BtRDP and anti-NtRLP4 serum**

421 The coding sequence of BtRDP (excluding the signal peptide) was PCR-amplified and cloned
422 into the pET-28a vector (Novagen) to generate a C-terminal 6×His-tagged fusion protein. The
423 recombinant plasmid was transformed into *Escherichia coli* Transetta (DE3) competent cells
424 (TransGen Biotech, Beijing, China). Protein expression was induced with 0.5 mM isopropyl-β-D-
425 thiogalactoside (IPTG) at 28°C for 8 h. Bacterial cells were harvested by centrifugation and lysed
426 via ultrasonication for 30 min. The recombinant BtRDP^{-sp}-His protein was purified under native
427 conditions using Ni-NTA agarose (Qiagen, Hilden, Germany) according to the manufacturer's
428 protocol.

429 Purified BtRDP^{-sp}-His protein was used to immunize rabbits (Hua'an Biotechnology,
430 Hangzhou, China) for custom polyclonal antibody production. The anti-NtRLP4 serum, prepared
431 by immunizing rabbits with peptide GQNSDRPISTKNST, was produced via the custom service of
432 Genscript Biotechnology Company (Nanjing, China). The anti-BtRDP serum was subsequently
433 conjugated to Alexa Fluor™ 488 NHS Ester (#A20000, Thermo Fisher Scientific) following
434 standard labeling protocols.

435 The specificity of anti-BtRDP serum was tested by comparing ds*GFP*- and ds*BtRDP*-treated
436 *Bemisia tabaci*. The results showed that ds*BtRDP* significantly reduced the target gene. Similarly,
437 the specificity of anti-NtRLP4 serum was tested by comparing RNAi-EV and RNAi-NtRLP4 plants,
438 which showed a reduced NtRLP4 expression in *RNAi-NtRLP4* plants.

439

440 **Immunohistochemistry (IHC) staining**

441 Dissected *B. tabaci* heads with attached salivary glands and Parafilm-embedded salivary
442 sheaths were fixed in 4% paraformaldehyde (#E672002, Sango Biotechnology, Shanghai) for 30
443 min. Salivary sheaths adherent to Parafilm were similarly excised and fixed under identical
444 conditions. After fixation, samples were washed three times with PBST (PBS containing 0.1%
445 Tween-20) and blocked with 10% FBS for 2 h at room temperature. The tissues were then incubated
446 overnight at 4°C with Alexa Fluor 488-conjugated anti-BtRDP serum (1:200 dilution), followed by
447 co-staining with phalloidin-rhodamine (1:500, Thermo Fisher Scientific) for 30 min and 4',6-

448 diamidino-2-phenylindole (DAPI) solution (#ab104139, Abcam, Cambridge, USA) for nuclear
449 visualization. Fluorescent images were acquired using a Leica SP8 confocal microscope (Leica
450 Microsystems) to examine BtRDP localization patterns
451
452 **Protein extraction and Western-blotting assays**
453 To identify secreted salivary proteins in *N. tabacum* plants, approximately 200 *B. tabaci* adults
454 were confined in a 3-cm diameter feeding cage and allowed to feed on host plants for 24 h. After
455 feeding, the eggs deposited on the infested tobacco leaves were removed. The leaves showing no
456 visible insect contamination were immediately frozen in liquid nitrogen and ground to a fine powder.
457 The powdered tissue was then homogenized in RIPA Lysis Buffer (#89900, Thermo Fisher
458 Scientific) for protein extraction. To examine the effects of insect feeding on NtRLP expression,
459 groups of approximately 200 *B. tabaci* were allowed to feed on 4-5 true-leaf stage tobacco plants
460 for 12, 24, or 48 h, with uninfested plants serving as controls. For silencing/overexpression
461 efficiency tests, leaf samples were collected at 48 h post-*Agrobacterium* infiltration, along with
462 transgenic tobacco plants at the 4-5 true-leaf stage. For insect tissue analysis, various *B. tabaci*
463 organs were carefully dissected in 1×PBS buffer, including carcasses (20), fat bodies (20), guts (40),
464 salivary glands (60), and ovaries (10), with sample sizes indicated in parentheses. All dissected
465 tissues were transferred to lysis buffer for protein extraction. Total protein concentrations in both
466 insect and plant homogenates were quantified using a BCA Protein Assay Kit (#CW0014S,
467 CwBiotech, Taizhou, China). Equal protein amounts were separated by SDS-PAGE and electro-
468 transferred to PVDF membranes.
469 Membranes were probed with the following primary antibodies: anti-FLAG (1:10,000, #MA1-
470 91878, Thermo Fisher Scientific), anti-MYC (1:10,000, #MA1-21316, Thermo Fisher Scientific),
471 anti-GFP (1:10,000, #MA5-15256, Thermo Fisher Scientific), anti-NtRLP4 (1:5,000, GenScript
472 Biotechnology, Nanjing, China), and anti-BtRDP serum (1:5,000, Huaan Biotechnology, Hangzhou,
473 China). Following primary antibody incubation, membranes were treated with HRP-conjugated
474 secondary antibodies: goat anti-mouse IgG (1:10,000, #31430, Thermo Fisher Scientific) or goat
475 anti-rabbit IgG (1:10,000, #31460, Thermo Fisher Scientific). Protein bands were visualized using
476 an AI 680 image analyzer (Amersham Pharmacia Biotech, Buckinghamshire, UK), with Ponceau S
477 staining used to verify equal protein loading.

478

479 **Quantitative real-time PCR (qRT-PCR) analysis**

480 To prepare tissue-specific samples from *B. tabaci*, adult females were dissected to isolate
481 carcasses (10), fat bodies (10), guts (20), salivary glands (40), and ovaries (10). Additionally,
482 different developmental stages, including eggs (50), nymphs (20), pupae (20), and adult males (20)
483 and females (20), were collected for analysis. The number of insects in each sample is indicated in
484 parentheses. To extract RNA from *N. tabacum* plants, the samples were grinded using liquid
485 nitrogen after collection. Total RNA was extracted using the TRIzol Total RNA Isolation Kit (#9109,
486 Takara, Dalian, China) following the manufacturer's instructions. RNA purity and concentration
487 were assessed using a NanoDrop spectrophotometer (Thermo Fisher Scientific). First-strand cDNA
488 was synthesized from equal amounts of RNA (1 μg) using the HiScript II Q RT SuperMix (#R212-
489 01, Vazyme, Nanjing, China). Gene expression analysis was performed using a Roche LightCycler®
490 480 system (Roche Diagnostics, Mannheim, Germany) with SYBR Green Supermix (#11202ES08,
491 Yeasen, Shanghai, China). The thermal cycling protocol consisted of initial denaturation at 95°C for
492 5 min, and amplification for 40 cycles of 95°C for 10 s and 60°C for 30 s. Primers were designed
493 with Primer Premier v6.0 (Table S4). *B. tabaci Tubulin* and *N. tabacum Tubulin* served as internal
494 controls for normalization. Relative gene expression was calculated using the $2^{-\Delta\Delta Ct}$ method [49].
495 Three to six independent biological replicates, each repeated twice, were performed.

496

497 **RNA interference**

498 The target gene DNA sequences were amplified using primers listed in Table S4 and
499 subsequently cloned into the pClone007 Vector (#TSV-007, Tsingke Biotechnology, Beijing, China).
500 For dsRNA production, PCR-generated DNA templates containing T7 promoter sequences were
501 transcribed *in vitro* using the T7 High Yield RNA Transcription Kit (#TR101-01, Vazyme Biotech,
502 Nanjing, China). The RNAi experiments were performed according to established methods [50].
503 Briefly, newly emerged adult whiteflies were anesthetized with carbon dioxide for 5-10 seconds.
504 Approximately 50 nL of dsRNA solution (2 μg/μL) was microinjected into the mesothorax of each
505 insect using a FemtoJet microinjection system (Eppendorf, Hamburg, Germany). Following
506 injection, the whiteflies were maintained on healthy *N. tabacum* leaves under standard rearing
507 conditions. Only actively moving insects were selected for subsequent analyses. Gene silencing

508 efficiency was evaluated on day 4 post-injection using both qRT-PCR and Western-blotting
509 approaches.
510
511 **Generation of transgenic plants**
512 We generated two transgenic *N. tabacum* lines expressing different BtRDP variants: one
513 containing the full coding sequence (oeBtRDP) and another lacking the signal peptide (oeBtRDP^{-}
514 ^{sp}), which may affect protein secretion. The target sequences, along with the full-length NtRLP4
515 coding sequence and an NtRLP4 hairpin RNAi construct, were each cloned into the pBWA(V)HS
516 vector. The oeBtRDP and oeBtRDP^{-sp} were fused with C-terminal flag tags, while no tag was fused
517 to oeNtRLP4. All constructs were transformed into *A. tumefaciens* strain GV3101 and used to
518 generate transgenic tobacco plants (K326 background) through *Agrobacterium*-mediated
519 transformation performed by Wuhan Boyuan Biological Company. Transgenic lines were verified
520 by qRT-PCR and western blotting, with empty vector-transformed plants serving as controls, and
521 two independent lines for each construct were selected for further experiments.
522
523 **Target gene silencing in plants**
524 The hairpin RNAi construct targeting *NtSOBIR1* was generated by cloning the specific
525 fragment into the pBWA(V)HS plasmid using BsaI and Eco31I restriction enzymes. The
526 recombinant vector was then transformed into *A. tumefaciens* strain GV3101 and subsequently
527 infiltrated into *N. tabacum* leaves using the agroinfiltration method. Following a 48-h incubation
528 period under standard growth conditions, silencing efficiency was quantitatively evaluated by qRT-
529 PCR analysis.
530
531 **Transcriptomic sequencing**
532 To investigate the transcriptional effects of NtRLP4, BtRDP, and BtRDP^{-sp} in *N. tabacum*, leaf
533 samples from EV, oeRLP4#1, oeBtRDP#1, and oeBtRDP^{-sp}#1 transgenic plants were homogenized
534 in TRIzol Reagent (#10296018, Invitrogen, Carlsbad, CA, USA) for total RNA extraction following
535 the manufacturer's protocol. Afterwards, total RNA was extracted according to the instructions of
536 the manufacturer, and the RNA samples were sent to Novogene Institute (Novogene, Beijing, China)
537 for transcriptomic sequencing. Briefly, poly(A)+ RNA was isolated from 20 μg pooled total RNA

using oligo(dT) magnetic beads, followed by fragmentation in divalent cation buffer at 94°C for 5 min. First-strand cDNA synthesis was performed using N6 random primers, with subsequent second-strand synthesis to generate double-stranded cDNA. After end-repair and Illumina adapter ligation, the products were PCR-amplified (15 cycles) and purified using a QIAquick PCR Purification Kit (#28104, Qiagen, Hilden, Germany). The resulting cDNA libraries were quantified and quality-checked before paired-end sequencing on an Illumina NovaSeq 6000 platform. All raw sequencing data were deposited in the National Genomics Data Center under accession number PRJCA025907.

Analysis of transcriptomic data

The raw sequencing reads were quality-filtered using Illumina's internal software, and the resulting clean reads from each cDNA library were aligned to the *N. tabacum* reference genome in Sol Genomics Network (https://solgenomics.net/ftp/genomes/Nicotiana_tabacum/edwards_et_al_2017/) using HISAT v2.1.0 [51]. Low-quality alignments were removed using SAMtools (v1.7) with default parameters [52]. Transcript abundance was quantified as Transcripts Per Million (TPM) using Cufflinks (v2.2.1) [53]. Differential expression analysis was performed with DESeq2 (v2.2.1) [54], identifying significantly DEGs using thresholds of |log2(fold change)| > 1 and adjusted *p*-value < 0.05. PCA of transcriptome profiles was conducted using a custom R script plotPCA (github.com/franco-ye/TestRepository/blob/main/PCA_by_deseq2.R). For functional annotation, KEGG pathway enrichment analysis was performed in TBtools (v2.083) using a one-sided hypergeometric test: $P = 1 - \sum_{i=0}^{m-1} \left(\frac{\binom{M}{i}\binom{N-M}{n-i}}{\binom{N}{n}} \right)$, [55]. In this software, enriched *P*-values were calculated according to one-sided hypergeometric test: with *N* representing the number of gene with KEGG annotation, *n* standing for the number of DEGs in *N*, *M* indicating the number of genes in each KEGG term, and *m* suggesting the number of DEGs in each KEGG term.

Insect bioassays

To survivorship analysis, newly emerged *B. tabaci* adults were microinjected with dsRNA and placed on *N. tabacum* leaves. After 24 h, any dead individuals (potentially due to injection injury)

567 were removed. For each treatment, 20-30 surviving adults were transferred to leaf cages, and
568 mortality was recorded daily for 10 days. Three independent biological replications were performed.
569 For fecundity analysis, dsRNA-treated virgin females were paired with untreated males in
570 leaf cages. Five such pairs were maintained per cage (n=10-12 cages per treatment). Egg deposition
571 was quantified daily for 3 consecutive days under controlled conditions. Each male-female pair was
572 considered an experimental replicate.
573 For host preference test, detached *N. tabacum* leaves with moist cotton-wrapped petioles were
574 arranged in a 50-cm diameter choice arena with a central release chamber. Forty adult whiteflies
575 were released per chamber, and settling preference was recorded at 3, 6, 12, 24, 36, and 48 h post-
576 release. The experiment included 10-12 replicates per treatment, with leaf positions randomized
577 between replicates to eliminate positional bias.
578
579 **EPG recording and analysis**
580 Feeding behavior of *B. tabaci* was monitored using a GiGA-8d EPG amplifier (Wageningen
581 Agricultural University; 10 TΩ input resistance, <1 pA input bias current) with 50× gain and ±5 V
582 output range. Prior to recording, dsRNA-treated whiteflies were starved for 12 h on moist filter
583 paper, briefly anesthetized with CO_2 (10 s), and connected to the amplifier via a gold wire electrode
584 (20 μm diameter × 5 cm length) attached to the pronotum using conductive silver glue. Plant
585 electrodes consisted of copper wires (2 mm diameter × 10 cm length) inserted into the soil of potted
586 *N. tabacum*. Recordings were conducted for 8 h in a Faraday cage (120×75×67 cm; Dianjiang,
587 Shanghai), with only insects surviving the full duration retained for analysis.
588 Recorded waveforms were processed using PROBE 3.4 software (Wageningen Agricultural
589 University) and categorized into four distinct feeding phases: nonpenetration (np), pathway duration
590 (C), phloem salivation (E1), and phloem ingestion (E2) as defined in a previous study [31]. Each
591 treatment included ⩾10 biological replicates, with ds*GFP*-injected and untreated whiteflies
592 serving as controls.
593
594 ***Agrobacterium*-mediated plant transformation in *N. tabacum* and *N. benthamiana***
595 The recombinant expression vectors were introduced into *A. tumefaciens* strain GV3101 via
596 heat shock transformation. Transformed cells were selected on LB agar plates supplemented with

597 50 μg/mL kanamycin and 10 μg/mL rifampicin, followed by incubation at 28°C for 60 h. Positive
598 colonies were inoculated into liquid LB medium with the same antibiotics and grown to log phase.
599 Bacterial cells were then pelleted by centrifugation at 2,400 *g* for 2 min and resuspended in induction
600 buffer (10 mM $MgCl_2$, 10 mM MES [pH 5.6], 200 μM acetosyringone) adjusted to specific OD_{600}
601 values depending on the experiment.
602 For standard experiments, bacterial suspensions were normalized to OD_{600} = 1.0, while
603 degradation assays used three concentrations (OD_{600} = 0.05, 0.3, and 1.0). Equal volumes of selected
604 bacterial suspensions were mixed and infiltrated into leaves of 4–5-week-old *N. tabacum* and *N.*
605 *benthamiana* plants using a needleless syringe. Infiltrated plants were maintained under controlled
606 conditions for subsequent analysis.
607
608 **Diaminobenzidine (DAB) staining**
609 To detect H_2O_2 accumulation in *N. tabacum* leaves, leaf samples were immersed in 1 mg/mL
610 3,3'-diaminobenzidine tetrahydrochloride (DAB-HCl, #D8001, Sigma-Aldrich, St. Louis, MO,
611 USA) solution (pH 3.8) for 6 hours at room temperature, allowing H_2O_2-dependent brown
612 polymerization to occur. Following incubation, the DAB solution was replaced with 100% ethanol
613 for chlorophyll removal, and samples were decolorized overnight at 65°C. The destained leaves
614 were then photographed under standardized conditions using a Canon EOS 80D digital camera
615 (Canon Inc., Tokyo, Japan).
616
617 **Interaction assays between two proteins**
618 In the Y2H screening assay, the coding sequence of $BtRDP^{-sp}$ was cloned into the pGBKT7
619 bait vector (Clontech, USA), while a *N. benthamiana* cDNA library was constructed in the pGADT7
620 prey vector (Biogene Biotech, Shanghai, China). These recombinant vectors were co-transformed
621 into yeast strain Y2HGold and plated on QDO medium (SD/-Ade/-His/-Leu/-Trp, #630428, Takara)
622 for 3 days at 30°C. Positive colonies were cultured in QDO liquid medium, and plasmids were
623 extracted using a yeast DNA kit (#DP112-02, TIANGEN, Beijing, China) before transformation
624 into E. coli DH5α (#TSC-C14, Tsingke) for sequencing (YouKang Biotech, China) to identify
625 interacting partners.
626 In the Y2H point-to-point verification assay, $BtRDP^{-sp}$ and $NlSP104^{-sp}$, and mutant variants of

627 NtRLP4/SlRLP4/ OsRLP4 were cloned into either pGBKT7 or pGADT7 vectors using primers
628 from Table S4. Yeast co-transformants were first selected on DDO medium (SD/-Leu/-Trp)
629 (#630417, Takara) for 3 days at 30°C, then spotted onto QDO medium to confirm interactions
630 through growth after another 3 days of incubation.

631 In the Co-IP assays, Full-length sequences of *BtRDP*, *NlSP104*, *NtSOBIR1*, *NtRLP4*, *SlRLP4*,
632 and *OsRLP4* were cloned into lic-myc or lic-flag vectors for C-terminal tagging, with BtFTSP-flag
633 serving as a negative control. Five-week-old *N. benthamiana* leaves were agroinfiltrated with these
634 constructs or collected from oeBtRDP transgenic plants. Total proteins were extracted from 1 g
635 frozen tissue in IP lysis buffer (#87788, Thermo Scientific) with protease inhibitors (#56079200,
636 Roche, Switzerland), followed by centrifugation at 1,000 × *g* for 20 min. Cleared lysates were
637 incubated with anti-flag beads (#L00432-1, GenScript, Nanjing, China) for 4 h at 4°C, washed with
638 PBS, and eluted in 2× SDS-PAGE buffer (500 mM Tris-HCl, pH=6.8, 50% glycerin, 10% SDS, 1%
639 bromophenol blue, and 2% β-mercaptoethanol) for Western-blotting assay.

640 In the BiFC assay, $BtRDP^{-sp}$, $BtFTSP^{-sp}$, NtRLP4, and NtCf9-like were cloned into the pCV-
641 cYFP or pCV-nYFP vectors, respectively. After transforming *A. tumefaciens* GV3101, pairwise
642 combinations were co-infiltrated into *N. benthamiana* leaves. Following 36-48 h incubation in a
643 growth chamber, reconstituted YFP fluorescence was visualized using a Leica SP8 confocal
644 microscope with standard filter sets for YFP detection.

645

646 **RLP degradation by salivary effectors among different herbivorous insects**

647 To examine salivary protein effects on RLPs, we co-infiltrated *A. tumefaciens* GV3101 strains
648 carrying various constructs into *N. benthamiana* leaves. The recombinant vectors expressed C-
649 terminally tagged proteins: BtRDP-flag, NlSP104-flag, GUS-flag, NlSP7-flag, and myc-tagged
650 RLPs (NtRLP4, SlRLP4, OsRLP4, SlCf9, NtCf9). Bacterial suspensions were mixed at
651 predetermined OD_{600} ratios before infiltration, with leaf samples collected 48 hours post-infiltration
652 for subsequent analysis.

653 For confocal microscopy studies, *N. benthamiana* leaves were co-infiltrated with *A.*
654 *tumefaciens carrying*: (1) NtRLP4-GFP plus BtRDP-mCherry, (2) NtRLP4-GFP plus RFP-mCherry,
655 or (3) NtRLP4-GFP plus BtFTSP-mCherry. The samples were imaged by confocal microscopy at
656 48 h post injection. The same parameters were used in photographing.

657 This study also conducted a treatment on *N. benthamiana* plants that were overexpressing
658 NtRLP4-myc using purified proteins. Briefly, the BtRDP^{-sp} and GFP coding sequences were cloned
659 into pET-28a for 6×His-tagged expression in *E. coli* Transetta (TransGen Biotech). Protein
660 expression was induced with 0.5 mM IPTG at 25°C for 8 h, followed by purification using Ni-NTA
661 agarose and buffer exchange into PBS using a 3-kDa molecular-weight cutoff Amicon Ultra-4
662 Centrifugal Filter Device (Millipore, MA, USA). Different concentrations of purified proteins were
663 infiltrated into leaves of *N. benthamiana* plants stably expressing NtRLP4-myc, with samples
664 collected 24 h post-treatment.

665 To investigate degradation pathways, we infiltrated *N. benthamiana* leaves with: 50 μM
666 MG132 (#M7449, Sigma-Aldrich, Steinheim, Germany), 5 μM 3-MA (#M9281, Sigma-Aldrich,),
667 or 10 nM BAF (#BML-CM110-0100, Enzo Life Sciences, Farmingdale, USA) at 24 h post-
668 agroinfiltration. The samples were incubated for additional24 h. Protein levels were detected using
669 Western-blotting assay.

670

671 ***In planta* ubiquitination assay**

672 Ubiquitination detection in *N. benthamiana* was performed according to the methods
673 previously reported [56]. The recombinant vector for transient expression of the HA-fused ubiquitin
674 protein was kindly provided by Dr. Chao Zheng (Ningbo University). Myc-tagged proteins were co-
675 expressed with HA-UBQ by agroinfiltration, and 50 μM MG132 was injected into the *N.*
676 *benthamiana* leaves one day post *A. tumefaciens* infiltration. Immunoprecipitation was performed
677 using anti-myc beads (ytma-20, ChromoTek , Planegg-Martinsried, Germany). Ubiquitination
678 signals were detected by immunoblot with anti-HA antibody (HT301, TransGen Biotech, Beijing,
679 China).

680

681 **Scanning electron microscopy (SEM)**

682 *B. tabaci* adults were allowed to feed on artificial diet solutions for 24 h. Parafilm sections
683 containing salivary sheaths were carefully excised and rinsed with 1× PBS (pH 7.4) to remove
684 residual diet. The samples were mounted on aluminum stubs, desiccated under vacuum, and sputter-
685 coated with gold before imaging with a TM4000 II Plus SEM (Hitachi, Tokyo, Japan). Salivary
686 sheath length (from apex to base) was measured, with 20 sheaths analyzed per treatment to ensure

statistical reliability.

Statistical analysis

The log-rank test (SPSS Statistics 19, Chicago, IL, USA) was used to determine the statistical significance of survival distributions. Two-tailed unpaired Student's *t*-test (comparisons between two groups) or one-way ANOVA test followed by Tukey's multiple comparisons test (comparisons among three groups) was used to analyze the results of qRT-PCR, fecundity analysis, and host choice analysis. The EPG data were first checked for the normality and homogeneity of variance, and those not fitting a normal distribution were $\log_{10}$ transformed before Student's *t* test, as described in previous studies [31]. Statistical tests, including Student's *t*-test and one-way ANOVA, and data visualization were conducted in GraphPad Prism 9.

Data availability

All data is included in the manuscript and/or supporting information. The transcriptomic data have been submitted to the National Genomics Data Center under accession number PRJCA025907. The original blot images have been displayed in Fig. S29-S32.

References

1. Howe GA & Jander G (2008). Plant immunity to insect herbivores. *Annu Rev Plant Biol* 59, 41-66.
2. Wang H, *et al*. (2024), Release brake and set plant defense in motion. *New Plant Prot* 1: e11.
3. Nürnberger T, Brunner F, Kemmerling B, & Piater L (2004) Innate immunity in plants and animals: striking similarities and obvious differences. *Immunol Rev* 198(1):249-266.
4. Macho AP & Zipfel C (2014) Plant PRRs and the activation of innate immune signaling. *Mol Cell* 54(2):263-272.
5. Zipfel C (2014) Plant pattern-recognition receptors. *Trends Immunol* 35(7):345-351.
6. Gust AA & Felix G (2014) Receptor like proteins associate with SOBIR1-type of adaptors to form bimolecular receptor kinases. *Curr Opin Plant Biol* 21:104-111.
7. Adam D. Steinbrennera, *et al.* (2020) A receptor-like protein mediates plant immune responses to herbivore-associated molecular patterns. *Proc Natl Acad Sci USA* 117(49):31510-31518.

717 8. Chinchilla D, Bauer Z, Regenass M, Boller T, & Felix G (2005) The *Arabidopsis* receptor kinase
718 FLS2 binds flg22 and determines the specificity of flagellin perception. *Plant Cell* 18(2):465-
719 476.
720 9. Zipfel C, *et al.* (2006) Perception of the bacterial PAMP EF-Tu by the receptor EFR restricts
721 *Agrobacterium*-mediated transformation. *Cell* 125(4):749-760.
722 10. Ron M & Avni A (2004) The receptor for the fungal elicitor ethylene-inducing xylanase is a
723 member of a resistance-like gene family in tomato. *Plant Cell* 16(6):1604-1615.
724 11. Tian T, *et al.* (2021) A salivary calcium-binding protein from *Laodelphax striatellus* acts as an
725 effector that suppresses defense in rice. *Pest Manag Sci* 77(5): 2272-2281.
726 12. Huang HJ, *et al.* (2019) Salivary DNase II from *Laodelphax striatellus* acts as an effector that
727 suppresses plant defence. *New Phytol* 224(2):860-874.
728 13. Chen CY, *et al.* (2019) An effector from cotton bollworm oral secretion impairs host plant
729 defense signaling. *Proc Natl Acad Sci USA* 116(28):14331-14338.
730 14. Xu HX, *et al.* (2019) A salivary effector enables whitefly to feed on host plants by eliciting
731 salicylic acid-signaling pathway. *Proc Natl Acad Sci USA* 116(2):490-495.
732 15. Chen CY & Mao YB (2020) Research advances in plant-insect molecular interaction. *F1000Res*
733 9(F1000 Faculty Rev):198.
734 16. Guiguet A, *et al.* (2016) Shared weapons of blood- and plant-feeding insects: Surprising
735 commonalities for manipulating hosts. *J Insect Physiol* 84:4-21.
736 17. Wu J & Baldwin IT (2009) Herbivory-induced signalling in plants: perception and action. *Plant*
737 *Cell Environ* 32(9):1161-1174.
738 18. Jiang YJ, Zhang CX, Chen RZ, & He SY (2019) Challenging battles of plants with phloem-
739 feeding insects and prokaryotic pathogens. *Proc Natl Acad Sci USA* 116(47):23390-23397.
740 19. Gao H，*et al*. (2023) The salivary chaperone protein NlDNAJB9 of *Nilaparvata lugens* activated
741 plant immune responses. *J Exp Bot* 74(21):6874-6888.
742 20. Guo H, *et al*. (2020) An aphid-secreted salivary protease activates plant defense in phloem. *Curr*
743 *Biol* 30(24): 4826-4836.
744 21. Bos JI, *et al*. (2010) A functional genomics approach identifies candidate effectors from the
745 aphid species *Myzus persicae* (green peach aphid). *PLoS Genet* 6(11):e1001216.
746 22. Zhang Y & Zeng L (2020) Crosstalk between ubiquitination and other post-translational protein

747 modifications in plant immunity. *Plant Commun* 1(4):100041.

748 23. Huang J*, et al.* (2020) *Phytophthora* effectors modulate genome-wide alternative splicing of
749 host mRNAs to reprogram plant immunity. *Mol Plant* 13(10):1470-1484.

750 24. Shan L*, et al.* (2008) Bacterial effectors target the common signaling partner BAK1 to disrupt
751 multiple MAMP receptor-signaling complexes and impede plant immunity. *Cell Host Microbe*
752 4(1):17-27.

753 25. Huang HJ*, et al.* (2016) Screening and functional analyses of *Nilaparvata lugens* salivary
754 proteome. *J Proteome Res* 15(6):1883-1896.

755 26. Huang HJ, *et al.* (2021) Identification of salivary proteins in the whitefly *Bemisia tabaci* by
756 transcriptomic and LC-MS/MS analyses. *Insect Sci* 28(5):1369-1381.

757 27. Gao H, *et al*. (2022) *Nilaparvata lugens* salivary protein NlG14 triggered defense response in
758 plants. *J Exp Bot* 73(22):7477-7487.

759 28. Mukhtar M, *et al*. (2011) Independently evolved virulence effectors converge onto hubs in a
760 plant immune system network. *Science* 333(6042):596-601.

761 29. Wang Y, *et al*. (2023) Horizontally transferred salivary protein promotes insect feeding by
762 suppressing ferredoxin-mediated plant defenses. *Mol Biol Evol* 40(10):msad221.

763 30. Huang HJ*, et al.* (2023) Planthopper salivary sheath protein LsSP1 contributes to manipulation
764 of rice plant defenses. *Nat Commun* 14(1):737.

765 31. Lu S, *et al*. (2021) EPG-recorded feeding behaviors reveal adaptability and competitiveness in
766 two species of *Bemisia tabaci* (Hemiptera: Aleyrodidae). *J Insect Behav* 34: 26-40.

767 32. Yan ZW, *et al.* (2023) Endocytosis-mediated entry of a caterpillar effector into plants is
768 countered by Jasmonate. *Nat Commun* 14(1):6551.

769 33. Jones DA, *et al*. (1994) Isolation of the tomato Cf-9 gene for resistance to *Cladosporium fulvum*
770 by transposon tagging. *Science* 266 (5186): 789-793 (1994).

771 34. Varshavsky A, *et al*. (2017) The ubiquitin system, autophagy, and regulated protein degradation.
772 *Annu Rev Biochem* 86: 123-128.

773 35. Li L*, et al.* (2022) Independently evolved viral effectors convergently suppress DELLA protein
774 SLR1-mediated broad-spectrum antiviral immunity in rice. *Nature Commun* 13(1):6920.

775 36. Takatsuka C*, et al.* (2004) 3-Methyladenine inhibits autophagy in tobacco culture cells under
776 sucrose starvation conditions. *Plant Cell Physiol* 45: 265-274.

37. Tariqjaveed M, *et al.* (2021) Versatile effectors of phytopathogenic fungi target host immunity. *J Integr Plant Biol* 63(11):1856-1873.

38. Doblas VG, *et al.* (2018) Cell wall integrity signaling in plants: Malectin-domain kinases and lessons from other kingdoms. *Cell Surf* 3:1-11.

39. Albert I, *et al.* (2015). An RLP23–SOBIR1–BAK1 complex mediates NLP-triggered immunity. *Nat Plants* 1: 15140.

40. Li B, Lu D, & Shan L (2014) Ubiquitination of pattern recognition receptors in plant innate immunity. *Mol Plant Pathol* 15(7):737-746.

41. Chen Y, Song Y, Liu J, Xu G, & Dou D (2022) Ubiquitination of receptorsomes, frontline of plant immunity. *Int J Mol Sci* 23(6):2937.

42. Langin G, González-Fuente M, & Üstün S (2023) The plant ubiquitin–proteasome system as a target for microbial manipulation. *Annu Rev Phytopathol* 61:351-375.

43. Rosas-Diaz T, *et al.* (2018) A virus-targeted plant receptor-like kinase promotes cell-to-cell spread of RNAi. *Proc Natl Acad Sci USA* 115(6):1388-1393.

44. Irieda H, *et al.* (2019) Conserved fungal effector suppresses PAMP-triggered immunity by targeting plant immune kinases. *Proc Natl Acad Sci USA* 116(2):496-505.

45. Qin J, *et al.* (2018) The Xanthomonas effector XopK harbours E3 ubiquitin-ligase activity that is required for virulence. *New Phytol* 220(1):219-231.

46. Xu FQ, Xue HW (2019) The ubiquitin-proteasome system in plant responses to environments. *Plant Cell Environ* 42(10):2931-2944.

47. Katoh K & Standley DM (2013) MAFFT multiple sequence alignment software version 7: improvements in performance and usability. *Mol Biol Evol* 30(4):772-780.

48. Kozlov AM, Darriba D, Flouri T, Morel B, & Stamatakis A (2019) RAxML-NG: a fast, scalable and user-friendly tool for maximum likelihood phylogenetic inference. *Bioinformatics* 35(21):4453-4455.

49. Livak, K.J., and Schmittgen, T.D. (2001). Analysis of relative gene expression data using real-time quantitative PCR and the $2^{-\Delta\Delta CT}$ method. *Methods* 25, 402-408.

50. Xu HJ, *et al.* (2015) Two insulin receptors determine alternative wing morphs in planthoppers. *Nature* 519(7544):464-467.

51. Kim, D., Langmead, B., and Salzberg, S.L. (2015). HISAT: A fast spliced aligner with low

memory requirements. *Nature Methods* 519(7544):464-467.

52. Li, H. (2009). The Sequence Alignment/Map format and SAMtools. *BIOINFORMATICS - OXFORD*.

53. Trapnell, C., Roberts, A., Goff, L., Pertea, G., Kim, D., Kelley, D.R., Pimentel, H., Salzberg, S.L., Rinn, J.L., and Pachter, L. (2012). Differential gene and transcript expression analysis of RNA-seq experiments with TopHat and Cufflinks. *Nature Protocols* 7, 562-578.

54. Wang, L., Feng, Z., Wang, X., Wang, X., and Zhang, X. (2010). DEGseq: an R package for identifying differentially expressed genes from RNA-seq data. *Bioinformatics* 26, 136-138.

55. Chen, C., Chen, H., Zhang, Y., Thomas, H.R., Frank, M.H., He, Y., and Xia, R. (2020). TBtools: an integrative toolkit developed for interactive analyses of big biological data. *Mol Plant* 13, 1194-1202.

56. Wang, N., Yin, Z., Zhao, Y., Wang, J., Pei, Y., Ji, P., Daly, P., Li, Z., Dou, D., and Wei, L. (2022). An F-box protein attenuates fungal xylanase-triggered immunity by destabilizing LRR-RLP NbEIX2 in a SOBIR1-dependent manner. *New Phytol* 236(6):2202-2215.

Acknowledgements

This project has received funding from the National Key Research and Development Plan in the 14th five-year plan (2021YFD1401100: H.J.H, C.X.Z.), National Natural Science Foundation of China (32422075: H.J.H.; U23A6006: J.P.C and C.X.Z.), and the Natural Science Foundation of Zhejiang Province (LDQ24C140001: H.J.H).

Author Contributions Statement

H-JH, J-ML, C-XZ, and J-PC planned and designed the research. XW, J-BL, Y-ZW, and H-JH performed experiments and analyzed data. X-HZ provided the EV plants. H-JH and XW drafted the manuscript.

Competing Interests Statement

The authors declare no competing interests.

837 **Figure Legends**

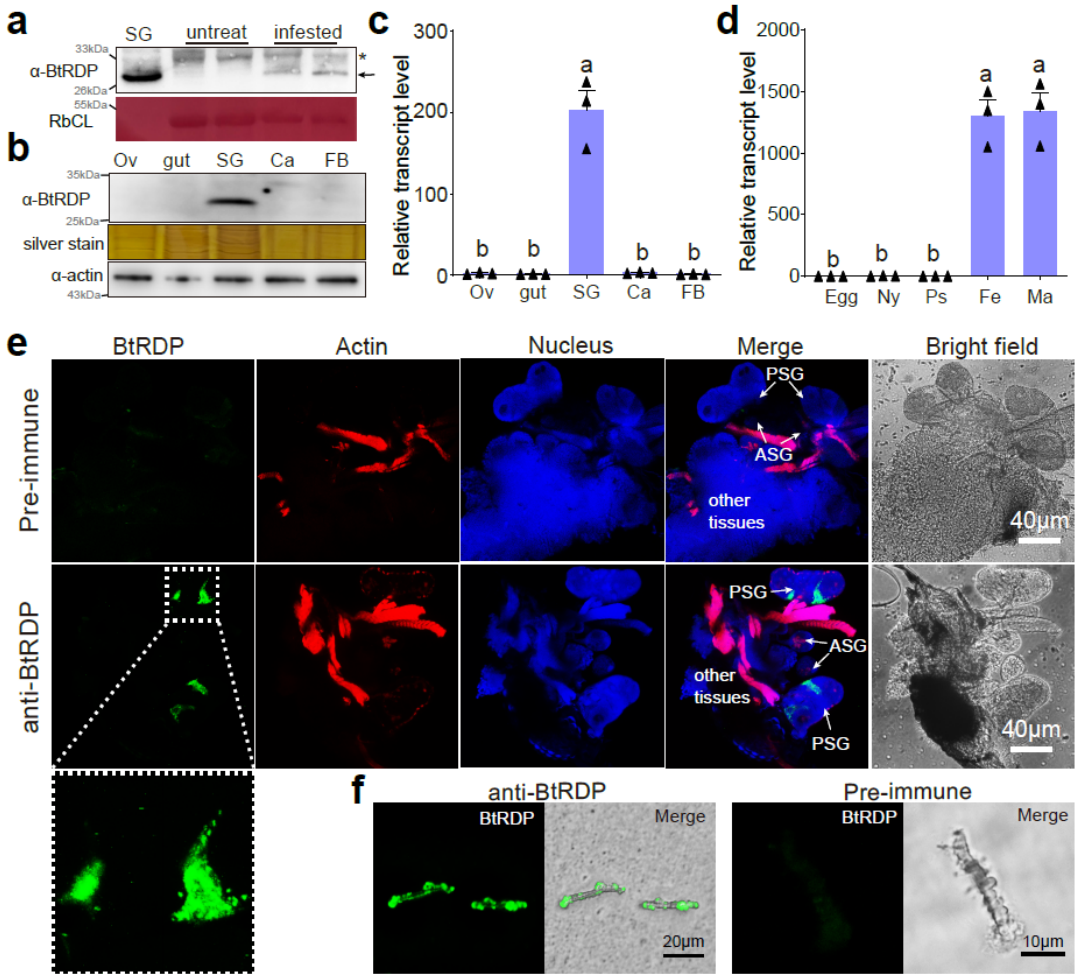

838

839 **Fig. 1. BtRDP is a salivary protein and secreted into plants.** (**a**) Detection of BtRDP in *Nicotiana*
840 *tabacum* plants. The untreated and *Bemisia tabaci*-infested tobacco plants, as well as the salivary
841 gland samples, are collected for western-blotting assays. Asterisk indicates non-specific binding.
842 Rubisco staining (RbcL) is conducted to visualize the amount of sample loading. **(b**, **c)** Detection
843 of BtRDP in different tissues by western-blotting and qRT-PCR assays. Ov, ovary; SG, salivary
844 gland; Ca, carcass; FB, fat body. Silver staining and anti-actin serum are used to visualize the sample
845 loading. (**d**) Expression patterns of BtRDP in different development stages. Ny, nymph; Ps,
846 pseudopupa; Fe, female; Ma, male. *B. tabaci tubulin* is used as an internal control. The relative
847 quantitative method ($2^{-\Delta\Delta Ct}$) is used to evaluate the quantitative variation. Data are presented as mean
848 values ± SEM (n= 3 independent biological replicates). Different lowercase letters indicate
849 statistically significant differences at the $P < 0.05$ level according to one-way ANOVA test followed
850 by Tukey's multiple comparisons test. **(e, f)** Immunohistochemical staining of BtRDP in salivary
851 glands **(e)** and salivary sheath secreted from *B. tabaci* **(f)**. The salivary gland and its nearby tissues

are dissected and incubate with anti-BtRDP serum or pre-immune serum conjugated with Alexa Fluor™ 488 NHS Ester (green) and actin dye phalloidinrhodamine (red). The nucleus is stained with DAPI (blue). PSG, principal salivary gland; ASG, accessory salivary gland. The lower images represent the enlarged images of the boxed area in the upper image. Experiments are repeated thrice for **(a** and **b**), while twice for **(e** and **f**). Similar results are observed and representative images are displayed.

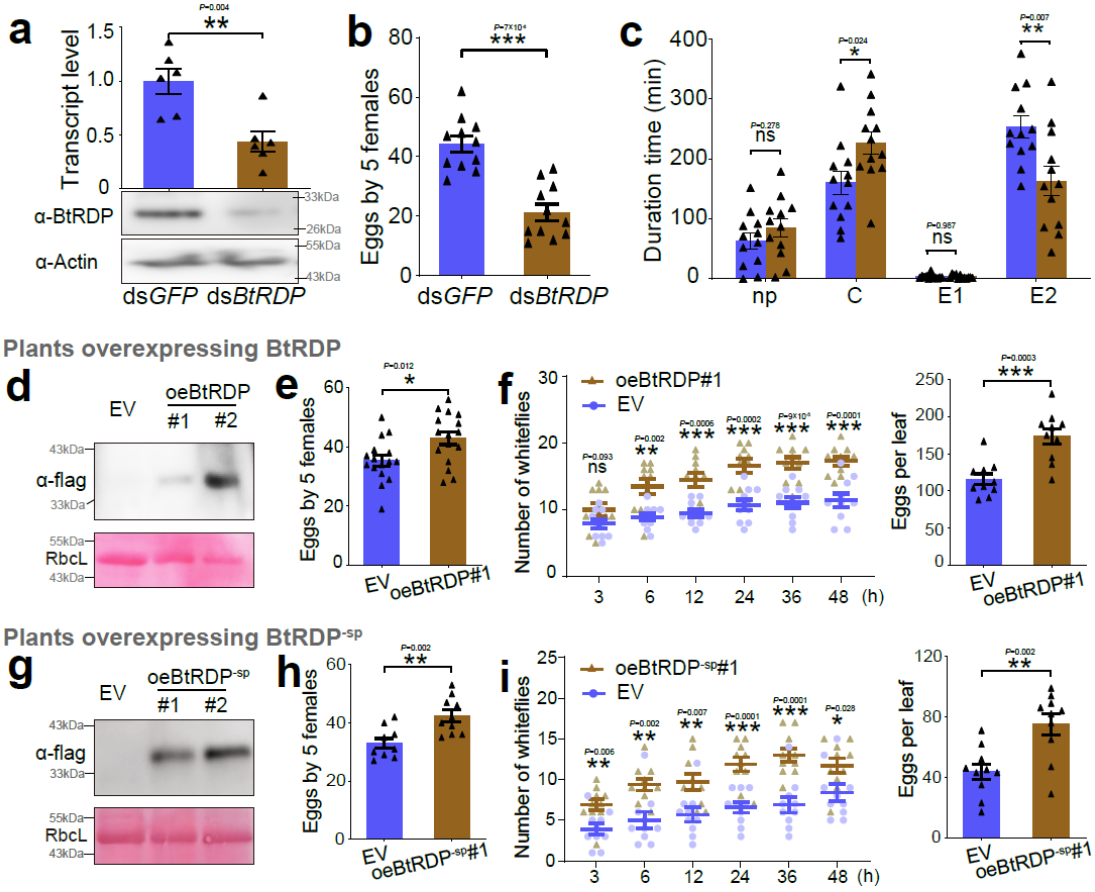

Fig. 2. Effects of BtRDP on *Bemisia tabaci*. (**a**) Treating *B. tabaci* with ds*BtRDP* significantly reduces the transcript and protein level of target gene. The ds*GFP*-treated *B. tabaci* is used as a control. **(b–c)** Effects of *BtRDP* knockdown on insect reproduction **(b)** and feeding behavior **(c)**. Electrical penetration graph (EPG) is used to monitor the insect feeding behavior, which can be classified into nonpenetration (np), pathway duration (C), phloem salivation (E1) and phloem ingestion (E2) phases. All EPG recordings are performed for 8 h. Typical EPG waveforms are displayed in Fig. S7. **(d-f)** Insect performance on transgenic plants overexpressing BtRDP (oeBtRDP). **(d)** Detection of BtRDP in transgenic *Nicotiana tabacum* overexpressing a complete

868 coding region of *BtRDP*. The empty vector (EV) plants are used as the control. The flag tag is fused
869 to the C-terminal ends of recombinant proteins. **(e)** Comparison of insect reproduction on
870 oeBtRDP#1 and EV plants. Five *B. tabaci* individuals are confined to indicated plants for 3 days,
871 and the oviposited eggs are counted. **(f)** Attraction of oeBtRDP#1 and EV leaves to *B. tabaci* in a
872 two-choice equipment. A group of 40 female *B. tabaci* are released into a device containing
873 oeBtRDP#1 and EV leaves. The number of insects settling on each leaf is counted. After 48 h, the
874 number of eggs on each leaf is counted. **(g-i)** Insect performance on transgenic plants overexpressing
875 $BtRDP^{-sp}$ ($oeBtRDP^{-sp}$). **(g)** Detection of $BtRDP^{-sp}$ in transgenic *N. tabacum* overexpressing BtRDP
876 without a signal peptide. The insect reproduction **(h)** and settlement **(i)** on $oeBtRDP^{-sp}$ transgenic
877 plants are recorded. The EPG data are first checked for normality and homogeneity of variance, and
878 data not fitting a normal distribution are subjected to log10 transformation. Data are presented as
879 mean ± SEM. Statistical significance in panels **(a)**, **(b)**, **(c)**, **(e)**, **(f)**, **(h)**, and **(i)** was assessed using
880 two-tailed unpaired Student's *t*-tests. ***$P < 0.001$; **$P < 0.01$; *$P < 0.05$; ns, not significant.
881 Western-blotting assays are repeated thrice with the similar results.

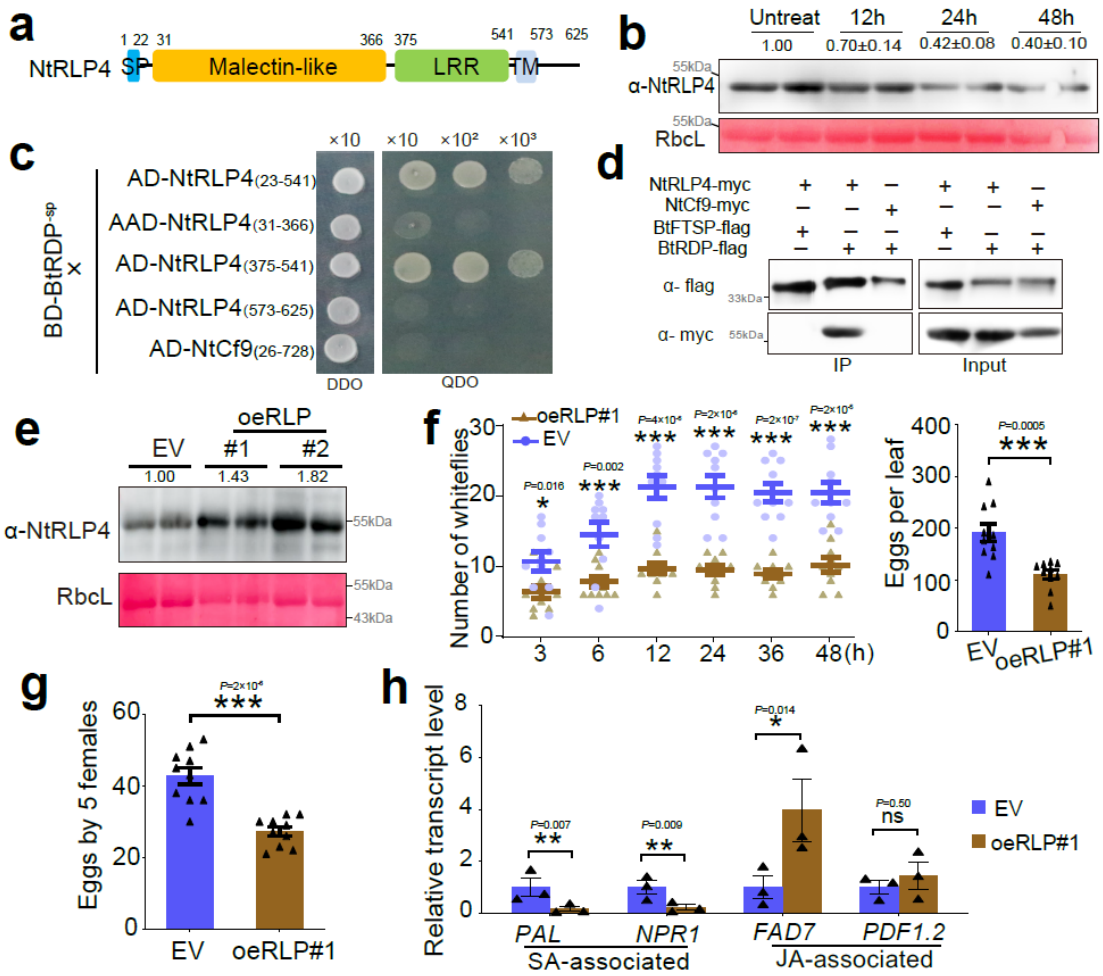

Fig. 3. NtRLP4 interacts with BtRDP and confers plant resistance to *Bemisia tabaci*. (a) Domain organization of NtRLP4. NtRLP4 contains a predicted N-terminal signal peptide (SP), a malectin-like domain, a LRR domain, and a transmembrane domain (TM). **(b)** The protein level of NtRLP4 in response to *B. tabaci* infestation. The untreated *Nicotiana tabacum* is used as a negative control. Four independent biological replicates are performed, and the representative images are displayed. The band density is measured using ImageJ. The density values from 4 biological replicates are calculated and the mean value in the controls is set at 1.0. **(c)** Yeast two hybrid assays showing the interaction between BtRDP and NtRLP4. The different combinations of constructs are transformed into yeast cells, and are grown on the selective medium SD/-Trp/-Leu (DDO), and the interactions are tested with SD/-Trp/-Leu/-His/-Ade (QDO). **(d)** Co-immunoprecipitation assay showing the interaction between BtRDP and NtRLP4. Total proteins are extracted from *N. benthamiana* leaves transiently co-expressing NtRLP4-myc/NtCf9-myc with BtFTSP-flag/BtRDP-flag. All genes are expressed with a complete coding region, and the myc/flag tags are fused at the C-terminus. Precipitation is performed using flag beads. The samples are probed with anti-flag and

anti-myc antibodies for immunoblotting analysis. **(e–h)** Analysis of transgenic *N. tabacum* overexpressing NtRLP4 (oeRLP). **(e)** Detection of NtRLP4 level in oeRLP plants. The empty vector (EV) plant is used as a control. Two independent oeRLP lines are selected. The samples are probed with an anti-NtRLP4 antibody. Rubisco staining (RbcL) is used to visualize the amount of sample loading. **(f)** Attraction of oeRLP#1 and EV leaves to *B. tabaci* in a two-choice equipment. A group of 40 female *B. tabaci* are released into a device containing oeRLP#1 and EV leaves. The number of insects settling on each leaf is counted at each time point. After 48 h, the number of eggs on each leaf is counted. **(g)** Comparison of insect reproduction on oeRLP#1 and EV plants. Five *B. tabaci* individuals are confined to indicated plants for 3 days, and the oviposited eggs are counted. **(h)** Relative transcript levels of salicylic acid (SA)- and jasmonic acid (JA)-associated genes in oeRLP#1 and EV plants. PAL, phenylalanine ammonia lyase; NPR1, nonexpressor of pathogenesis-related protein 1; FAD7, fatty acid desaturase 7; PDF1.2, plant defensin 1.2. Two independent biological replicates are performed in **(d)** and **(e)**. Data in **(f)**, **(g)**, and **(h)** are presented as mean values ± SEM. For insect bioassays in (**f**) and (**g**), n= 10 independent biological replicates. For qRT-PCR in (**h**), n= 3 independent biological replicates. *P*-values are determined by two-tailed unpaired Student's *t* test. ***$P < 0.001$; **$P < 0.01$; *$P < 0.05$; ns, not significant.

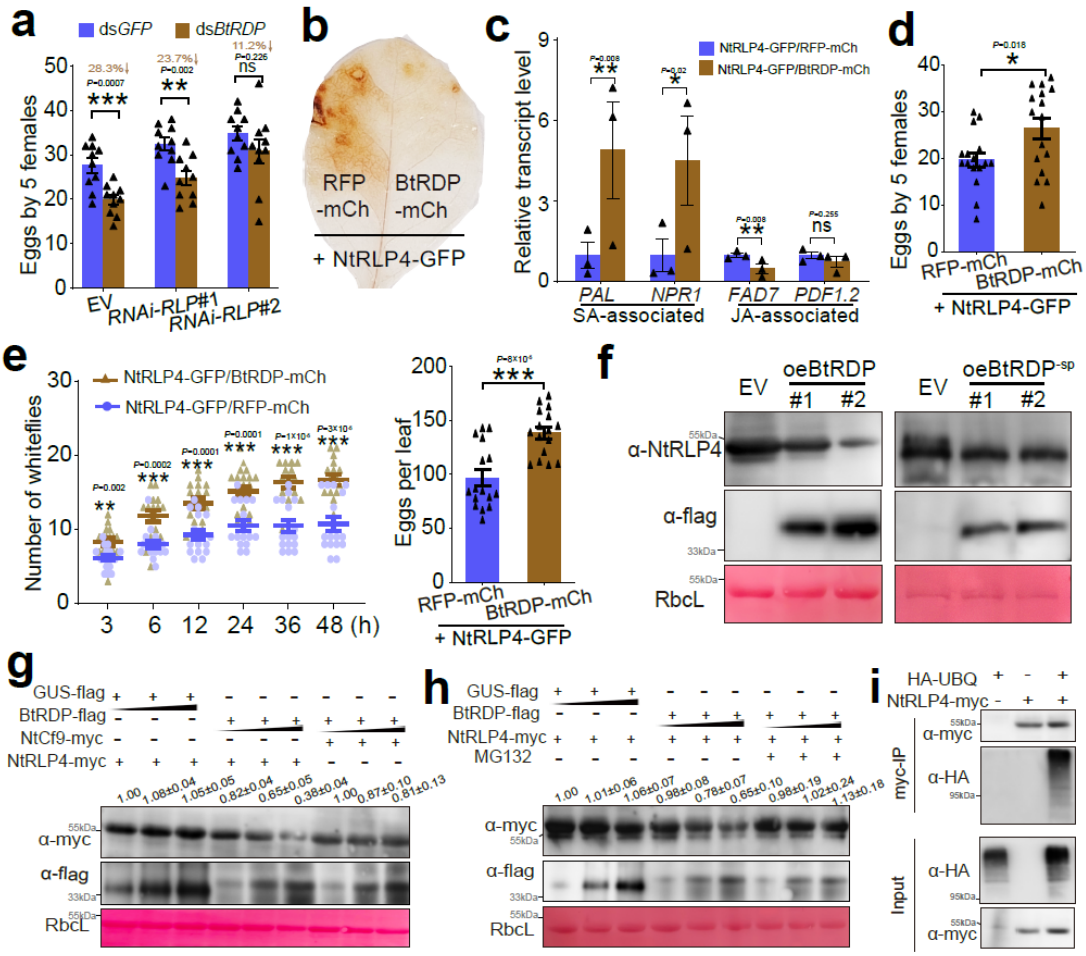

Fig. 4. BtRDP suppress plant defenses by promoting NtRLP4 degradation. (a) Effects of ds*BtRDP* suppression on insect reproduction (n= 10 independent biological replicates) when feeding on empty vector (EV) and NtRLP4-silenced (*RNAi-RLP*) transgenic *Nicotiana tabacum*. **(b)** Transient overexpressing BtRDP-mCherry attenuates H_2O_2 accumulation caused by NtRLP4-GFP overexpression. *N. tabacum* co-expressing RFP-mCherry and NtRLP4-GFP is used as a control. All genes are expressed with a complete coding region. The experiment is repeated 5 times with the similar results. **(c)** Relative transcript level of salicylic acid (SA)- and jasmonic acid (JA)-associated genes in BtRDP-mCherry/NtRLP4-GFP and RFP-mCherry/NtRLP4-GFP plants (n=3 independent biological replicates). PAL, phenylalanine ammonia lyase; NPR1, nonexpressor of pathogenesis-related protein 1; FAD7, fatty acid desaturase 7; PDF1.2, plant defensin 1.2. **(d)** Comparison of insect reproduction (n= 16 independent biological replicates) on transient-expressed BtRDP-mCherry/NtRLP4-GFP and RFP-mCherry/NtRLP4-GFP plants. **(e)** Attraction of BtRDP-mCherry/NtRLP4-GFP and RFP-mCherry/NtRLP4-GFP leaves to *B. tabaci* in a two-choice equipment (n= 16 independent biological replicates). The number of eggs on each leaf is counted at

928 48 h post insect release. (**f**) Effects of BtRDP and BtRDP^{-sp} overexpression on NtRLP4
929 accumulation. Transgenic oeBtRDP (left) and oeBtRDP^{-sp} (right) plants are probed with anti-
930 NtRLP4 and anti-flag antibodies for immunoblotting analysis. The experiments are repeated twice
931 with the similar results. **(g)** Degradation of NtRLP4 by BtRDP in *N. benthamiana* leaves. NtRLP4-
932 myc and BtRDP-flag are transiently co-expressed in *N. benthamiana* plants through *Agrobacterium*
933 infiltration. *Agrobacterium* carrying NtCf9-myc and GUS-flag are used as negative controls. **(h)**
934 Effects of 26S proteasome inhibitor (MG132) on NtRLP4 accumulation. Co-infiltrated leaves are
935 treated with MG132 at 24 h post injection. The samples are probed with anti-flag and anti-myc
936 antibodies for immunoblot analysis. Rubisco staining (RbcL) is conducted to visualize the amount
937 of sample loading. The small triangle indicates the different concentrations of *Agrobacterium*
938 (OD_{600} = 0.05, 0.3, and 1.0). **(i)** NtRLP4 is ubiquitinated *in planta*. NtRLP4-myc is co-expressed
939 transiently with HA-UBQ in *N. benthamiana* leaves. Extracted total proteins are
940 immunoprecipitated by anti-myc beads and immunoblotted with anti-myc or anti-HA antibody.
941 Experiments are repeated thrice for (**g**) and (**h**), while twice for (**i**). Band density is measured using
942 ImageJ. The density values from three biological replicates are calculated and the mean value in the
943 first lane is set at 1.0. Data are presented as mean values ± SEM. *P*-values are determined by two-
944 tailed unpaired Student's *t* test. ***$P < 0.001$; **$P < 0.01$; *$P < 0.05$; ns, not significant.

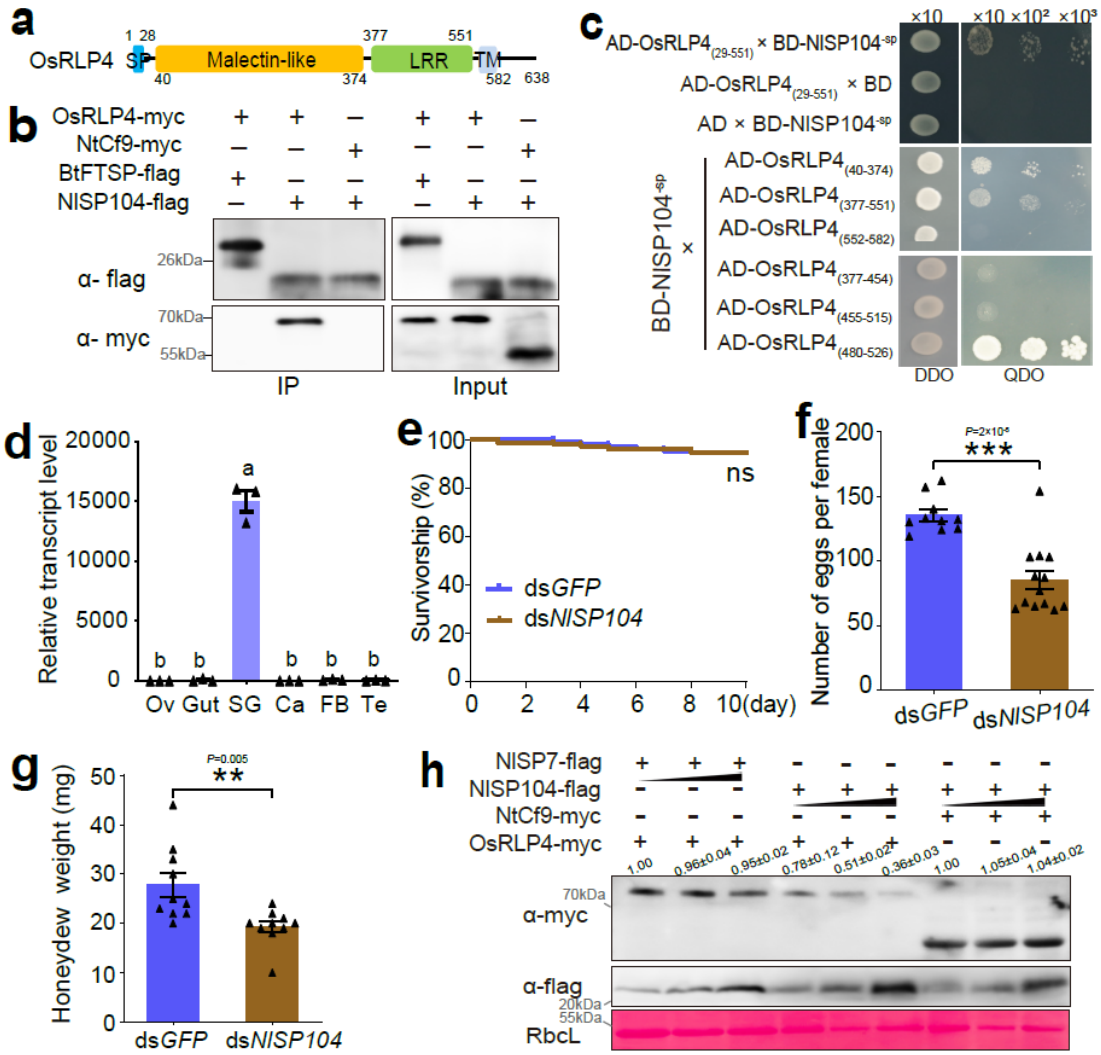

Fig. 5. Rice RLP4 are targeted by salivary protein NlSP104 from *Nilaparvata lugens*. (a) Domain organization of *Oryza sativa* RLP4 (OsRLP4). **(b, c)** Yeast two-hybrid and Co-IP assays showing the interaction between OsRLP4 and NlSP104. All genes are expressed with a complete coding region in Co-IP assays, while NlSP104 without a signal peptide is used in yeast two-hybrid assays. Experiments in (**b**) are repeated twice with the similar result. **(d)** The expression patterns of *NlSP104* in different *N. lugens* tissues. Te, testis; Ov, ovary; SG, salivary gland; Ca, carcass; FB, fat body. Data are presented as mean values ± SEM (n= 3 independent biological replicates). Different lowercase letters indicate statistically significant differences at $P < 0.05$ level according to one-way ANOVA test followed by Tukey's multiple comparisons test. **(e-g)** Effects of dsRNA treatment on insect survivorship (**e**), reproduction (**f**), and honeydew excretion (**g**). For survivorship analysis, a group of 30 *N. lugens* are reared in a cage. Three independent biological replications are performed. Differences in survivorship between the two treatments are tested by log-rank test. ns, not significant.

958 For reproduction analysis, n= 10 and 13 individuals are tested in ds*GFP*- and ds*NlSP104*-treatment,
959 respectively. The sterile females are excluded from data analysis. For honeydew analysis, n= 10
960 independent biological replicates. *P*-values in **(f)** and **(g)** are determined by two-tailed unpaired
961 Student's *t* test. ***$P < 0.001$; **$P < 0.01$. **(h)** Effect of NlSP104 on the accumulation of transient-
962 expressed OsRLP4. OsRLP4-myc is agro-injected into *Nicotiana benthamiana* together with
963 different concentrations of NlSP104-flag and NlSP7-flag. NtCf9-myc is used as a negative control.
964 The small triangle indicates the different concentrations (OD_{600} = 0.05, 0.3, and 1.0) of
965 *Agrobacterium*. Rubisco staining (RbcL) is conducted to visualize the amount of sample loading.
966 Experiments are repeated three times with the similar results. Band density is measured using
967 ImageJ. The density values from three biological replicates are calculated with the mean value in
968 the first lane being set at 1.0.

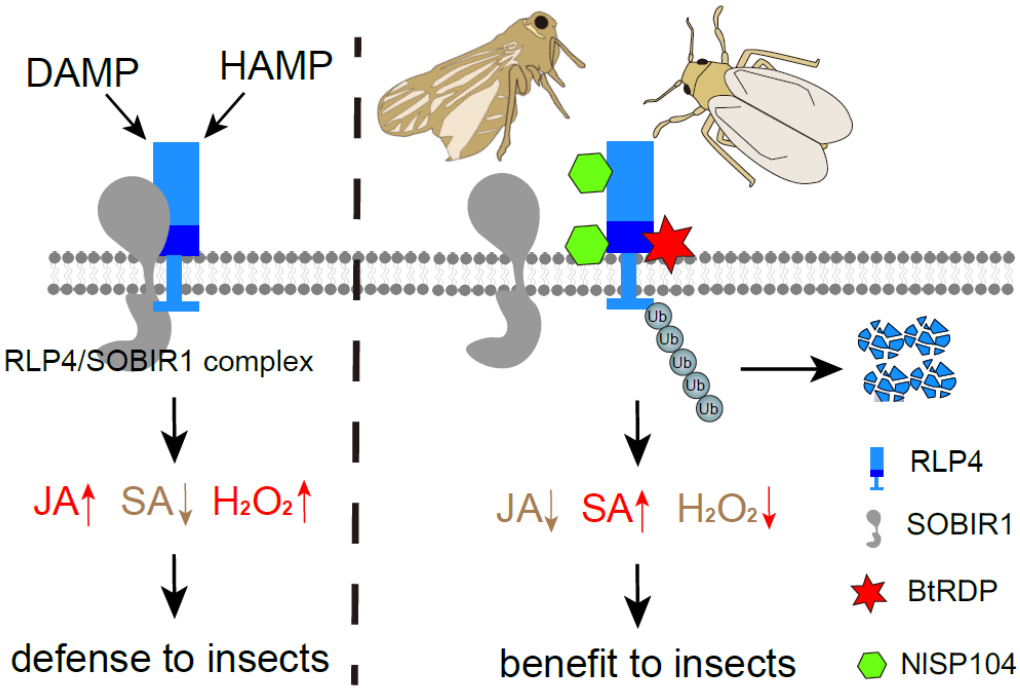

969

970 **Fig. 6. The proposed model for the suppression of receptor-like proteins (RLPs)-mediated**
971 **plant defenses by salivary effectors.** Host plants employ pattern-recognition receptors (PRRs) to
972 detect various damage-associated molecular patterns (DAMPs) and herbivore-associated molecular
973 patterns (HAMPs) triggered by insect feeding. The RLP4/SOBIR1 complex plays a vital role in
974 initiating pattern-triggered immunity (PTI), including H_2O_2 burst, upregulation of jasmonic acid
975 (JA), and downregulation of salicylic acid (SA), which hinders insect feeding. The whitefly *Bemisia*
976 *tabaci* and planthopper *Nilaparvata lugens* independently evolved salivary proteins that targeted

977 plant RLP4. *B. tabaci* salivary sheath protein BtRDP interacts with the leucine-rich repeat (LRR)
978 domain of RLP4 from *Nicotiana tabaci* and *Solanum lycopersicum*, while *N. lugens* NlSP104 targets
979 both the LRR domain and the malectin-like domain of *Oryza sativa* RLP4. These interactions
980 promote the ubiquitin-dependent degradation of RLP4, thereby disrupting the stability of the
981 RLP4/SOBIR1 complex. The presence of salivary effectors causes a hormonal shift and suppresses
982 the H_2O_2 burst, finally favoring insect feeding.
983

1. Supplementary Figures

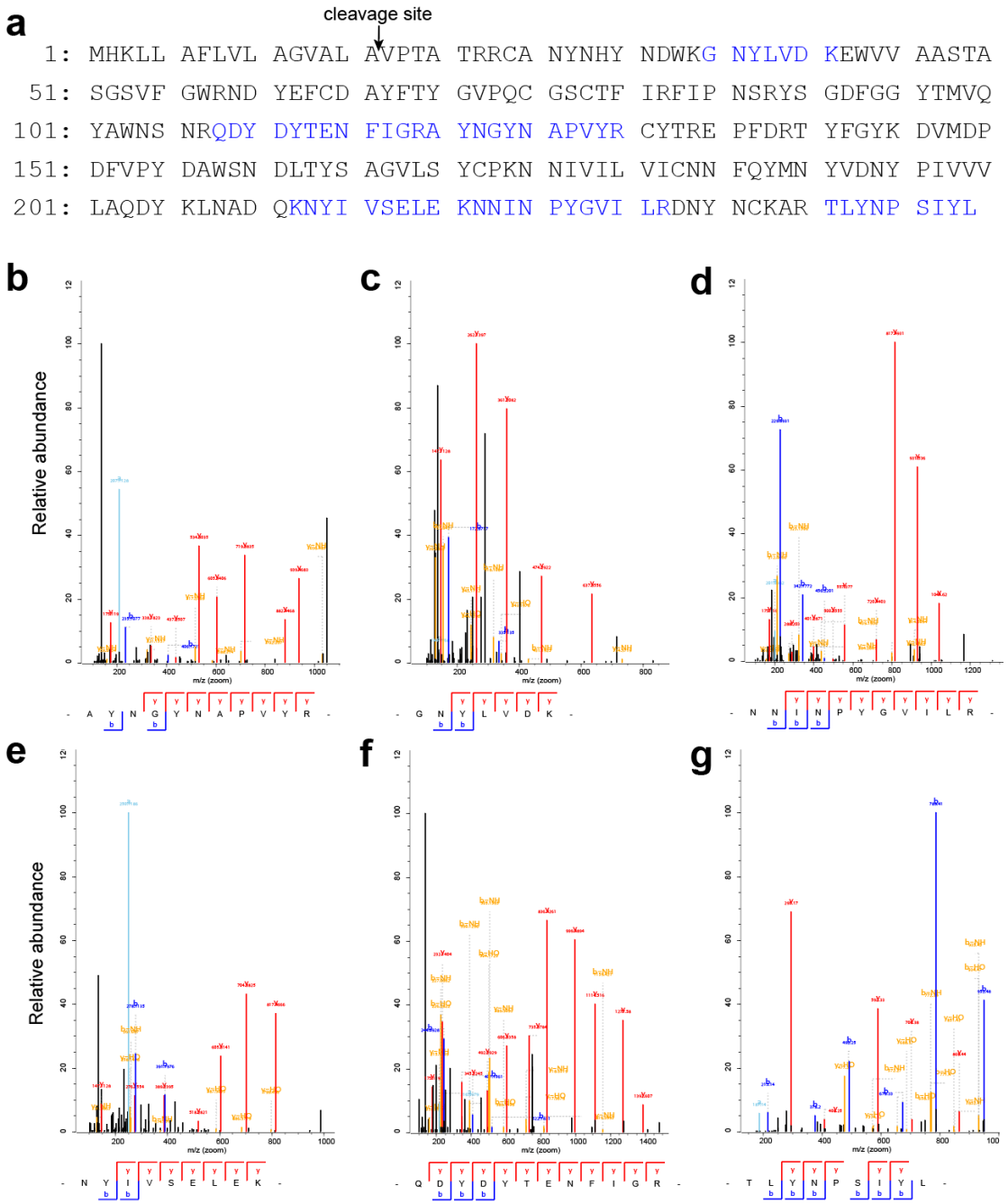

Fig. S1. Characteristic of BtRDP. (a) Deduced amino acid sequence of BtRDP. Arrow indicates the signal peptide cleavage site. **(b-g)** Mass spectrums of the identified unique peptides in watery saliva of *Bemisia tabaci*.

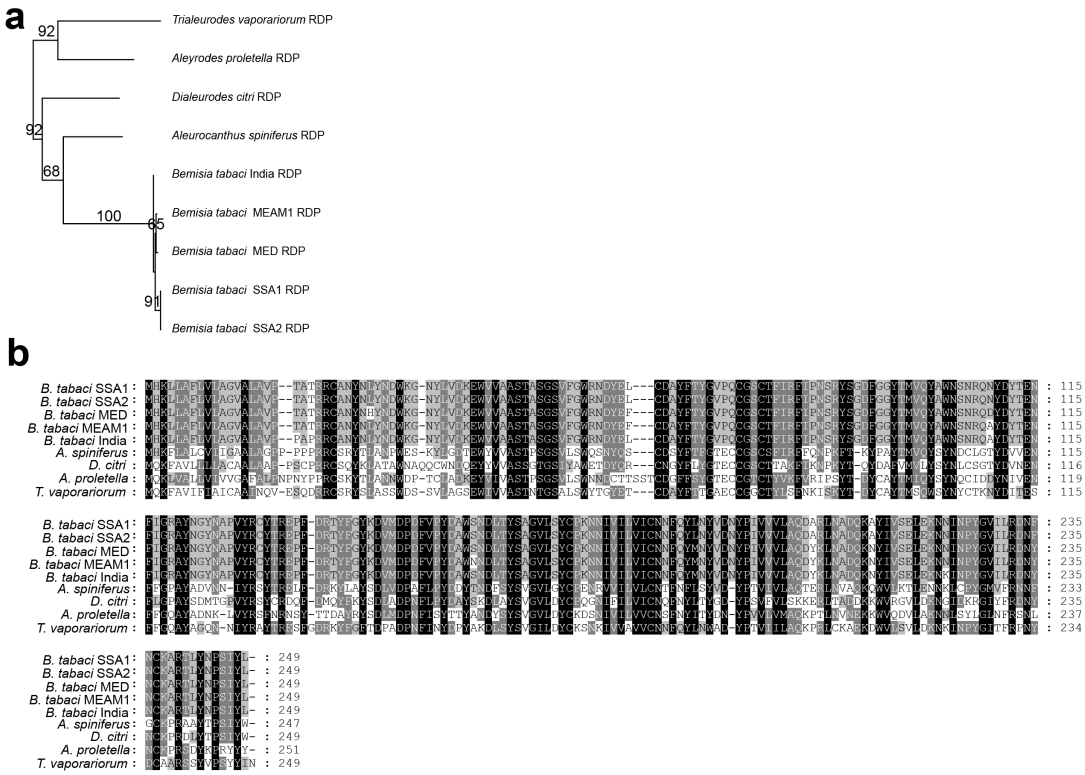

Fig. S2. Analysis of insect RDP. (**a**) Phylogenetic tree of RDP sequences from Aleyrodidae species. The trees are constructed by RAxML v0.9.0 using the maximum likelihood method with 1000 bootstrap replicates. Nodes with bootstrap values greater than 50 are displayed. (**b**) Sequence alignments of RDPs. The amino acid sequence of RDPs used for phylogenetic tree construction are aligned using ClusterX software. Black shades indicate the conserved regions.

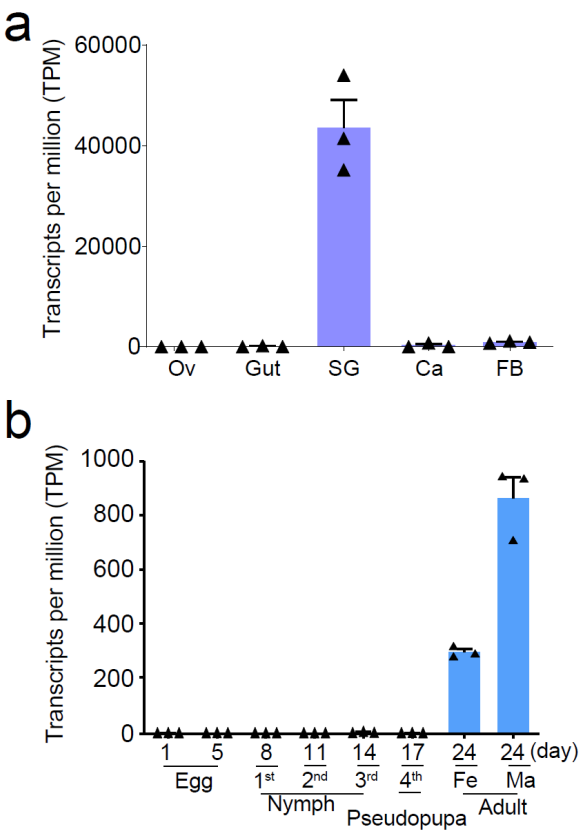

Fig. S3. Expression patterns of *Bemisia tabaci BtRDP*. Transcripts per million (TPM) expression values of *BtRDP* in different tissues (**a**) and at different developmental stages (**b**) are determined based on the transcriptomic data. Data are presented as mean values ± SEM (n=3 independent biological replicates).

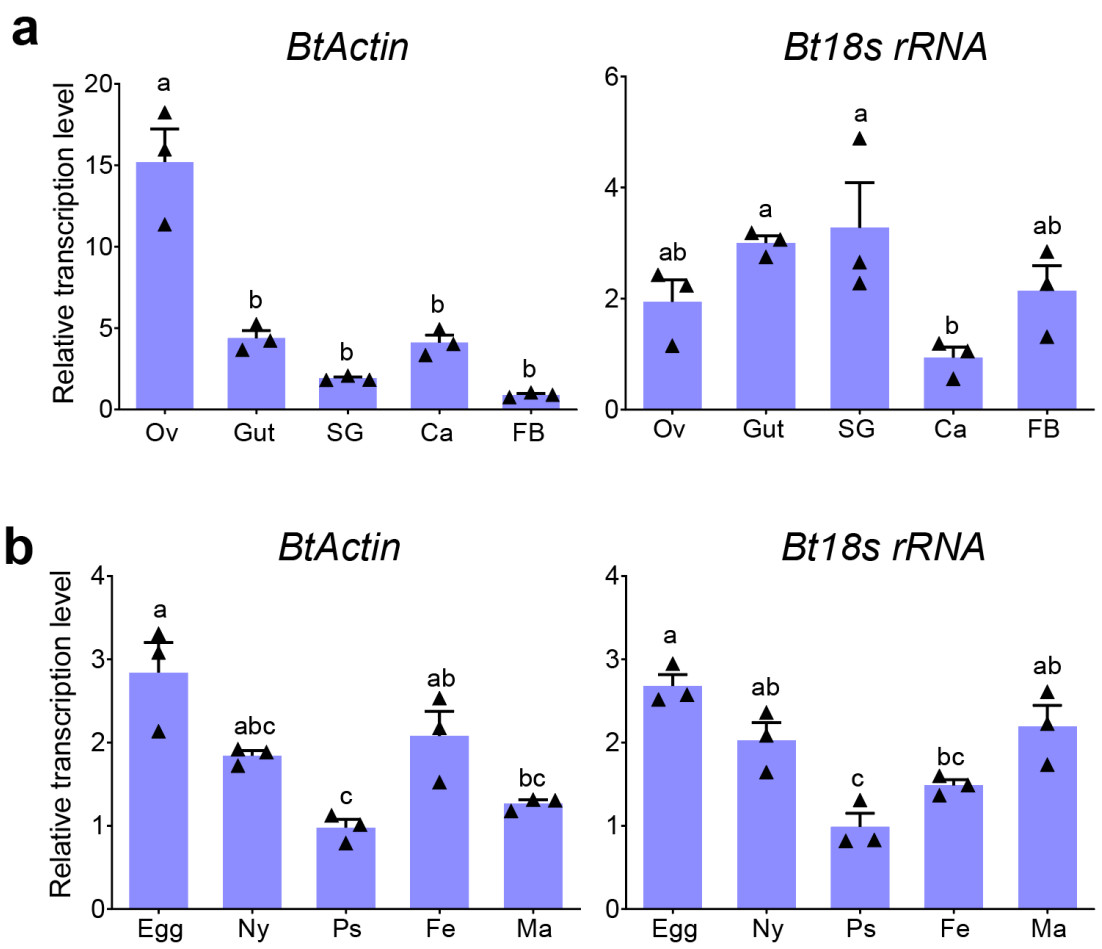

Fig. S4. Expression patterns of *BtActin* and *Bt18s rRNA*. The transcript level of each gene in different tissues (**a**) and at different developmental stages (**b**) is quantified by qRT-PCR. *Bemisia tabaci tubulin* is used as an internal control. The relative quantitative method ($2^{-\Delta\Delta Ct}$) is used to evaluate the quantitative variation. Ov, ovary; SG, salivary gland; Ca, carcass; FB, fat body; Ny, nymph; Ps, pseudopupa; Fe, female; Ma, male. Data are presented as mean values ± SEM (n=3 independent biological replicates). Different lowercase letters indicate statistically significant differences at $P < 0.05$ level according to one-way ANOVA test followed by Tukey's multiple comparisons test.

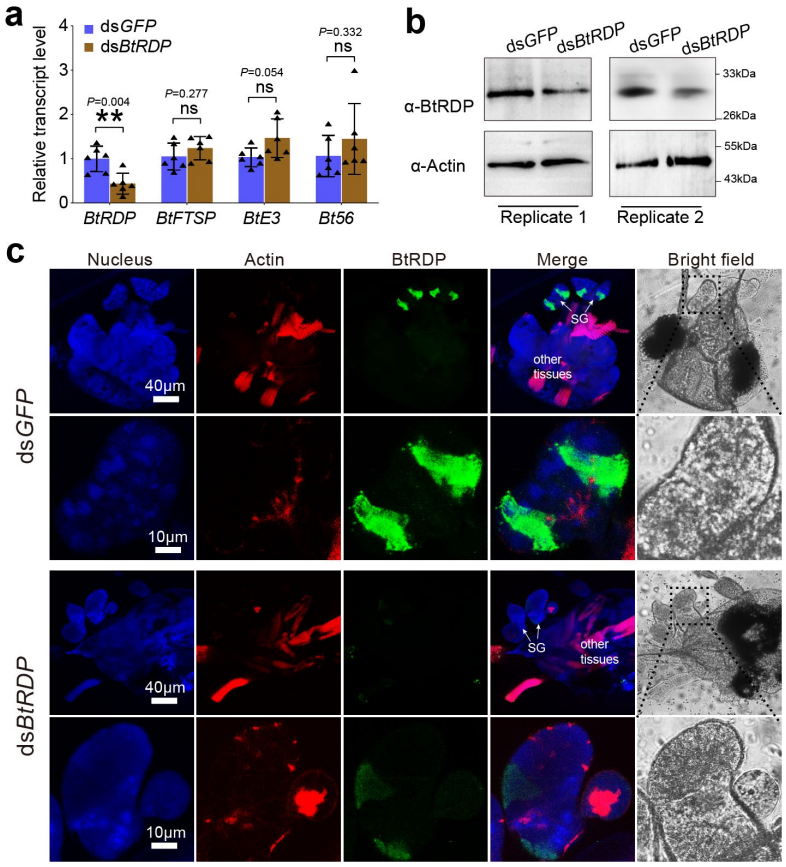

Fig. S5. BtRDP is efficiently and specifically suppressed by ds*BtRDP*. (**a**) Relative transcript level of *BtRDP*, *BtFTSP*, *BtE3*, and *Bt56* after dsRNA treatments. *Bemisia tabaci* are treated with ds*GFP* and ds*BtRDP*. The expression pattern of each gene is determined 4 days post treatment using qRT-PCR methods. *B. tabaci tubulin* is used as an internal control. The relative quantitative method ($2^{-\Delta\Delta Ct}$) is used to evaluate the quantitative variation. Data are presented as mean values ± SEM (n= 3 independent biological replicates) (**b**) Protein level of BtRDP after dsRNA treatments. Actin is used as an internal control. Two independent biological replicates are displayed. (**c**) Immunohistochemical staining of BtRDP after dsRNA treatment. The salivary gland (SG) and its nearby tissues are collected from ds*GFP*- and ds*BtRDP*-treated *Bemisia tabaci*. The samples are incubated with anti-BtRDP serum conjugated with Alexa Fluor™ 488 NHS Ester (green) and actin dye phalloidinrhodamine (red), and examined by Leica SP8. The nucleus is stained with DAPI (blue). The lower image in each treatment represents the enlarged images of the boxed area in the upper image. Experiments are repeated twice, with each inspecting more than 10 salivary glands.

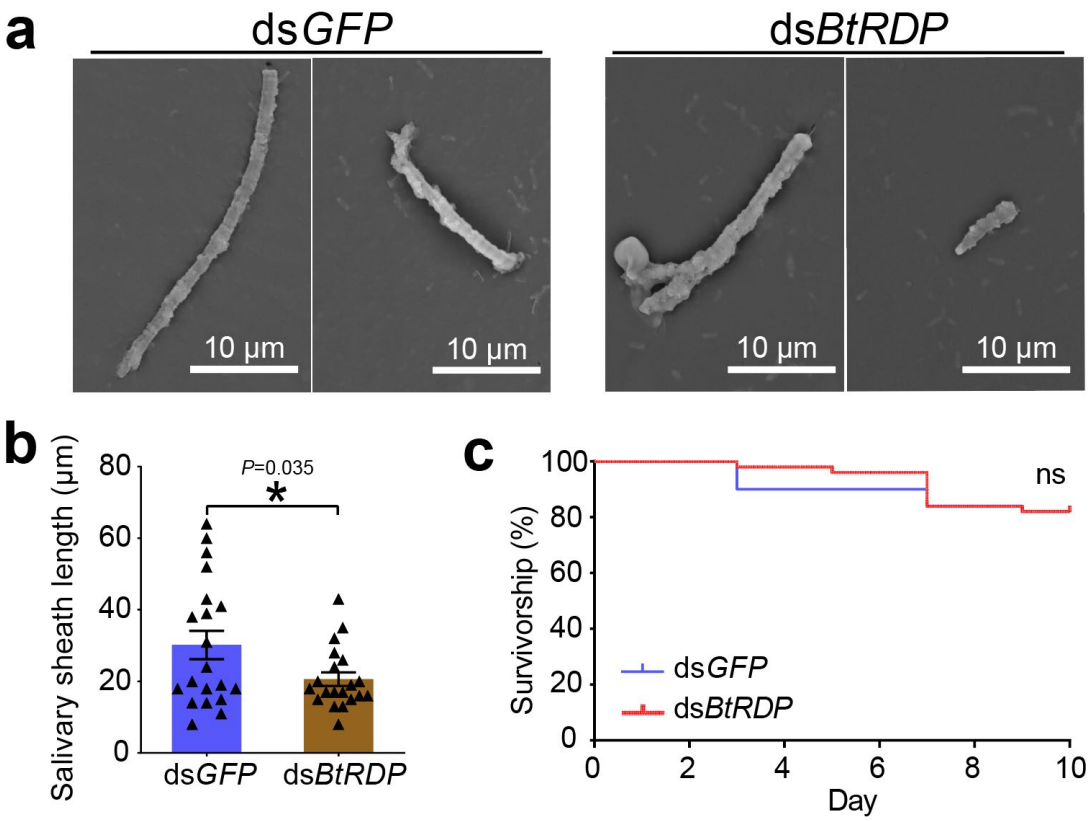

Fig. S6. Effects of dsRNA treatment on insect survivorship and salivary sheath formation. (**a**, **b**) Effects of dsRNA treatment on salivary sheath formation. Newly emerged *Bemisia tabaci* adults are injected with ds*GFP* and ds*BtRDP*. The dsRNA-treated *B. tabaci* are fed on artificial diets. The salivary sheaths left on parafilm are inspected by scanning electron microscopy **(a)**, and the length of salivary sheath is measured from the top to base of salivary sheath **(b)**. Data are presented as mean values ± SEM. Twenty salivary sheaths from each treatment are measured. *P*-value is determined by two-tailed unpaired Student's *t* test. $*P < 0.05$. **(c)** Effects of dsRNA treatment on insect survivorship. A group of 20-30 *B. tabaci* are placed in a leaf cage, and their mortality is recorded for ten consecutive days. Three independent biological replications are performed. Differences in survivorship between the two treatments are tested by log-rank test. ns, not significant.

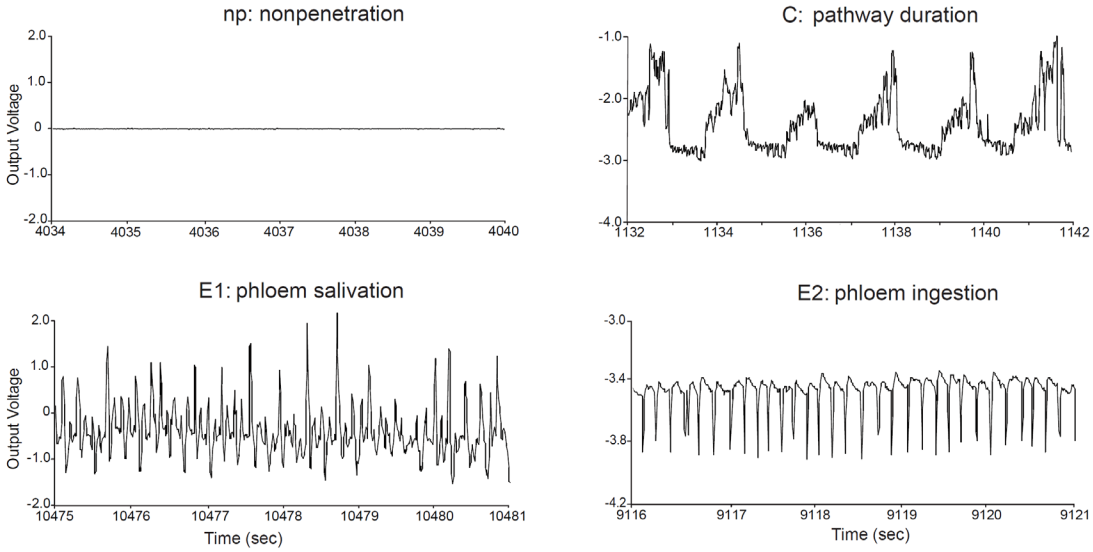

Fig. S7. Typical EPG waveforms for *Bemisia tabaci* feeding on *Nicotiana tabacum*. The *B. tabaci* feeding behavior can be classified into nonpenetration (np), pathway duration (C), phloem salivation (E1) and phloem ingestion (E2).

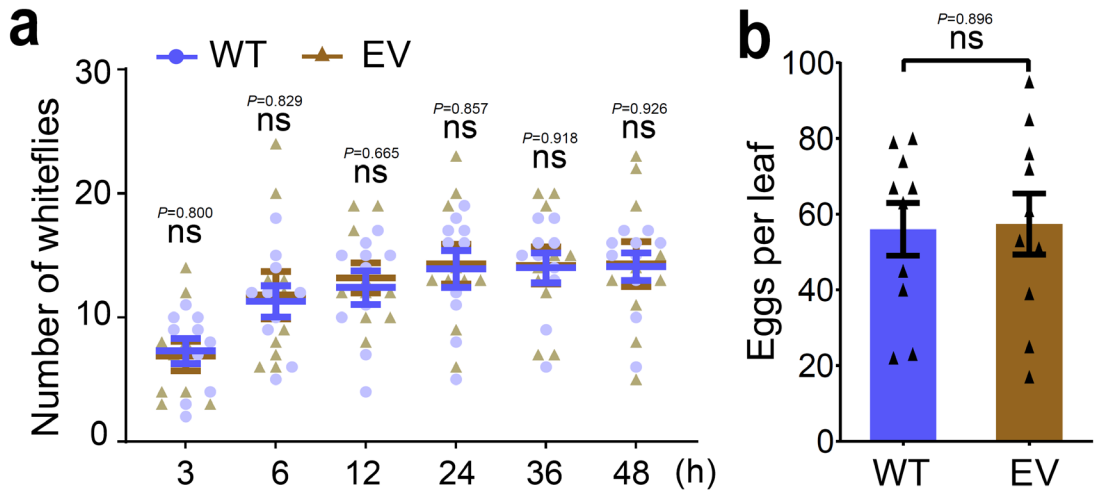

Fig. S8. Effects of empty vector (EV) transgenic plants on *Bemisia tabaci*. Two-choice experiment is performed to investigate the attraction of wild type (WT) and EV transgenic plants to *B. tabaci*. A group of 40 female *B. tabaci* are released into a device containing EV and WT leaves. The number of insects settling on each leaf is counted at 3, 6, 12, 24, 36, and 48 h (**a**). After 48 h, the number of eggs on each leaf is counted (**b**). Data are presented as mean values ± SEM. Ten independent biological replicates are performed. *P*-values are determined by two-tailed unpaired Student's *t* test. ns, not significant.

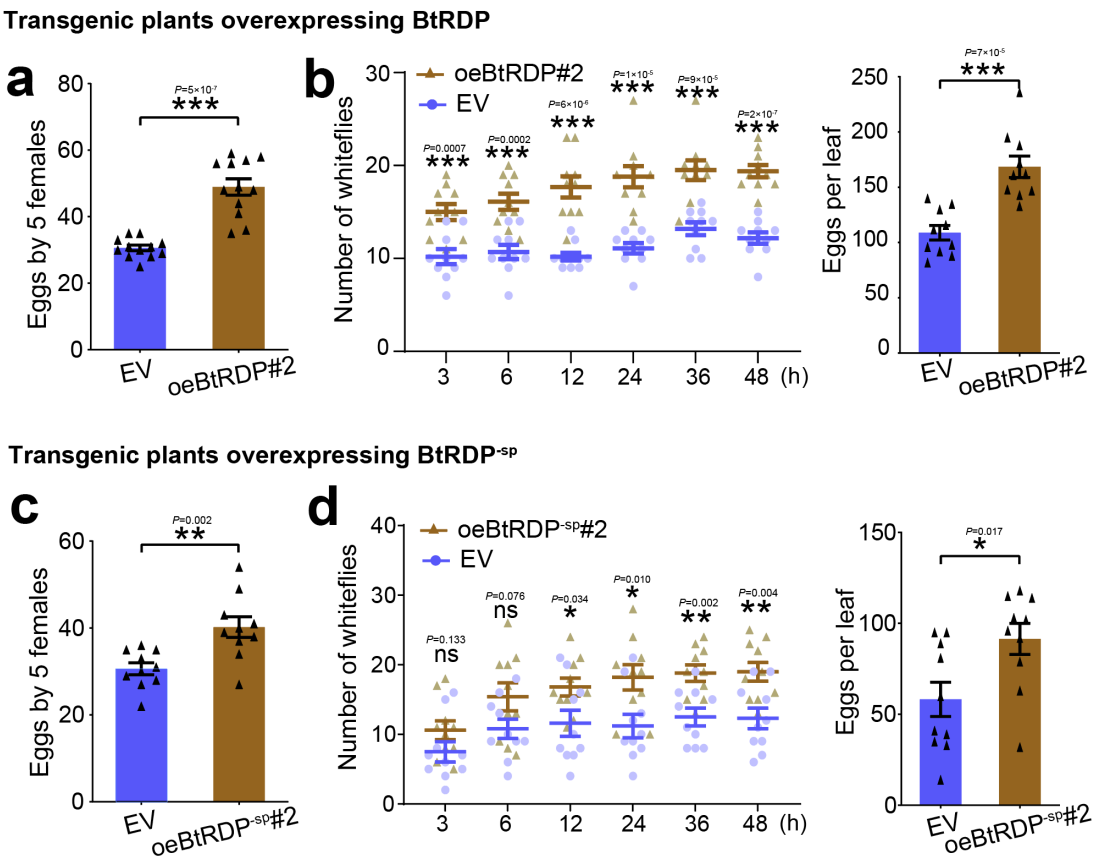

Fig. S9. Effects of BtRDP and BtRDP^{-sp} overexpression on *Bemisia tabaci*. Insect performance on oeBtRDP#2 (**a, b**) and oeBtRDP^{-sp}#2 (**c, d**) transgenic plants are tested. **(a, c)** Comparison of insect reproduction on empty vector (EV) and oeBtRDP#2/oeBtRDP^{-sp}#2 transgenic plants. Five *B. tabaci* individuals are confined to indicated plants for 3 days, and the oviposited eggs are counted. Twelve independent biological replicates are performed. **(b, d)** Attraction of EV and oeBtRDP#2/oeBtRDP^{-sp}#2 leaves to *B. tabaci* in a two-choice equipment. A group of 40 female *B. tabaci* are released into a device containing indicated leaves. The number of insects settling on each leaf is counted at 3, 6, 12, 24, 36, and 48 h. After 48 h, the number of eggs on each leaf is counted. Data are presented as mean values ± SEM. Ten independent biological replicates are performed. *P*-values are determined by two-tailed unpaired Student's *t* test. ***$P < 0.001$.

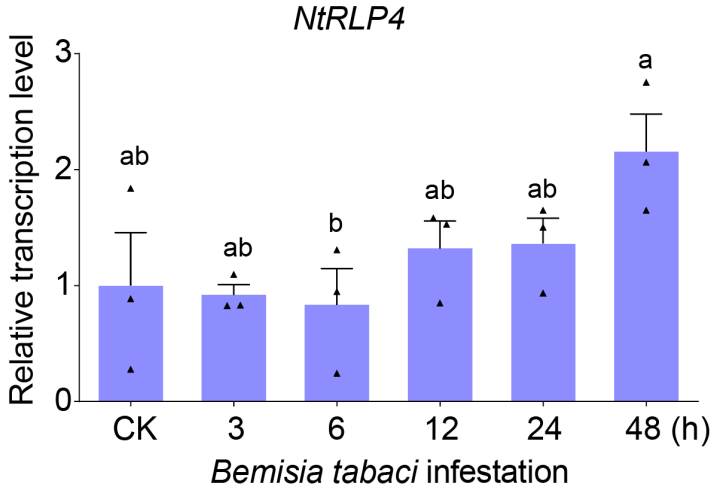

Fig. S10. Expression patterns of *NtRLP4* in response to *Bemisia tabaci* infestation. Relative transcript level of *NtRLP4* in response to *B. tabaci* infestation are determined by qRT-PCR. Data are presented as mean values ± SEM. Different lowercase letters indicate statistically significant differences at $P < 0.05$ level according to one-way ANOVA test followed by Tukey's multiple comparisons test. Three independent biological replicates are performed.

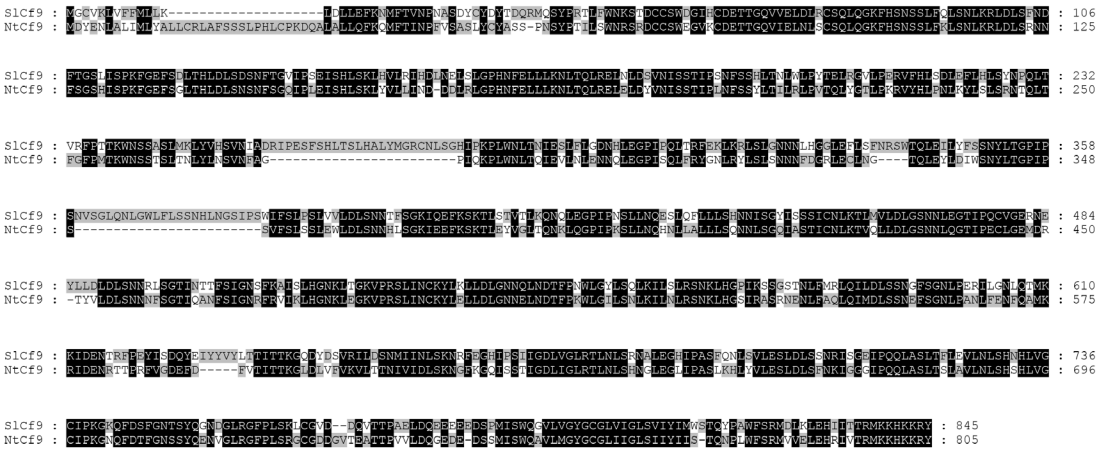

Fig. S11. Sequence alignments of SlCf9 and NtCf9. The amino acid sequence of SlCf9 and NtCf9 are aligned using ClusterX software. Black shades indicate the conserved regions.

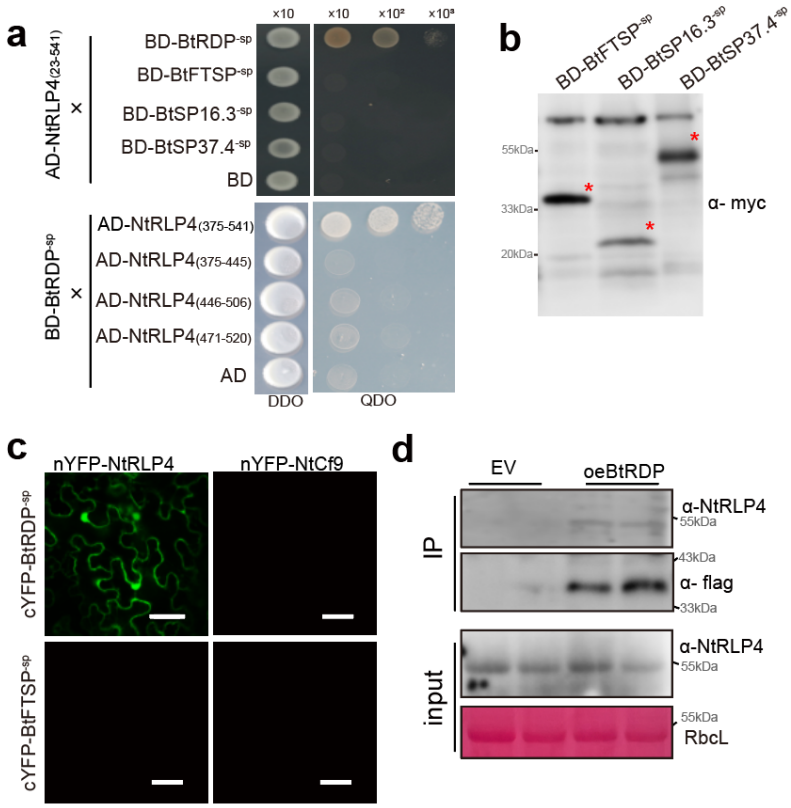

Fig. S12. BtRDP interacts with NtRLP4. (**a**) Yeast two hybrid assays showing the interaction between NtRLP4 and different whitefly salivary proteins (BtFTSP^{-sp}, BtSP16.3^{-sp} and BtSP37.4^{-sp}, without signal peptides), as well as BtRDP^{-sp} and truncated NtRLP4. The different combinations of constructs are transformed into yeast cells, and are grown on the selective medium SD/-Trp/-Leu (DDO), and the interactions are tested with SD/-Trp/-Leu/-His/-Ade (QDO). (**b**) Expression of three control salivary proteins at the protein level. The target bands are indicated by asterisks. **(c)** Bimolecular fluorescence complementation assay showing the specific interaction between BtRDP and NtRLP4. YFP fluorescence is observed when co-expressing the N-terminal nYFP tag fused NtRLP4 and N-terminal cYFP tag fused BtRDP^{-sp}. Bar =40 μm. **(d)** Co-immunoprecipitation (Co-IP) assays on oeBtRDP transgenic plants. oeBtRDP transgenic plants that overexpressing BtRDP-flag are incubated with anti-flag beads. Endogenous NtRLP4 can be immunoprecipitated by BtRDP-flag in oeBtRDP transgenic plants, while the flag tag alone in EV plants fails to immunoprecipitate endogenous NtRLP4. Rubisco staining (RbcL) is used to visualize the amount of sample loading.

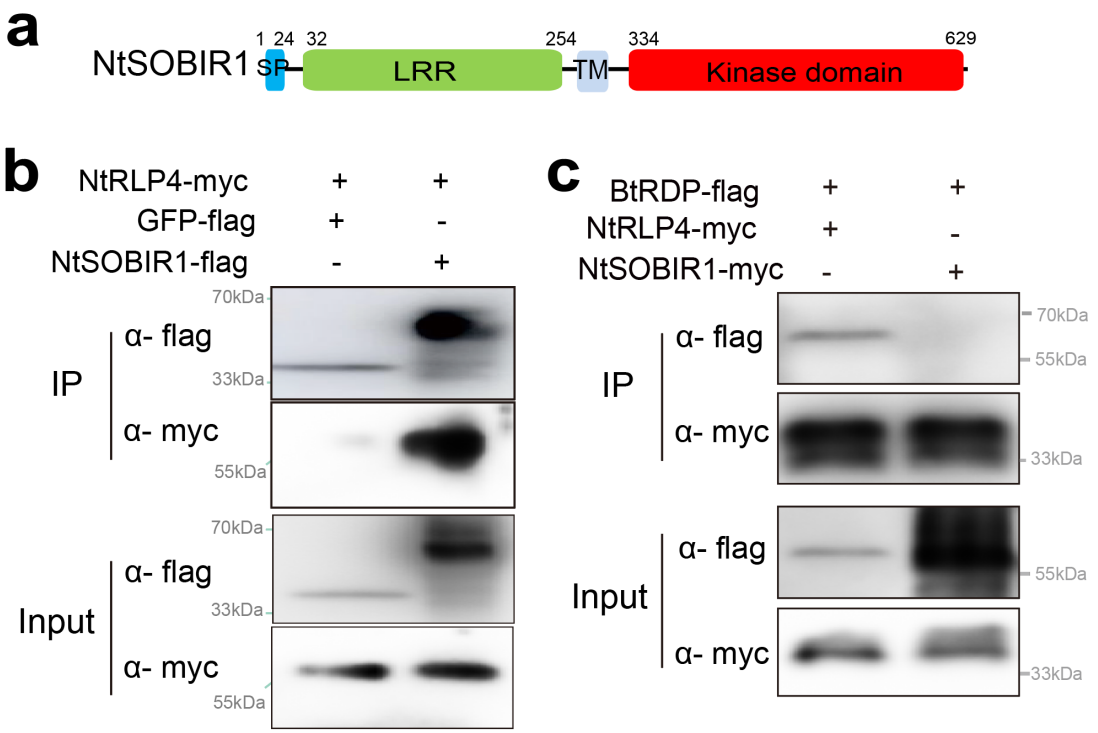

Fig. S13. NtSOBIR1 interacts with NtRLP4 but not BtRDP. (a) Domain organization of NtSOBIR1. NtSOBIR1 contains a predicted N-terminal signal peptide (SP), a leucine-rich repeat (LRR) domain, a transmembrane (TM) domain, and a kinase domain. **(b)** Co-immunoprecipitation assay showing the interaction between NtSOBIR1 and NtRLP4. **(c)** Co-immunoprecipitation assay showing the interaction between NtRLP4 and BtRDP, but not NtSOBIR1 and BtRDP. The complete coding region of *NtSOBIR1* and *NtRLP4* are fused with flag and myc tags at the C-terminal ends. Total proteins are extracted from *N. benthamiana* leaves co-expressing NtRLP4-myc with GFP-flag or NtSOBIR1-flag. Precipitation is performed using flag beads. The samples are probed with anti-flag and anti-myc antibodies for immunoblot analysis. Experiments are repeated twice with the similar results.

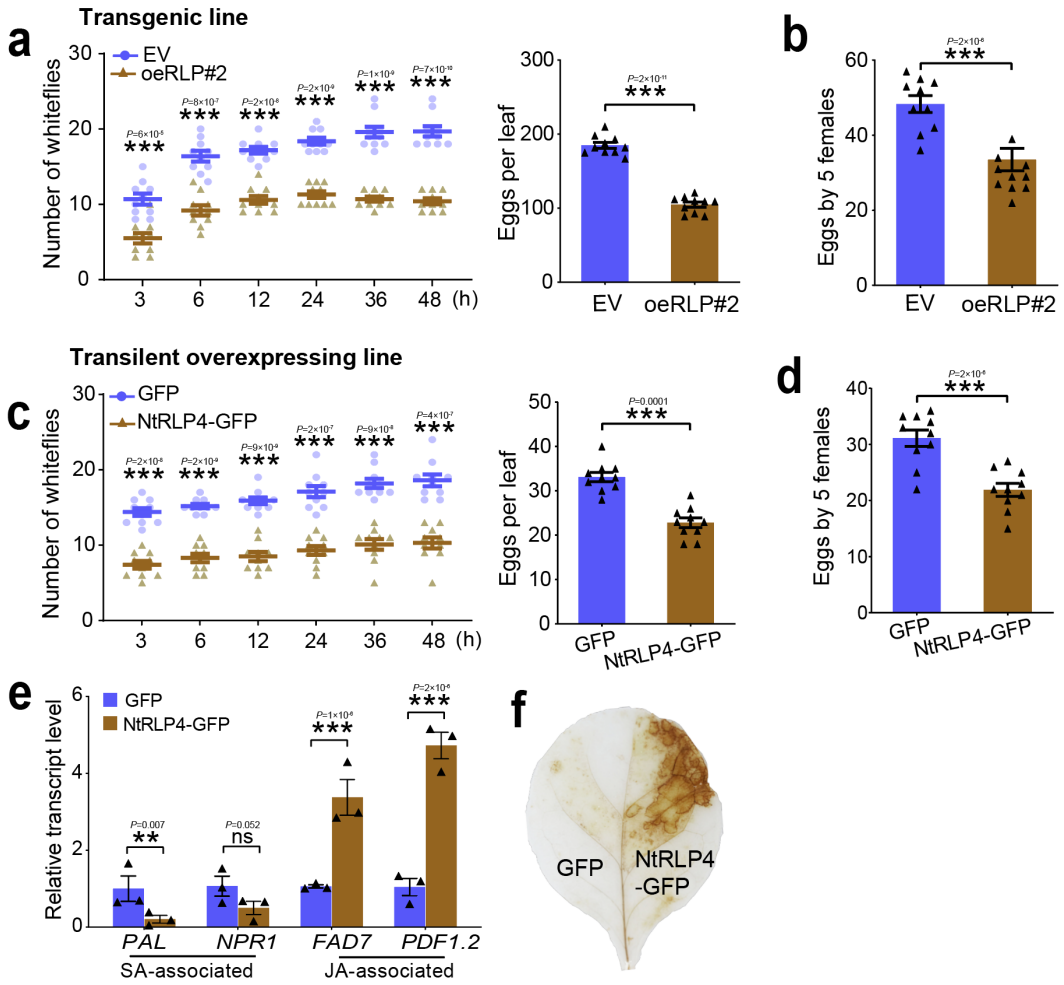

Fig. S14. Effect of NtRLP4 overexpression on *Bemisia tabaci* performance. (a) Attraction of empty vector (EV) and oeNtRLP4#2 (oeRLP#2) transgenic *Nicotiana tabacum* to *B. tabaci* in a two-choice equipment. A group of 40 female *B. tabaci* are released into a device containing oeRLP#2 and EV leaves. The number of insects settling on each leaf is counted at 3, 6, 12, 24, 36, and 48 h. After 48 h, the number of eggs on each leaf is counted. **(b)** Comparison of insect reproduction on EV and *oeRLP*#2 transgenic plants. Five *B. tabaci* individuals are confined to indicated plants for 3 days, and the oviposited eggs are counted. **(c)** Attraction of leaves transiently overexpressing GFP and NtRLP4-GFP to *B. tabaci* in a two-choice equipment. **(d)** Comparison of insect reproduction on *N. tabacum* leaves transiently overexpressing GFP and NtRLP4-GFP. **(e)** Relative transcript level of salicylic acid (SA)- and jasmonic acid (JA)-associated genes in *N. tabacum* leaves transiently overexpressing GFP and NtRLP4-GFP. PAL, phenylalanine ammonia lyase; NPR1, nonexpressor of pathogenesis-related protein 1; FAD7, fatty acid desaturase 7; PDF1.2, plant defensin

1.2. **(f)** Transiently overexpressing NtRLP4-GFP induces H_2O_2 accumulation. For bioassays in (**a**), (**b**), (**c**), and (**d**), ten independent biological replicates are performed. For qPCR analysis in (**e**), three independent biological replicates are performed. Data are presented as mean values ± SEM. *P*-values are determined by two-tailed unpaired Student's *t* test. ***$P < 0.001$. The experiment in (**f**) is repeated five times with the similar results.

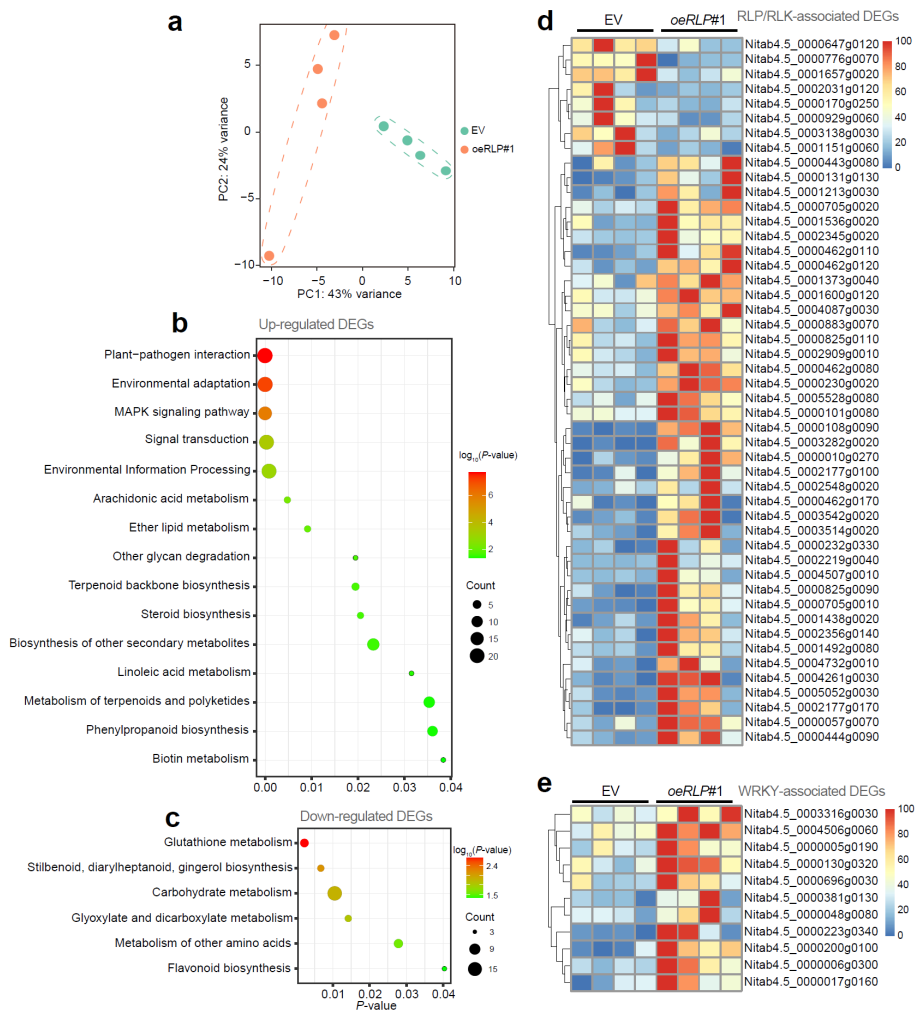

Fig. S15. Transcriptomic comparison of empty vector (EV) and oeNtRLP4#1 (oeRLP#1) transgenic plants. (**a**) Principal component analysis (PCA) of gene expression patterns in EV and oeRLP#1 transgenic *Nicotiana tabacum* plants. The first two principal components (PC1 and PC2) based on transcriptomic results are shown. Four independent biological replicates are performed. (**b**, **c**) Kyoto Encyclopedia of Genes and Genomes (KEGG) pathway enrichment analysis of differentially expressed genes (DEGs) that significantly up-regulated (**b**) and down-regulated (**c**). Enriched *P*-values are calculated according to one-sided hypergeometric test using TBtools software. (**d, e**) Expression pattens of DEGs that annotated as RLK/RLP (**d**) or WRKY transcription factor (**e**). Gene expression patterns are illustrated by a heatmap. The max transcripts per million value of each gene is set as 100.

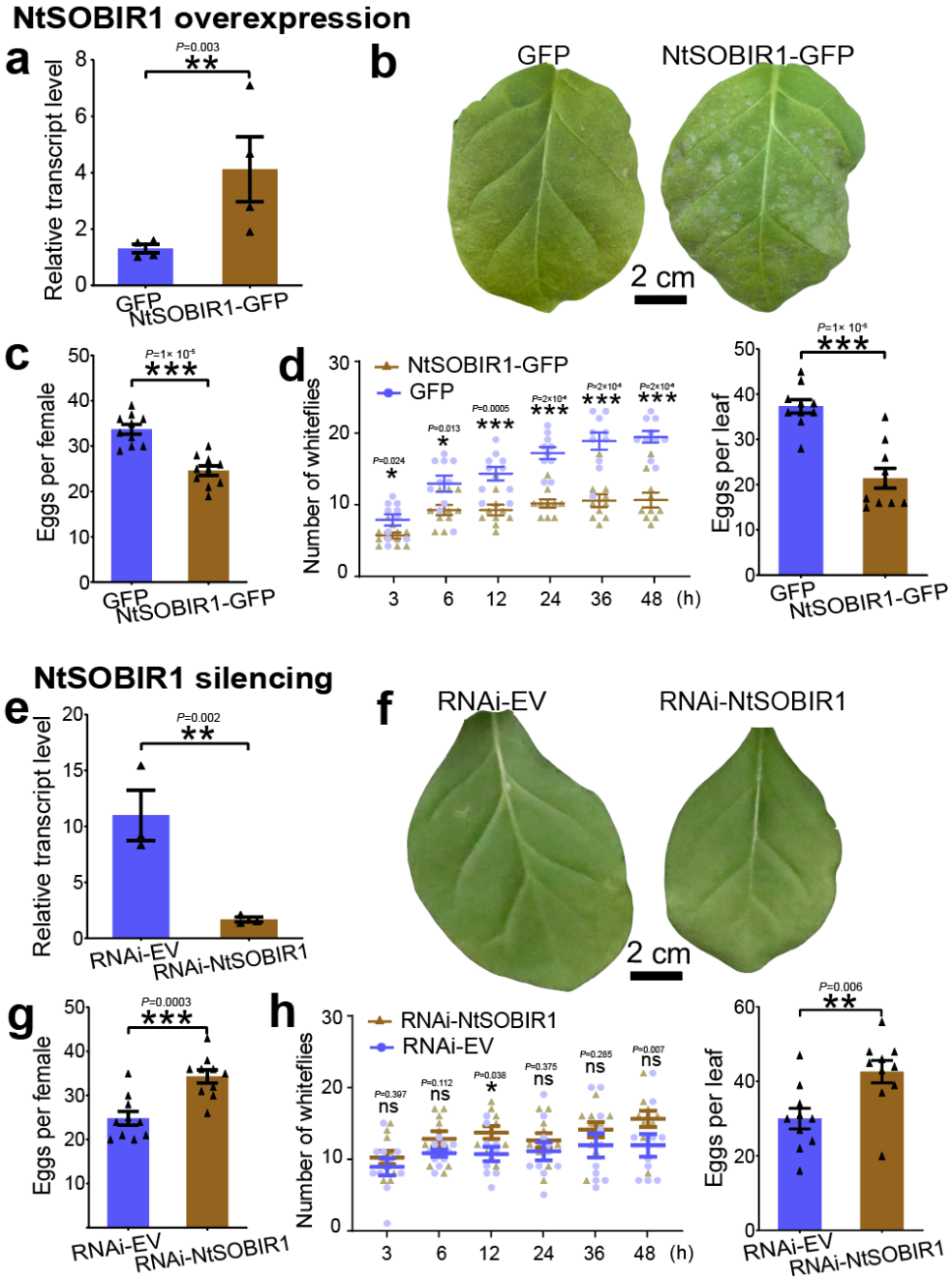

Fig. S16. Effect of NtSOBIR1 overexpression and silencing on *Bemisia tabaci* performance. (**a**) Validation of NtSOBIR1 transient overexpression using qRT-PCR (n= 4 biological replicates). (**b**) NtSOBIR1 transient overexpression induces cell death phenotype five days post agro-injection. **(c)** Comparison of insect reproduction on *Nicotiana tabacum* transiently overexpressing GFP and NtSOBIR1-GFP. Five *B. tabaci* individuals are confined to indicated plants for 3 days, and the oviposited eggs are counted. **(d)** Attraction of GFP and NtSOBIR1-GFP leaves to *B. tabaci* in a two-choice equipment. A group of 40 female *B. tabaci* are released into a device containing

GFP and NtSOBIR1-GFP leaves. The number of insects settling on each leaf is counted at 3, 6, 12, 24, 36, and 48 h (left). After 48 h, the number of eggs on each leaf is counted (right). (**e**) Silencing efficiency of hairpin NtSOBIR1 using qRT-PCR (n= 3 independent biological replicates). (**f**) Transiently silencing NtSOBIR1 affect growth of infiltrated leaves. **(g)** Comparison of insect reproduction on *Nicotiana tabacum* leaves infiltrated with hairpin empty vector (EV) and NtSOBIR1. **(h)** Attraction of hairpin EV and NtSOBIR1-treated leaves to *B. tabaci* in a two-choice equipment. The experiments in (**b**) and (**f**) are repeated ten times with the similar results. In (**c**), (**d**), (**g**), and (**h**), ten independent biological replicates are performed. *P*-values are determined by two-tailed unpaired Student's *t* test. ***$P < 0.001$; **$P < 0.01$.

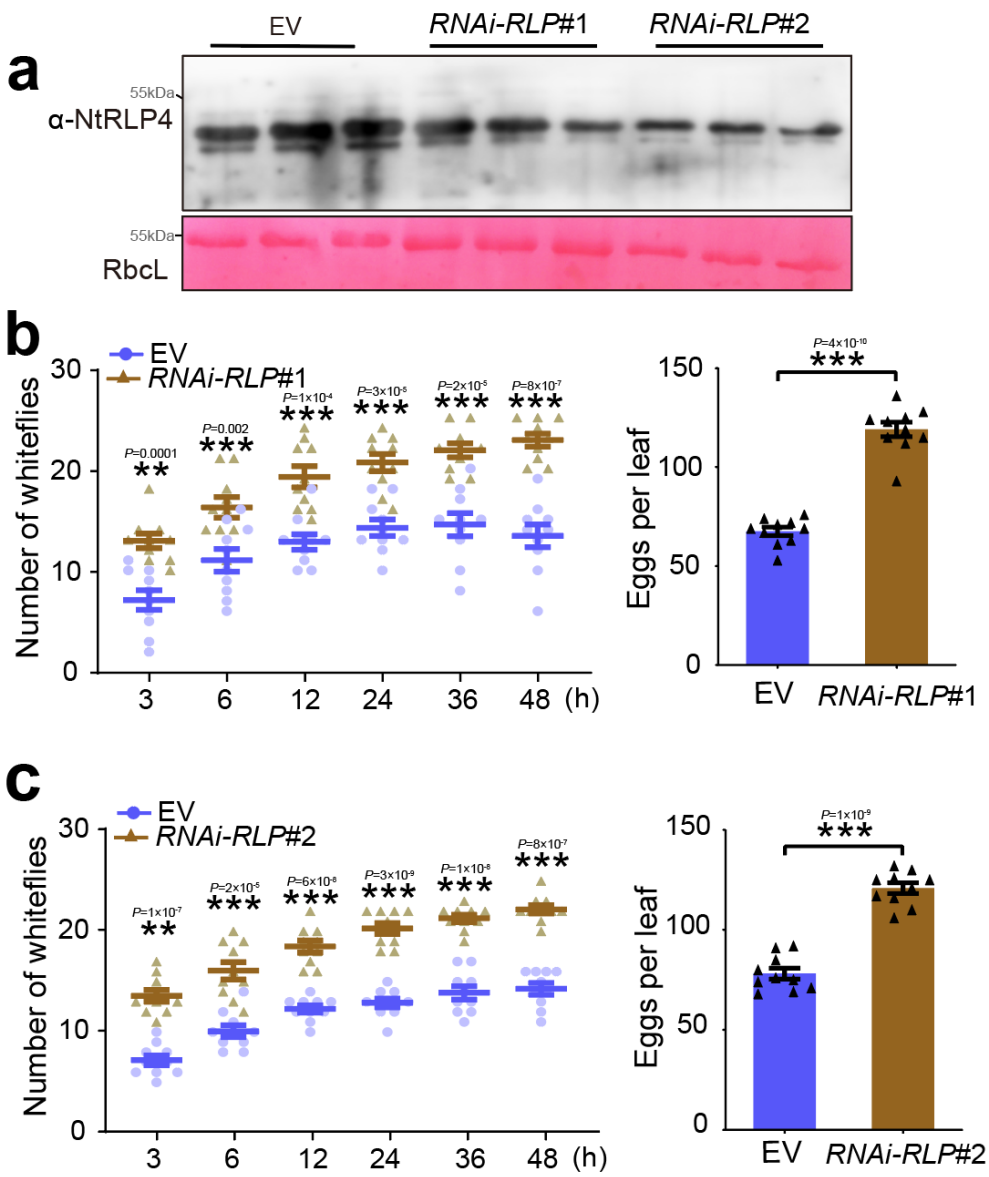

Fig. S17. Effects of *RLP* silencing on *Bemisia tabaci* performance. (**a**) Detection of NtRLP4 protein in empty vector (EV) and *NtRLP4*-silenced (*RNAi-RLP*) transgenic *Nicotiana tabacum*. Rubisco staining (RbcL) is conducted to visualize the amount of sample loading. **(b**, **c)** Attraction of EV and *RNAi-RLP* plants to *B. tabaci* in a two-choice equipment. Two NtRLP4-silenced plants (RNAi-RLP#1 in **b**; RNAi-RLP#2 in **c**) are assayed. A group of 40 female *B. tabaci* are released into a device containing two leaves. The number of insects settling on each leaf is counted at 3, 6, 12, 24, 36, and 48 h. After 48 h, the number of eggs on each leaf is counted. Ten independent biological replicates are performed. Data are presented as mean values ± SEM. *P*-values are determined by two-tailed unpaired Student's *t* test. ***$P < 0.001$.

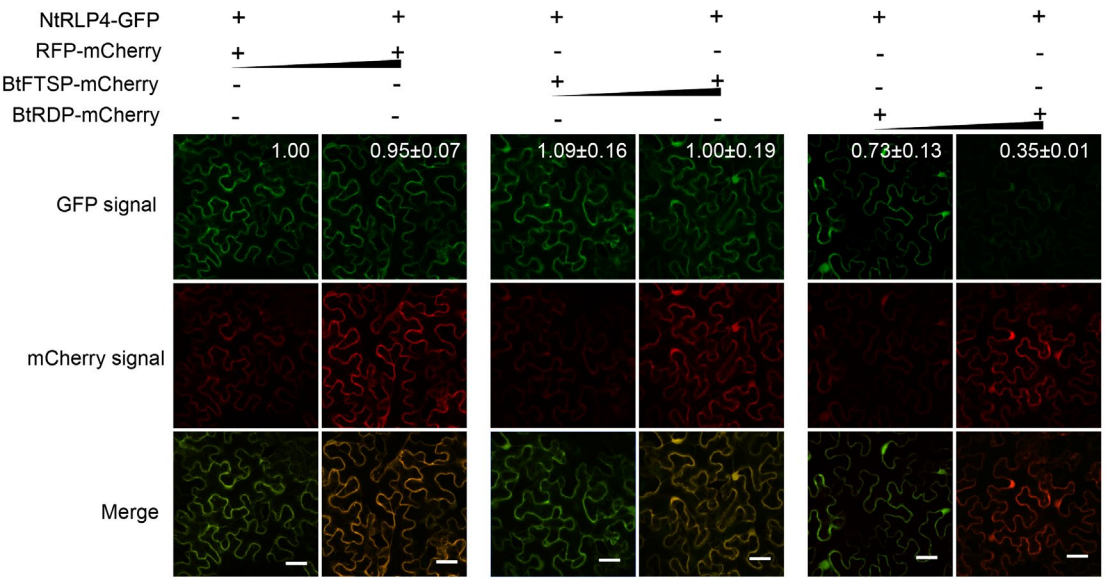

Fig. S18. Influence of BtRDP on NtRLP4 accumulation by fluorescent analysis. The NtRLP4-GFP is transiently co-expressed with red fluorescent protein (RFP)-mCherry, BtFTSP-mCherry, or BtRDP-mCherry via agroinfiltration. The samples are imaged by confocal microscopy at 48 h post injection. RFP-mCherry and BtFTSP-mCherry are used as negative controls. Three independent biological replicates are performed, and three representative images are taken in each biological replicate. Fluorescence intensity is measured using ImageJ. The intensity values from three biological replicates are calculated and the mean value in the upper left image is set at 1.0. Representative fluorescence images are displayed. The small triangle indicates the different concentrations (OD_{600} = 0.1 and 1.0) of *Agrobacterium*. Bar= 40 μm.

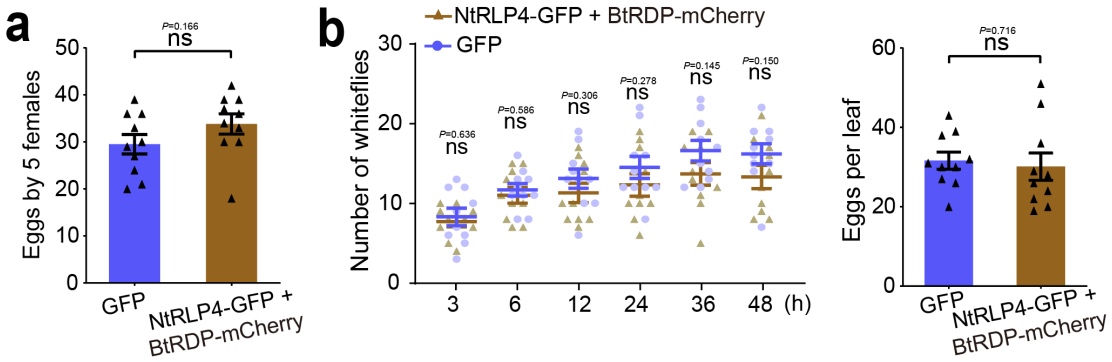

Fig. S19. Effects of BtRDP on suppressing NtRLP4-associated plant defenses. (a) Comparison of insect reproduction on *Nicotiana tabacum* plants transiently overexpressing GFP along and BtRDP-mCherry/NtRLP4-GFP. Five *Bemisia tabaci* individuals are confined to indicated plants for 3 days, and the oviposited eggs are counted. **(b)** Attraction of GFP- and BtRDP-mCherry/NtRLP4-GFP-expressed leaves to *B. tabaci* in a two-choice equipment. A group of 40 female *B. tabaci* are released into a device containing two leaves. The number of insects settling on each leaf is counted at 3, 6, 12, 24, 36, and 48 h. After 48 h, the number of eggs on each leaf is counted. Data are presented as mean values ± SEM. Ten independent biological replicates are performed. *P*-values are determined by two-tailed unpaired Student's *t* test. $*P < 0.05$; ns, not significant.

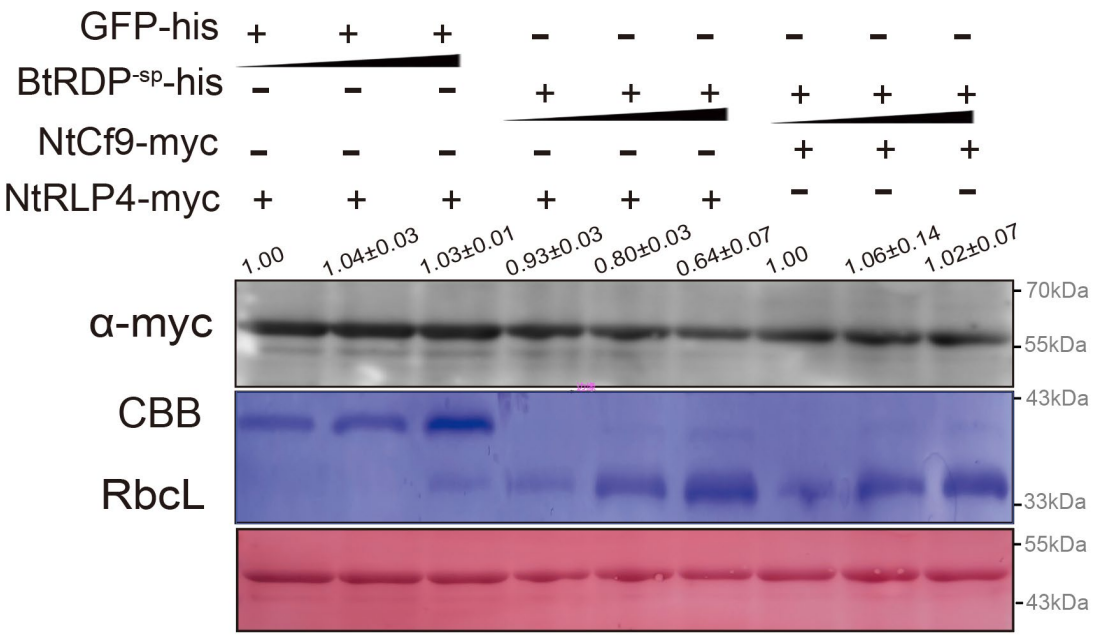

Fig. S20. Degradation of NtRLP4 by purified BtRDP^{-sp} in *Nicotiana benthamiana* leaves. Recombinant BtRDP^{-sp}-his and GFP-his proteins are expressed in *Escherichia coli*, and purified by Ni-NTA. *N. benthamiana* plants overexpressing NtRLP4-myc or NtCf9-myc are then infiltrated with different concentrations of purified BtRDP^{-sp}-his and GFP-his. The samples are probed with anti-myc antibodies for immunoblot analysis. Rubisco staining (RbcL) is conducted to visualize the amount of sample loading. Coomassie brilliant blue (CBB) staining is conducted to visualize the amount of recombinant BtRDP^{-sp}-his and GFP-his proteins. Experiments are repeated three times with the similar results. Band density is measured using ImageJ. The density values from three biological replicates are calculated and the mean value in the first lane is set at 1.0. Data are presented as mean values ± SEM.

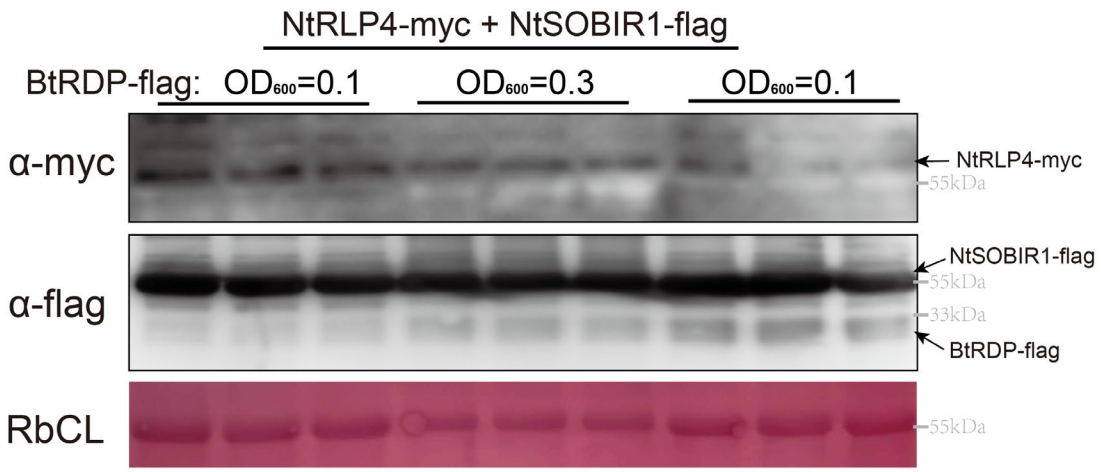

Fig. S21. Effect of BtRDP on NtRLP4 and NtSOBIR1. NtRLP4-myc and NtSOBIR1-flag were transiently co-expressed with different concentration of BtRDP-flag in *Nicotiana benthamiana* plants through *Agrobacterium* infiltration. The samples are probed with anti-flag and anti-myc antibodies for immunoblot analysis. Rubisco staining (RbcL) is conducted to visualize the amount of sample loading. The amount of BtRDP were controlled by infiltrating different concentrations of *Agrobacterium* (OD_{600} = 0.1, 0.3, and 1.0).

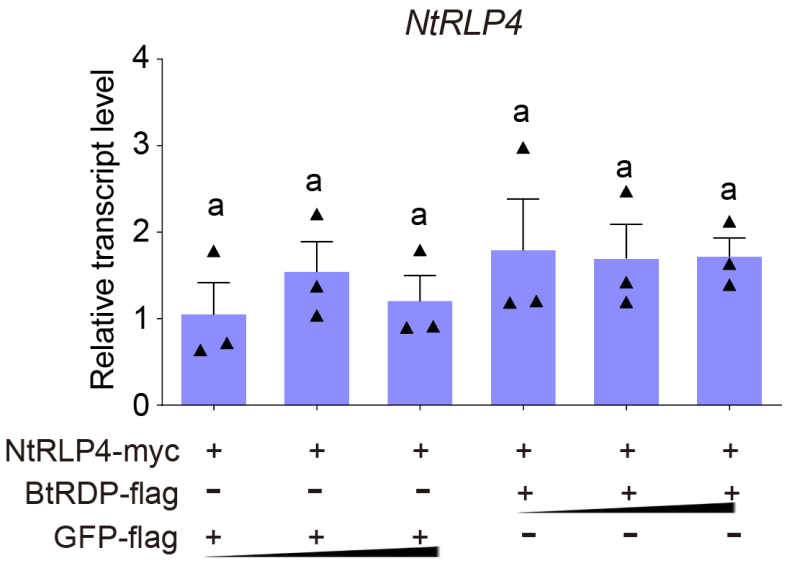

Fig. S22. Effect of BtRDP on the transcript level of *NtRLP4*. NtRLP4-myc is agroinfiltrated together with different concentration of BtRDP-flag or GFP-flag into *Nicotiana benthamiana* leaves. The transcript level of *NtRLP4* is determined by qRT-PCR. Data are presented as mean values ± SEM. Three independent biological replicates are performed. The same lowercase letters "a" indicate no statistically significant differences at $P < 0.05$ according to the one-way ANOVA test followed by Tukey's multiple comparisons test.

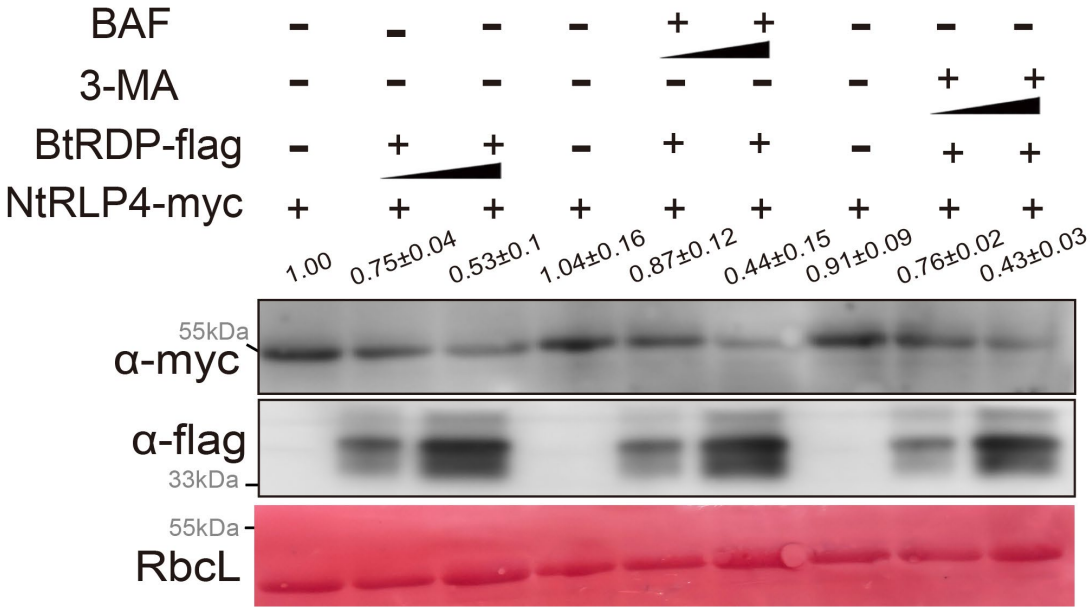

Fig. S23. Effects of autophagy inhibitor on NtRLP4 accumulation. NtRLP4-myc and BtRDP-flag were transiently co-expressed in *Nicotiana benthamiana* plants through *Agrobacterium* infiltration. Co-infiltrated leaves are treated with autophagy inhibitor BAF and 3-MA at 24 h post injection. The samples are probed with anti-flag and anti-myc antibodies for immunoblot analysis. Rubisco staining (RbcL) is conducted to visualize the amount of sample loading. The small triangle indicates the different concentrations of *Agrobacterium* (OD_{600} = 0.1 and 1.0). Experiments are repeated three times with the similar results. Band density is measured using ImageJ. The density values from three biological replicates are calculated and the mean value in the first lane is set at 1.0. Data are presented as mean values ± SEM. *P*-values are determined by two-tailed unpaired Student's *t* test. ***$P < 0.001$; **$P < 0.01$; *$P < 0.05$; ns, not significant.

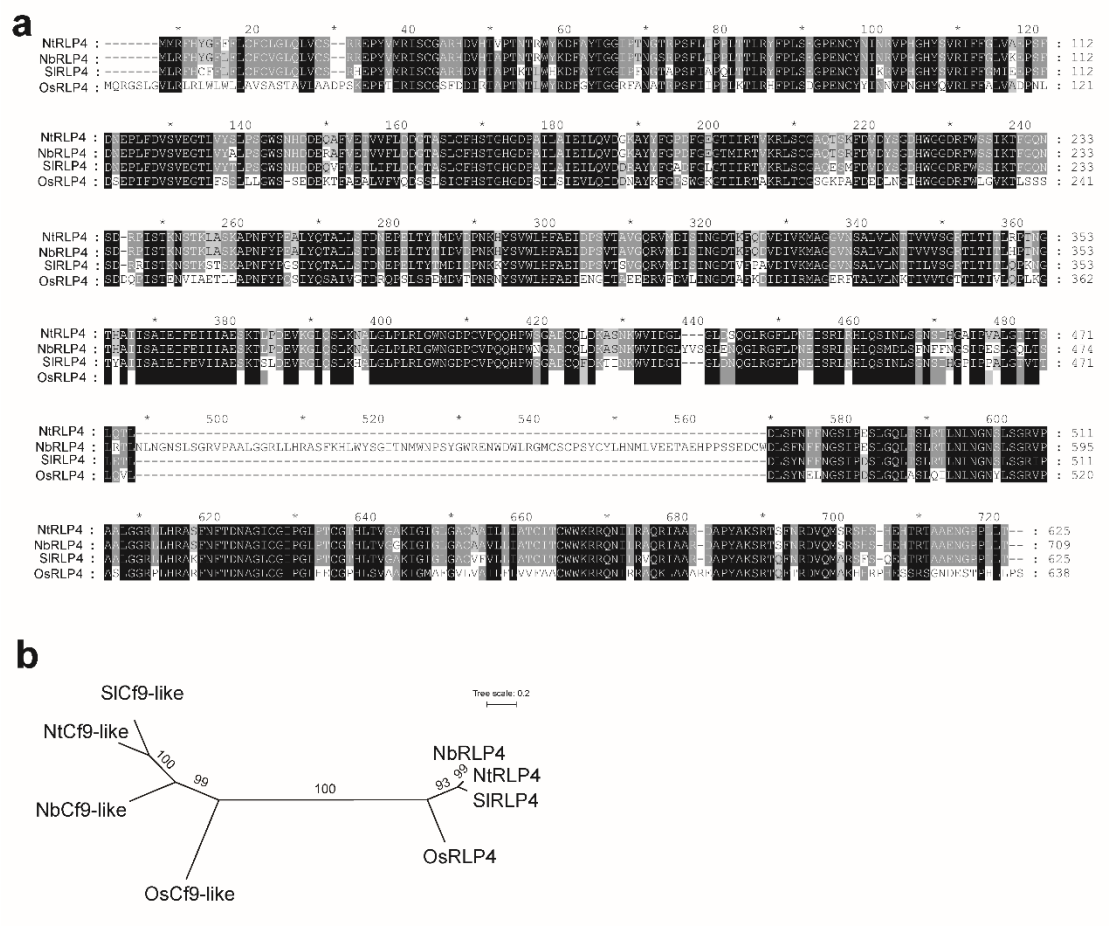

Fig. S24. Sequence alignment and phylogenetic tree of RLP4 homologs. (**a**) The amino acid sequence of RLP4s from *Nicotiana tabacum*, *N. benthamiana*, *Solanum lycopersicum*, and *Oryza sativa* are aligned using ClusterX software. Black shades indicate the conserved regions. (**b**) Phylogenetic analysis of RLP4 and Cf9-associated genes used in this study. The unrooted phylogenetic trees are constructed by RAxML v0.9.0 using the maximum likelihood method with 1000 bootstrap replicates.

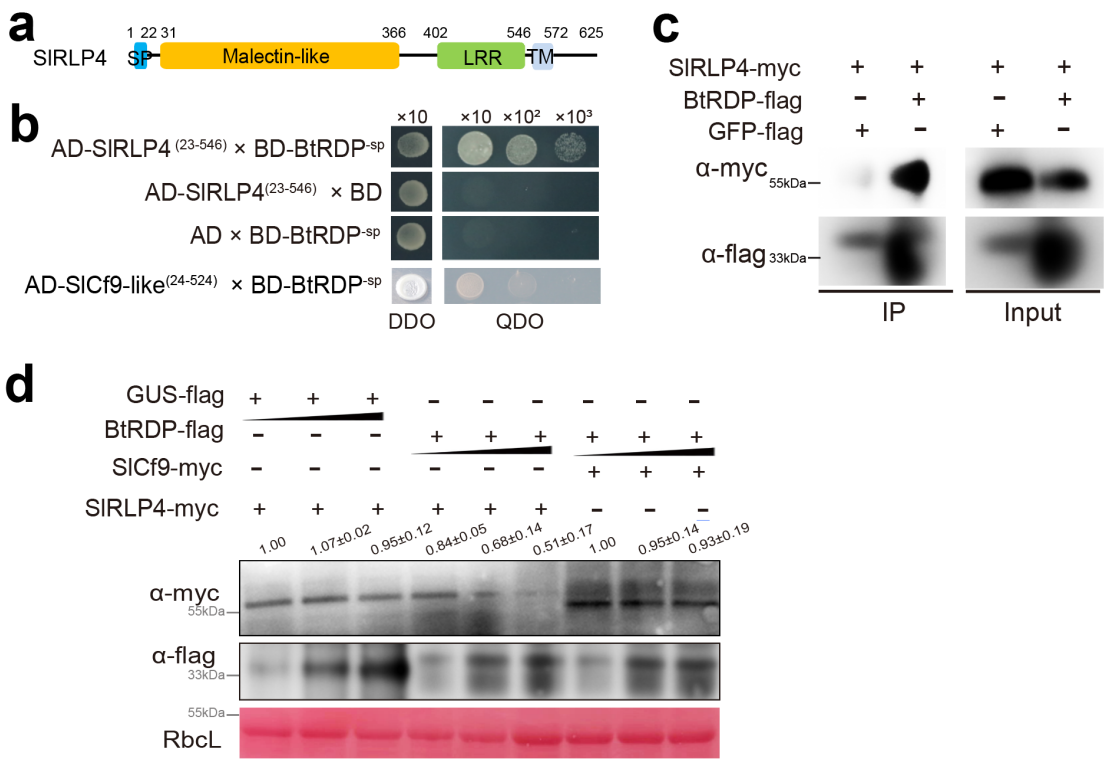

Fig. S25. Influence of BtRDP on RLP4 homology in *Solanum lycopersicum*. (a) Domain organization of *S. lycopersicum* RLP4 (SlRLP4). SlRLP4 contains a predicted N-terminal signal peptide (SP), a malectin-like domain, a LRR domain, and a transmembrane (TM) domain. (**b, c**) Yeast two-hybrid and co-immunoprecipitation (Co-IP) assays showing the interaction between BtRDP and SlRLP4. In (**b**), BtRDP is expressed without a signal peptide (BtRDP^{-sp}), while SlRLP4 and SlCf9 are expressed without a signal peptide and transmembrane domain (SlRLP4$^{(23-546)}$ and SlCf9$^{(24-524)}$). **(d)** Effect of BtRDP on the accumulation of SlRLP4. SlRLP4-myc and SlCf9-myc are agro-injected together with different concentration of BtRDP-flag or GFP-flag. In (**c, d**), the complete coding region of *BtRDP*, *SlRLP4*, *SfCf9* are fused with flag or myc tags at C-terminal ends, respectively. The small triangle indicates the different concentrations (OD_{600} = 0.05, 0.3, and 1.0) of *Agrobacterium*. Rubisco staining (RbcL) is conducted to visualize the amount of sample loading. Experiments are repeated three times with the similar results. Band density is measured using ImageJ. The density values from three biological replicates are calculated. For SlRLP4-myc bands (lane 1-6), the lane 1 is set at 1.0. For SlCf9-myc bands (lane 7-9), the lane 7 is set at 1.0.

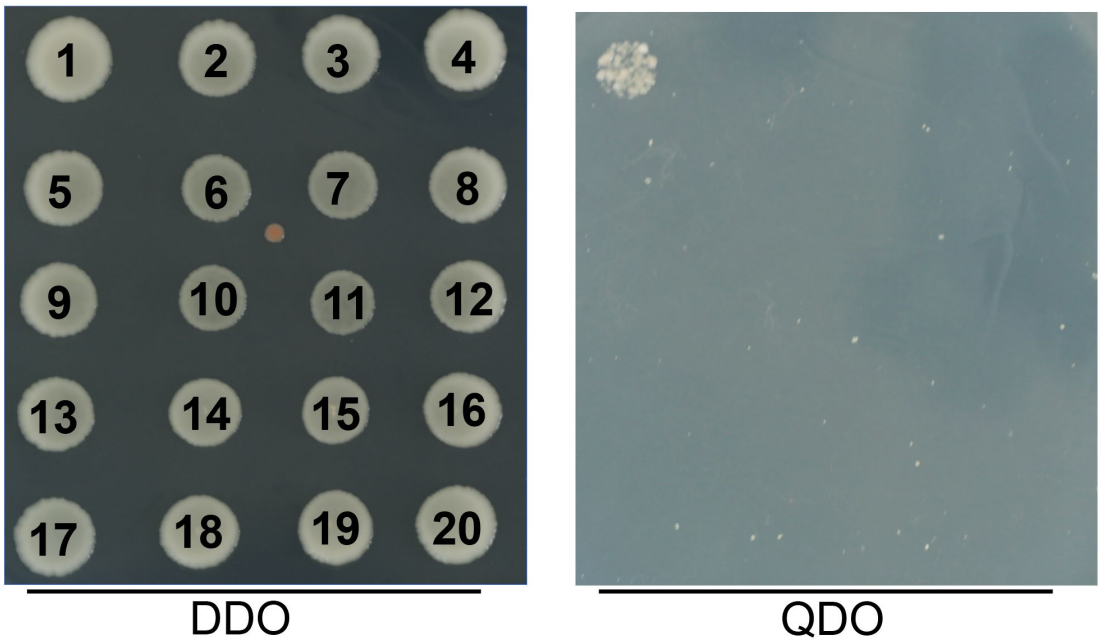

Fig. S26. Yeast two hybrid assays showing the interaction between OsRLP4 and salivary proteins from planthopper species. OsRLP4$_{(29\text{-}551)}$ (OsRLP4 without signal peptides and transmembrane domains) is fused to pGADT7 vector, while salivary proteins without signal peptides are fused to pGBKT7 vector, respectively. The different combinations of constructs are transformed into yeast cells, and are grown on the selective medium SD/-Trp/-Leu (DDO), and the interactions are tested with SD/-Trp/-Leu/-His/-Ade (QDO). Twenty salivary proteins are selected. The accession number of each protein is listed as follow: (1) MF278694.1, (2) XP_039291719.1, (3) KU365967.1, (4) MF278706.1, (5) MF278711.1, (6) MF278714.1, (7) MF278715.1, (8) MF278720.1, (9) XP_022195702.1, (10) XP_022196818.2, (11) XP_039284081.1, (12) XP_022192221.2, (13) XP_022207944.2, (14) KT764973,15) RZF44823.1, (16) RZF42644.1, (17) RZF33006.1, (18) RZF48570.1, (19) RZF42817.1, (20) RZF33751.1.

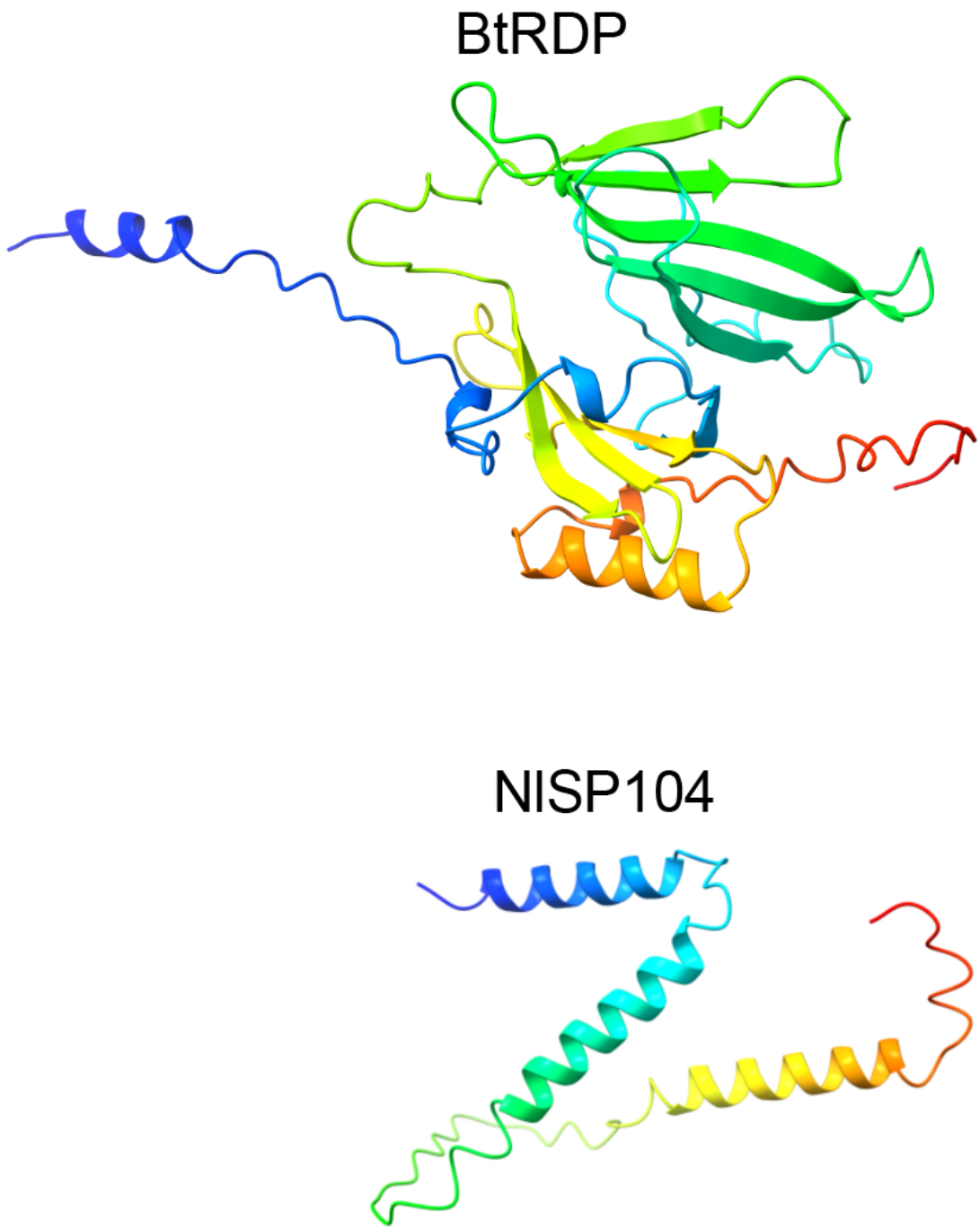

Fig. S27. Three-dimensional structure of BtRDP and NlSP104. AlphaFold2 is used to predicate the protein structure. The structures are colored as a spectrum from N-terminus (blue) to C-terminus (red).

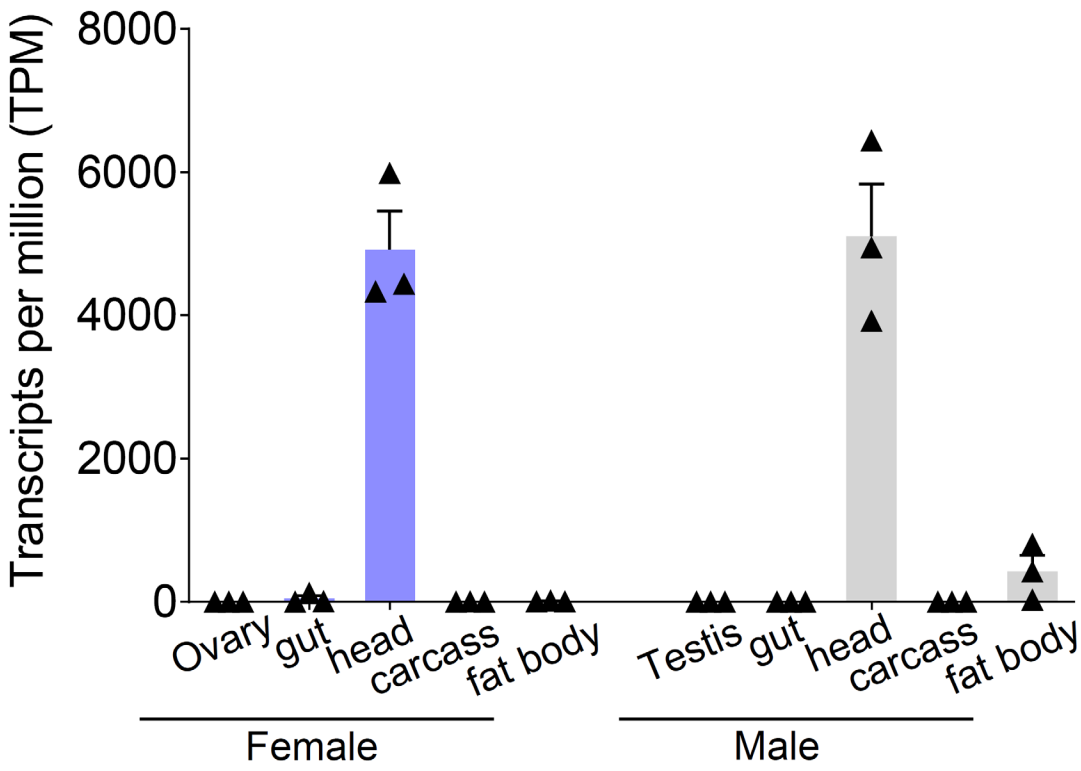

Fig. S28. Expression patterns of *Nilaparvata lugens NlSP104*. Transcripts per million (TPM) expression values of *NlSP104* in different tissues are determined based on the transcriptomic data. The head that contains salivary glands exhibits highest *NlSP104* expression in male and female *N. lugens*. Data are presented as mean values ± SEM (n=3 independent biological replicates).

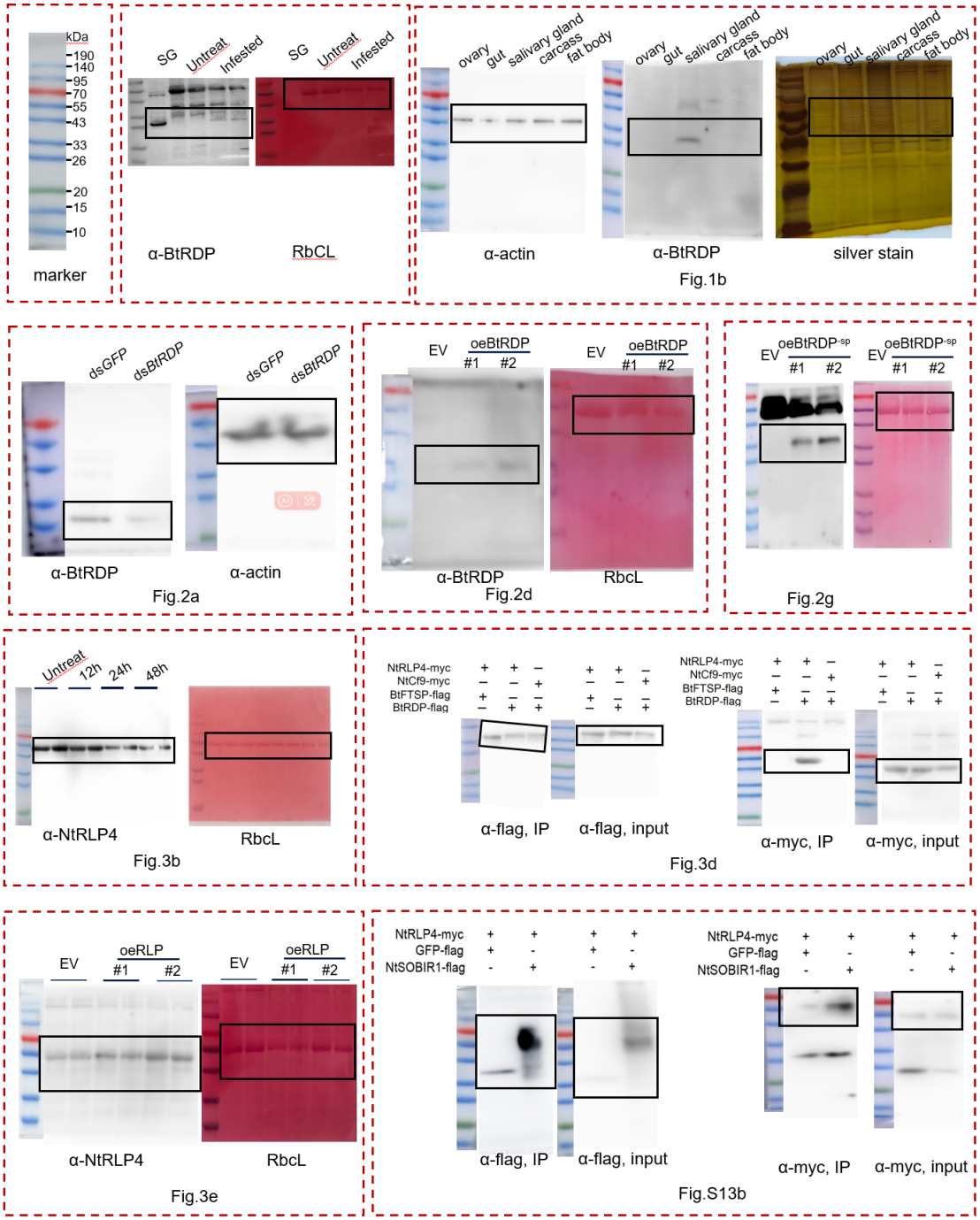

Fig. S29. Original images for blots in Figures 1-3 and Supplementary Figure S13b

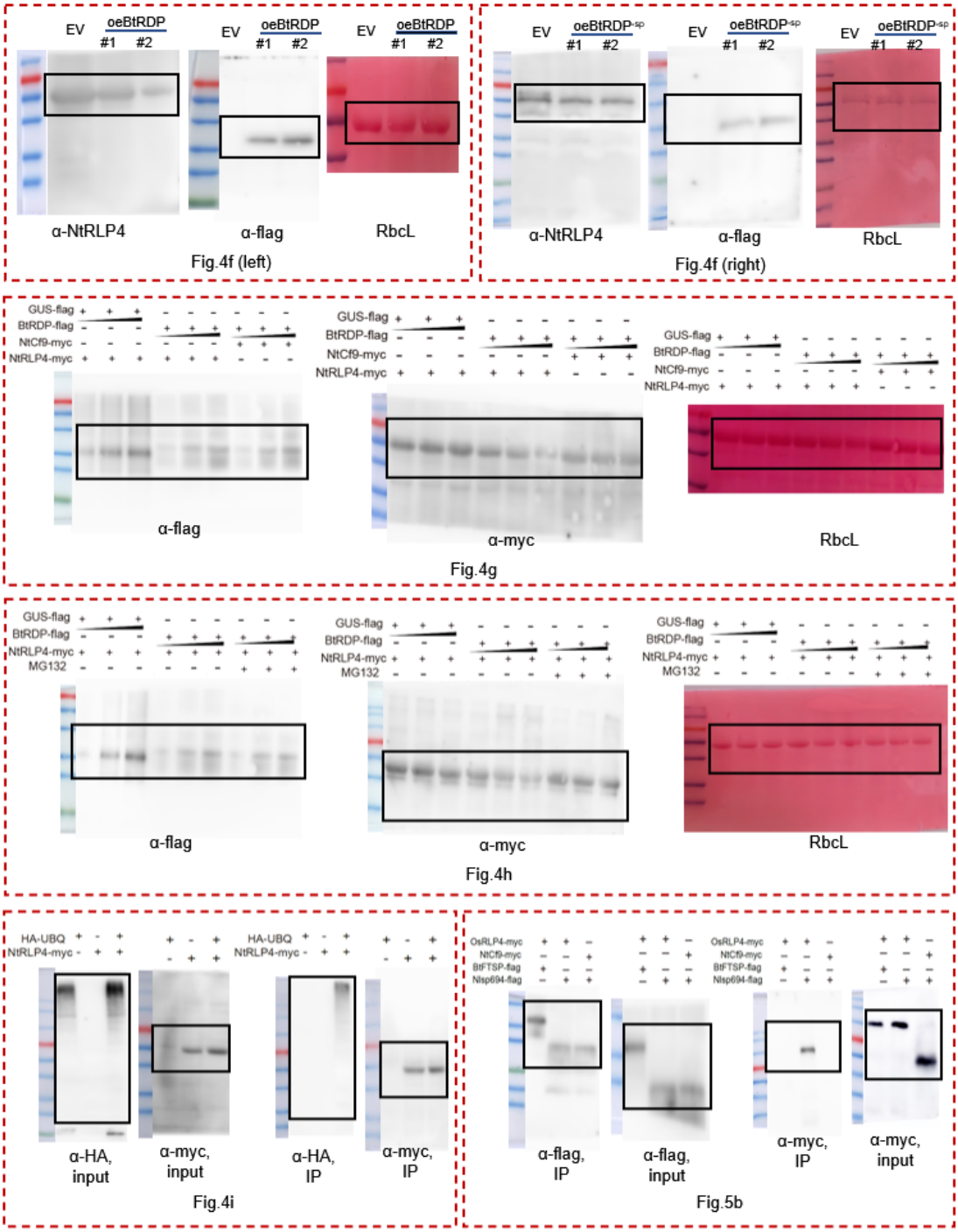

Fig. S30. Original images for blots in Figures 4-5

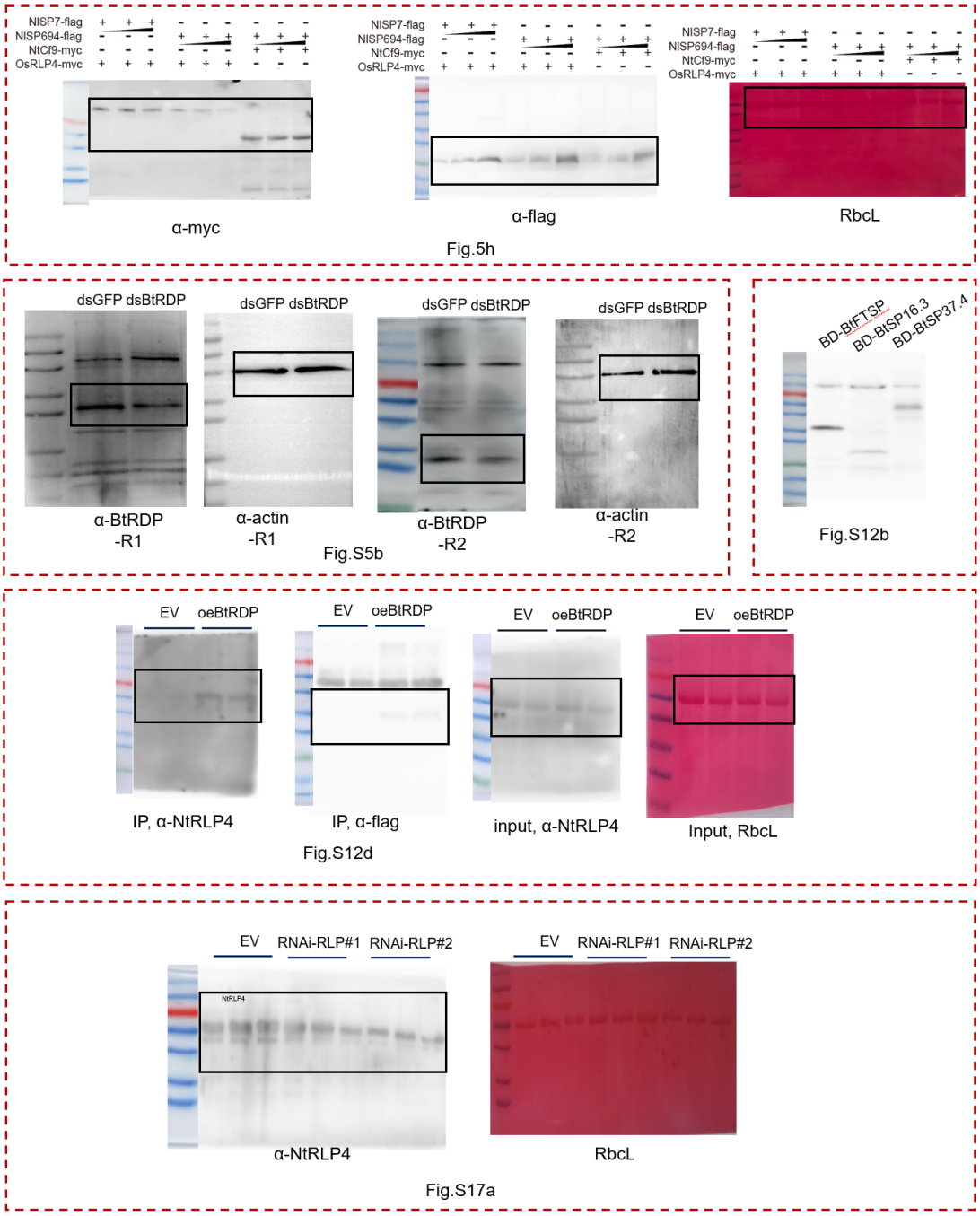

Fig. S31. Original images for blots in Figures 5 and Supplementary Figure 5-17.

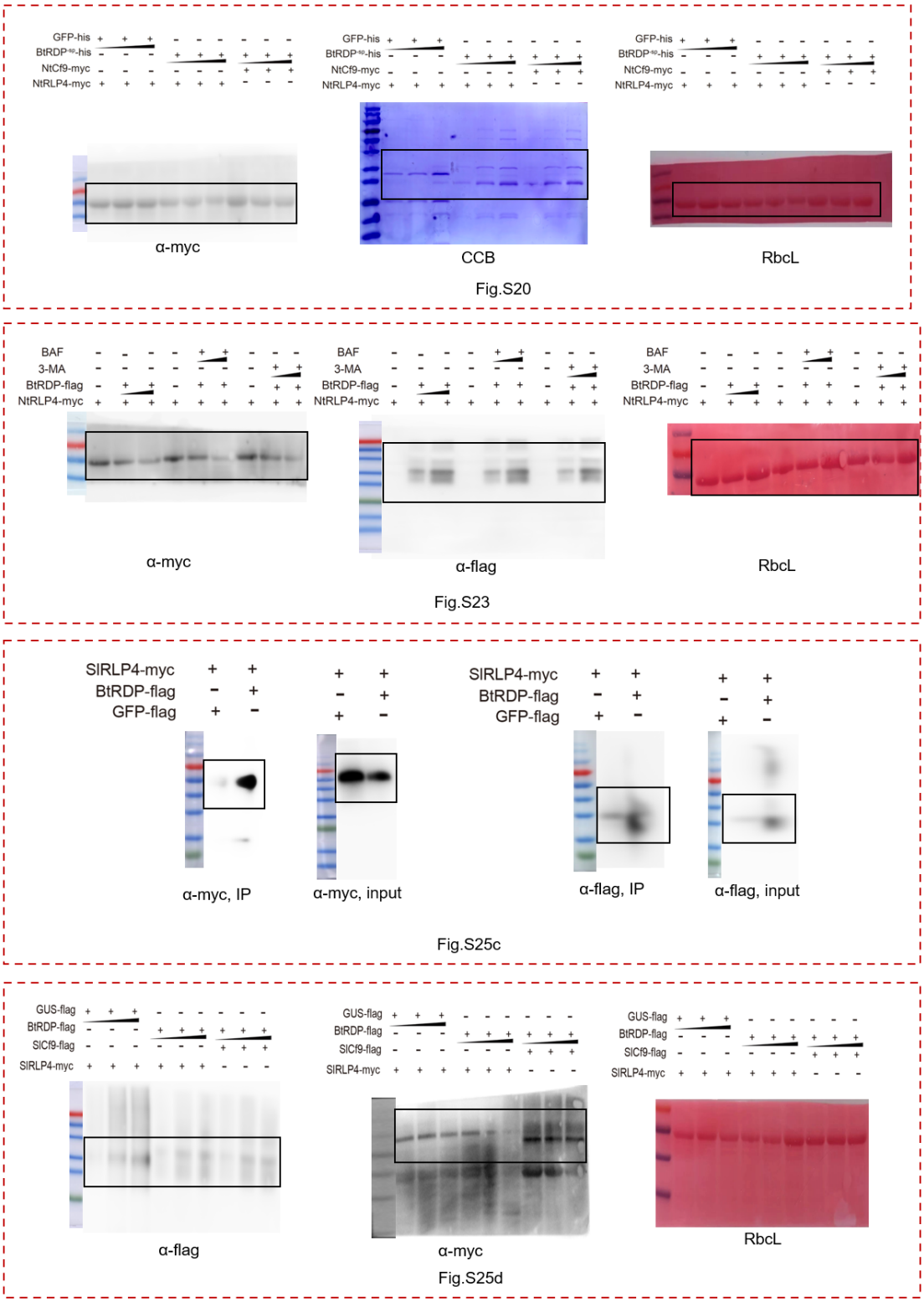

Fig. S32. Original images for blots in Supplementary Figure 20-25.

2. Supplementary Tables

Table S1. Identification of RDP and SP101 homologs in insect species

Family	Species	Accession	Total Base	Number of RDP homologs	Number of SP101 homologs	Note
Aleyrodidae	*Bemisia tabaci* MED	GCA_918797505	609.6 MB	1	0	Assembled genome
	Bemisia tabaci MEAM1	GCF_001854935	600.6 MB	1	0	Assembled genome
	Bemisia tabaci India	SRR1159209	9.7 GB*	1	0	Assembled genome
	Bemisia tabaci SSA1	GCA_902825415	657.8 MB	1	0	Assembled genome
	Bemisia tabaci SSA2	GCA_903994125	625.3 MB	1	0	Assembled genome
	Aleurocanthus spiniferus	SRR17330024	9.2 GB*	1	0	RNA-seq, whole body
	Aleyrodes proletella	SRX14998536	1.9 GB*	1	0	RNA-Seq, whole body
	Trialeurodes vaporariorum	GCA_011764245	814.7 MB	1	0	Assembled genome
	Dialeurodes citri	SRR2980521	5.0 GB*	1	0	RNA-Seq, whole body
Delphacidae	*Nilaparvata lugens*	GCF_014356525	1,088 MB	0	1	Assembled genome
	Laodelphax striatellus	GCA_017141395	510.2 MB	0	1	Assembled genome
	Sogatella furcifera	GCA_017141385	563.8 MB	0	1	Assembled genome
Aphididae	*Acyrthosiphon pisum*	GCA_005508785	533.6 MB	0	0	Assembled genome

	Myzus persicae	GCA_001856785	347.3 MB	0	0	Assembled genome
	Sitobion miscanthi	GCA_008086715	397.9 MB	0	0	Assembled genome
Aphalaridae	*Pachypsylla venusta*	GCA_012654025	482.0 MB	0	0	Assembled genome
	Diaci psyllid	GCA_000475195	485.7 MB	0	0	Assembled genome
Alydidae	*Riptortus pedestris*	GCA_019009955	1.0 GB	0	0	Assembled genome
Lygaeidae	*Oncopeltus fasciatus*	GCA_000696205	1.1 GB	0	0	Assembled genome
Pentatomidae	*Halyomorpha halys*	GCA_000696795	998.2 MB	0	0	Assembled genome
Cimicidae	*Cimex lectularius*	GCA_000648675	510.8 MB	0	0	Assembled genome
Reduviidae	*Rhodnius prolixus*	GCA_000181055	706.8 MB	0	0	Assembled genome
Gerridae	*Gerris buenoi*	GCA_001010745	994.4 MB	0	0	Assembled genome
Drosophilidae	*Drosophila melanogaster*	GCA_002310755	120.4 MB	0	0	Assembled genome
Culicidae	*Aedes albopictus*	GCA_018104305	1.3 GB	0	0	Assembled genome
Tenebrionidae	*Tribolium castaneum*	GCA_000002335	165.9 MB	0	0	Assembled genome
Chrysomeloidea	*Anoplophora glabripennis*	GCA_000390285	679.8 MB	0	0	Assembled genome
Bombycidae	*Bombyx mori*	GCA_027366755	456.6 MB	0	0	Assembled genome
Noctuidae	*Spodoptera frugiperda*	GCA_023101765	383.9 MB	0	0	Assembled genome
Pediculidae	*Pediculus humanus*	GCA_000006295	110.8 MB	0	0	Assembled genome

* The total base of raw data retrieved from SRA database.

Table S2. Proteins from a *Nicotiana benthamiana* cDNA library screened by yeast two hybrid using BtRDP as a bait

***N. benthamiana* v2.6.1 Accession** [1]	**Annotation**	**Number of colonies**	**Region**
Niben261Chr07g1310001.1	Putative leucine-rich repeat receptor-like serine/threonine-protein kinase	3	455-709
Niben261Chr13g1396009.1	Chloroplast stem-loop binding protein of 41 kDa b	1	162-374
Niben261Chr02g0086007.1	Sorbitol dehydrogenase-like	1	95-305
Niben261Chr17g0179002.1	Guanine nucleotide-binding protein subunit beta-like protein	1	92-326
Niben261Chr01g1673009.1	Ribulose bisphosphate carboxylase/oxygenase activase 2	2	228-420
Niben261Chr07g1128067.1	Ribulose-1,5-bisphosphate carboxylase/oxygenase small subunit	5	23-181
Niben261Chr14g0161005.1	Cytochrome b6-f complex iron-sulfur subunit 2	5	1-216

[1] The sequence can be downloaded from Sol Genomics Network (https://solgenomics.net/ftp/genomes/Nicotiana_benthamianaV261)